Set-up and Evaluation of Capacitive Deionization for Desalination Application

Gbenro Folaranmi

THÈSE

Pour obtenir le grade de Docteur

Délivré par **l'Université de Montpellier**

Préparée au sein de l'école doctorale **Sciences Chimiques Balard (ED459)**

Et de l'unité de recherche **Institut Européen des Membranes (IEM)**

Spécialité : **Chimie séparative matériaux et procédés**

Présentée par **Gbenro Folaranmi**

SET UP AND EVALUATION OF CAPACITIVE DEIONIZATION FOR DESALINATION APPLICATION

Soutenue le 16 Juillet 2021 devant le jury composé de

M. Hyacinthe Randriamahazaka, Professeur Université de Paris Diderot	**Rapporteur**
M. Patrick. Drogui, Professeur INRS Université du Québec	**Rapporteur**
Randa Khouri, Professeur Université Libanaise	**Examinatrice**
Mme. Sara Cavalière, Maître de Conférences HDR, Université de Montpellier	**Examinatrice**
M. Marc CRETIN, Professeur Université de Montpellier	**Directeur de thèse**
M. Mikhael BECHELANY, Directeur de Recherche (CNRS) Université de Montpellier	**Co-encadrant de thèse**
M. Philippe Sistat, Maître de Conférences Université de Montpellier	**Invité**
M. Francois Zaviska, Maître de Conférences Université de Montpellier	**Invité**

Abstract

Water purification is the rendering of non-potable water into water good enough for human consumption and use. Capacitive deionization is a promising emerging water desalination technique; a close relative to the established desalination technology such as reverses osmosis (RO) etc. It operates at low pressure and can potentially utilize less energy for brackish water desalination.

In a typical CDI cell, the feed water flows through the separator layer between two electrically charged carbon electrodes. This architecture results in significant performance limitations as electrodes are in solid state with limited exposed surface area of contact and pores for adsorption. Also, there is an inability to afford continuous mode of operation.

Here, we describe an alternative architecture, where the feed electrode is in liquid state and flows semi-continuously on carved channels. Using this technique, we show that flow capacitive deionization enables significant reductions in desalination time and can desalinate higher feed solution. We show these benefits using commercially made powdered activated carbon and superfine activated carbon as electrode materials. The superfine carbon at a moderate carbon loading rival the performance of powdered activated carbon due to its reduced particle size. Furthermore, the physico-chemical and electrochemical properties of the solid and flow electrodes (pristine and modified electrodes) were characterized by low-temperature nitrogen adsorption measurement, scanning electron microscope (SEM), X-ray diffraction (XRD), Raman spectroscopy, X-ray photoelectron spectroscopy (XPS), Fourier transform infra-red (FT-IR), cyclic voltammetry (CV), and electrochemical impedance spectroscopy (EIS).

We also present a strategy in reduction of concentration polarization of carbon based electrodes by utilization of electrospun nanofibers synthesized via electrospinning method and as a result, a notable improvement was made through experimental approaches by electrochemical impedance spectroscopy and cyclic voltammetry studies of the hybrid nanocomposites carbon electrodes. In furtherance, we demonstrate that our approaches are promising towards improving CDI/FCDI electrodes and in resolving some inherent challenges of carbon based electrodes.

Publications arising from this thesis

Gbenro Folaranmi, Mikhael Bechelany, Philippe Sistat, Marc Cretin and Francois Zaviska. Towards electrochemical water desalination techniques: A Review on Capacitive Deionization, Membrane Capacitive Deionization and Flow Capacitive Deionization. *Membranes.* **2020,** 10, 96

Gbenro Folaranmi, Mikhael Bechelany, Philippe Sistat, Marc Cretin and Francois Zaviska. Comparative Investigation of Activated Carbon Electrode and a Novel Activated Carbon/Graphene Oxide Composite Electrode for an Enhanced Capacitive Deionization. *Materials.* **2020**, 13, 5185

Gbenro Folaranmi, Mikhael Bechelany, Philippe Sistat, Marc Cretin and Francois Zaviska. Electronic improvement of AC electrode by RGO doping and it comparative effect on desalination by Capacitive Deionization. *Nanomaterials* **2021**, 11, 1090

Publications in progress

Gbenro Folaranmi, Myriam Tuak, Mikhael Bechelany, Philippe Sistat, Marc Cretin and Francois Zaviska. Investigation of superfine activated carbon as a viable flow electrode in capacitive deionization

Gbenro Folaranmi, Mikhael Bechelany, Philippe Sistat, Marc Cretin and Francois Zaviska. Activated carbon co-mixed electrospun titanium oxide nanofibers as flow electrode in capacitive deionization.

Participation in conferences

- **Oral communications**

Gbenro Folaranmi, Mikhael Bechelany, Philippe Sistat, Marc Cretin and Francois Zaviska. *Comparative Investigation of Activated Carbon Electrode and a Novel Activated Carbon/Graphene Oxide Composite Electrode for an Enhanced Capacitive Deionization*. Oral Communication, Journee Electrochimie at Montpellier, France. June 2019

Gbenro Folaranmi, Mikhael Bechelany, Philippe Sistat, Marc Cretin and Francois Zaviska. *Comparative Investigation of Activated Carbon Electrode and a Novel Activated Carbon/Graphene Oxide Composite Electrode for an Enhanced Capacitive Deionization*. Oral Communication, Journee Electrochimie (International) at Toulouse, France. July 2019

Gbenro Folaranmi, Mikhael Bechelany, Philippe Sistat, Marc Cretin and Francois Zaviska. *Comparative Investigation of Activated Carbon Electrode and a Novel Activated Carbon/Graphene Oxide Composite Electrode for an Enhanced Capacitive Deionization*. Oral Communication, FrancoFilt (International) at Hammamet South, Tunisia. September 2019

Gbenro Folaranmi, Mikhael Bechelany, Philippe Sistat, Marc Cretin and Francois Zaviska**.** *Investigation of superfine activated carbon as a viable flow electrode in capacitive deionization.* Oral Communication, Balard-Chemistry Conference at Montpellier, France. June 2021

- **Poster**

Gbenro Folaranmi, Mikhael Bechelany, Philippe Sistat, Marc Cretin and Francois Zaviska. *Investigation of superfine activated carbon as a viable flow electrode in capacitive deionization.* CDI-E Virtual Conference. May 2021

Acknowledgement

I would like to thank my PhD director, Prof. Marc Cretin, Dr. Mikhael Bechelany (Co-encadrant), and the other two supervisors (Dr. Francois Zaviska and Dr. Philippe Sistat) for their thorough technical guidance, tutelage, career advices, financial support and involvement in my research projects. This project and especially the thesis write-up would have been impossible without these wonderful people in my life. Your suggestions and comments during the course of this manuscript organization are highly appreciated. I couldn't find the right words to heartily express how much I god you people; I simply owe you a lot (especially Francois Zaviska).

I would like to further appreciate my many colleagues who have dedicated their time in one way or the other to assist me during the course of this program. I would like to thank the experts in IEM and the University of Montpellier who helped in characterizing my electrode materials.

I would also like to thank Dr. Mona Semsarilar for inviting me to IEM and after unsuccessful scientific adventures with her, introduced me to Francois Zaviska (a life changing opportunity in which the pedestal of my career is built).

Furthermore, I would like to heartily appreciate the members of Jury; Prof. Patrick Drogui (Rapporteur), Prof. Hyacinthe Randriamahazaka (Rapporteur), Prof. Randa Khouri (Examinatrice) and Dr. Sara Cavalière (Examinatrice) for dedicating their time to go through my report. Your time and scientific suggestions are appreciated.

I gratefully acknowledge funding for this research from the Federal government of Nigeria through TETFUND/AE-FUNAI/CAMPUS FRANCE with the funding number CAMPUS FRANCE 914886H and PAT eau Axe IEM.

Most importantly, I would like to thank my family, friends and Uncle whose support and help were instrumental for my mental health during the course of this program. To my girlfriend (Rixchie Mimi), I would like to say thank you for your dedication, unconditional love, and amazing enthusiasm.

Last but not the least, I would like to thank nature (OLODUMARE through IFA) for making me so privilege to meet amazing people (all my supervisors) and to be able to have a thorough scientific training in such an amazing and developed country like France.

Table of Contents

List of tables

List of Figures

List of Symbols

A	area	[cm^2]
F	Faraday Constant	[96487 C mol^{-1}]
I	current density	[A cm^{-2}]
Ie	electrical current passing through the cell	[A]
M	mass of carbon material in one pair of the electrodes	[g]
Q	salt adsorption per cycle	[mg of salt / gcarbon]
t	time	[s]
v	velocity in the flow channel	[m s^{-1}]
Vcell	electrical potential applied to the CDI/FCDI unit	[V]
V	volume	[m^3]
z	valency	-
λ	current efficiency	-

List of Abbreviations

abbreviation	Definition
ASAP	Accelerated surface area and porosimetry system
BET	Brunauer-Emmett-Teller
BJH	Barrett-Joyner-Halenda model
CDI	Capacitive deionization
DLS	Dynamic light scattering
ED	Electrodialysis
EDL	Electrical double layer
FCDI	Flow capacitive deionization
FESEM	Field emission scanning electron microscopy
FE	Feed electrode
FS	Feed saline solution
FT-IR	Fourier transform infrared
ID	D-band intensity
IEM	Ion exchange membrane
IG	G-band intensity
IR	Infrared
IUPAC	International union of pure and applied chemistry
MCDI	Membrane capacitive deionization
MSFD	multi-stage flash distillation
NMP	N-methyl-2-pyrrolidone
OFG	oxygenated functional group
PAC	Pristine activated carbon
PV	Photovoltaic
PVDF	Polyvinylidene difluoride
RO	Reverse osmosis
SAC	Salt adsorption capacity

S_{BET}	Brunauer-Emmett-Teller surface area
SCC	Short circuit close cycle
SEC	Specific energy consumption
SEM	Scanning electron microscopy
SFAC	Super fine activated carbon
SRR	Salt removal rate
STP	Standard temperature and pressure
SWRO	Seawater reverse osmosis
TDS	Total dissolved solids
TMO	Transition metal oxydes
ZrO_2	Zirconium oxide
TiG	Titanium graphene
PVA	Polyvinyl alcohol
OAC	Oxidized activated carbon
FCNT	Functionalized carbon nanotubes
SWCNT	Single walled carbon nanotubes
NG-CNFs	Nitrogen doped graphene carbon nanofibers
PANI	Polyanine
FRGO	Functionalized Reduced Graphene Oxide
NC	Nitrogen doped Carbon
MC	Mesoporous Carbon
HPC	Highly porous carbon
HCS	Hollow Carbon Spheres
VBTAC	Vinyl benzyl trimethyl ammonium chloride
S4VBS	Sodium 4-vinylbenzenesulfonate
MSC	Maxsorb Carbon
ACTi*	$ACTiO_2NFs$
*Th T	Thermal treatment
Tr*	Treatment
V_{MESO}	Mesopore volume

Chapter 1. Introduction

Availability of fresh and potable water for mankind consumption has been a major global challenge due to either man made or naturally occurring activities. Water reclamation or converting non-portable water for human consumption involves processes such as distillation, decontamination etc. Water desalination involves the removal of dissolved ions (salt ions) and water above dissolved salt level of 1000 mg L^{-1} is not considered healthy or fit for human consumption [1]. Contrary to other water pollutants, removing salt from water involves expensive technologies either on capital cost (CAPEX) or operational cost (OPEX) and there have been intensive scientific and engineering research for several decades to improve this aspect. Water desalination technologies such as reverse osmosis (RO), multi-stage flash distillation (MSFD), multi effect distillation (MED), electrodialysis (ED) etc., contribute most significantly to industrial water desalination from sea water and have been in the front line of major water treatment plants worldwide. RO plants currently supply over 50 % of the total worldwide desalination capacity [2], and over 90 % of the United States desalination capacity [3] with plant energy requirement of approximately 3-4 kWh m^{-3} of produced fresh water for seawater desalination at roughly 50 % water recovery.

A major cost of desalination involves electrical or thermal energy needed to extract salt and this could account for nearly 1/3 of the total costs in a sea water reverse osmosis (SWRO) desalination plant [3]. In 2008, the worldwide operational desalination capacity was reported as over 37 million m^{-3} fresh water per day [3, 4].

In this chapter, we summarized briefly the most utilized techniques i.e., RO for both brackish and seawater desalination and ED for basically brackish water desalination to combat water scarcity. For the rest of this thesis, we focused solely on the alternative techniques of brackish and seawater desalination.

1.1. A Brief Oversight into Reverse Osmosis (RO) and Electrodialysis (ED)

RO, being the most commonly used desalination technique is described in terms of principle of operation which involves the use of a semi-permeable membrane that prevents the flow of salt through its bulk, but allows the flow of water.

1.1.1 Reverse Osmosis

This is a membrane method of sea water purification process using pressure as a driving force to make feed solution pass through a membrane usually semi-permeable in nature. During this process, the ions in the feed solution are retained by the dense polymeric membranes. Basically, the sea water is fed into the system and made to permeate the semi-permeable membrane under pressure and recovered as clean water as shown in Figure 1.0. This is then followed by several post-treatment methods like disinfection, pH, and mineralization adjustment etc. to make it suitable for drinking [5] or agriculture. In RO as the ions are retained by membranes, generation of concentrate (concentrate brine) that is usually sent back to the environment is inevitable. Concentrate brine disposal is a real environmental challenge and many a times, this by-product (concentrate brine) is usually disposed into ocean bodies thus affecting the aqua-ecosystem. Brine concentration varies from 50 to 75 g/L and has a much higher density than seawater and therefore tends to fall on the sea floor near the brine outfall outlet (plume effect), creating a very salty layer which can have negative impacts on the flora and the marine life. The consequent effect of this could lead shorter life expectancy of the aquatic animals. However, research into brine utilization by International Center for Biosaline Agriculture in Dubai has shown that some species of fish i.e., tilapia thrive comfortably well in brine condition nonetheless, the reject brine should be checked for heavy metals and other chemicals before use in growing fish for human consumption. Other proposed possible way of safely disposing reject brine is: brine dilution in which the brine is diluted with another water source i.e., fresh water before deposition into the sea.

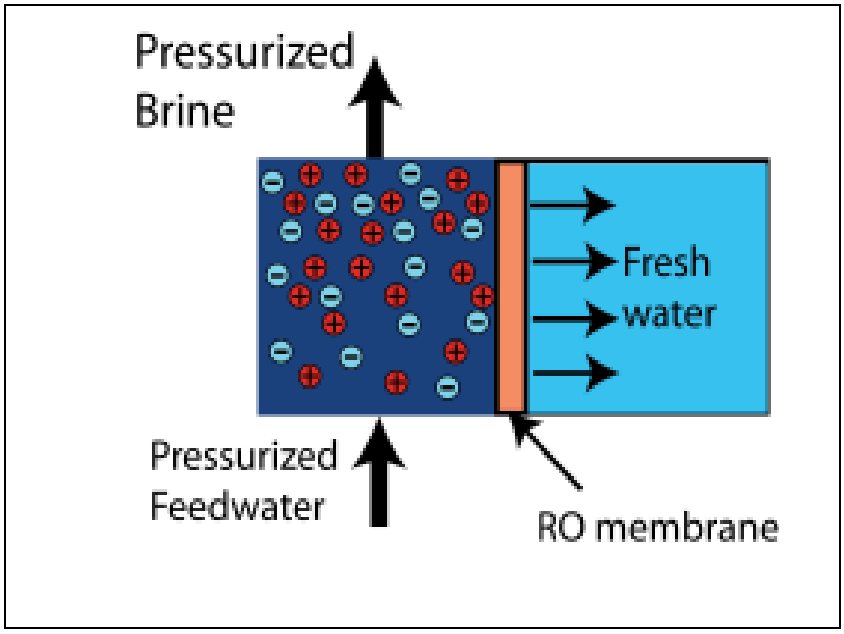

Figure 1: Schematic representation of reverse osmosis (RO) desalination system in which a semi-permeable membrane which allows a water flux but does not permit transport of dissolved salt ions. When the feed is pressurized to above its osmotic pressure, desalted water flows through the RO membrane.

1.1.2 Trend in Energy Consumption of Reverse Osmosis

Sea water desalination is energy intensive whatever the technique employed. Indeed, in a thermodynamic point of view, sea desalination consists of the generation of two streams (concentrate and permeate) with a very high salinity difference corresponding to high chemical potential difference and thus requires a high amount of energy. Concerning sea water reverse osmosis (SWRO), the energy consumption is affected by the work of the high-pressure pump, the aim of which is to drive water through a semi-permeable membrane. High pressure is required in order to overcome the osmotic pressure and also to compensate energy loss due to viscous friction in the membrane module (pressure drop) which transforms mechanical energy into thermal energy.

The energy consumption of SWRO has tremendously decreased in these last decades, passing from 15 $kWhm^{-3}$ in the early seventies to less than 2 $kWhm^{-3}$ nowadays (considering exclusively RO steps) [6, 7]. This energy decrease is attributed to both membrane materials improvement (membrane with a very good compromise between selectivity and permeability) and process aspect (operating and energy recovery device implementation). Plant energy requirements are minimized by recovering energy from the pressurized brine stream through use of turbines or pressure exchangers. Nowadays, the specific energy consumption (SEC) of sea water RO (SWRO) including both pre-treatment and post-treatment is around 3.5–4.5 $kWhm^{-3}$. Hence, RO is actually the most developed technology for sea water desalination which is due to the tremendous improvement of membrane material and process optimization for minimizing energy consumption. Table 1 shows the specific energy consumption for high capacity SWRO plants which is in the range of 3.5 to 6.7 $kWhm^{-3}$ confirming the important energy consumption reduction.

Table 1. Specification of some selected sea water reverses osmosis (SWRO) desalination plants working in single stage configuration in different countries.

Country	Plant	Capacity ($m^3.d^{-1}$)	SEC* ($kWhm^{-3}$)	Reference
Chile	El Coloso	45360	4.3	[8]
USA	Carlsbad	190000	3.5	[9]
Spain	Aguilas	200000	4.6	[10]
Algeria	Benisaf	200000	4.0	[11]
Egypt	Marsa	24000	6.7	[12]
China	Caofeidian	50000	4.0	[12]

SEC* here considers all the energy involved (pumping, pre-treatment, RO and post-treatment energy) and not just only RO

Actually, most sea water desalination plants around the world operate RO system below 2 $kWhm^{-3}$ which is becoming close to the thermodynamic limit (1.1 $kWhm^{-3}$ at 50 % water recovery from sea water) and even closer to the minimal practical energy consumption (1.54 $kWhm^{-3}$ Elimelech *et al*. [7]). However, as any other membrane process, RO is very sensitive to membrane fouling and thus requires strong pretreatment to assure long term filtration operation. While RO operation costs are directly linked to the feed water salinity, the pre-treatment cost is more or less constant even for low salinity water. From this point of view, RO is not the most suitable desalination technology for moderate and low salinity water (below 5 g L^{-1}). Electrochemical technologies such as ED and CDI seem much more appropriate for moderate and low salinity water as the functioning principle is at the opposite of the others desalination method by targeting solute (ions) instead of the solvent.

1.1.3 Electrodialysis

ED is a membrane-based desalination method for brackish water. Contrary to other desalination technologies, ED as shown in Figure 1.1 employs a difference of electrical potential (as well as CDI) as driving force in order to extract charged compounds (instead of

the solvent) from a saline solution. It involves ions migration through intercalation of anion and cation-exchange membranes when an electric field is created by difference of potential. Cation- and anion-exchange membranes (CEM and AEM) are alternatively oriented between the anode and the cathode. The application of potential difference in the system electrostatically attracts the cations to the cathode (negative pole) and anions towards the anode (positive pole). Concentrate is generated (brine solution) in ED compartments due to the retention of ions by opposite membranes and consequently fresh water is generated by another compartment as ions migrate through the desired membranes [13]. As shown in Figure 1.1, a unit of ED is made of an arrangement of CEM and AEM defining the concentrate and the dilute compartments.

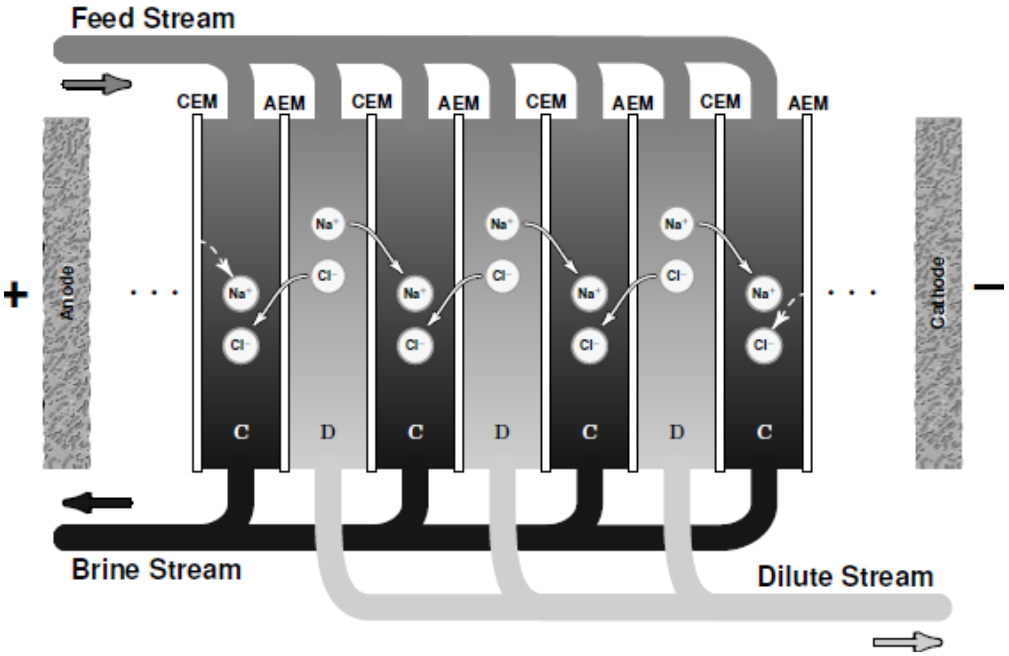

Fig 1.1 A schematic diagram of electrodialysis (ED) where C is the concentrate compartment and D is the dilute compartment.

1.1.4 Trend in Energy Consumption and Shortcomings of Electrodialysis

ED has been used in cooperation with other renewable energies such as solar and wind [14] to improve efficiency and reduce energy consumption. The integration is environmentally friendly as no pollution is recorded and offers low maintenance cost [15, 16]. In general, ED is advantageous by affording high removal salt rate and energy consumption of 0.8–1.5 kWh m^{-3} at a water productivity of 45 L m^{-2} h^{-1} for initial water salinity less than 5 g L^{-1} [16]. It is

noteworthy to keep in mind that both ED and CDI are not intended to compete with RO but are more interesting (i.e. in terms of energy consideration) for low and moderate saline water treatment (below 10 g L^{-1}). ED offers the advantage (unlike other desalination techniques) of being flexible either in terms of demineralization rate or recovery rates. In addition, CDI and ED are much less sensitive to clogging and therefore require less extensive pre-treatment and therefore are more applicable for the treatment of saline water.

In addition to the above desalination techniques; research effort in providing alternative means of water desalination has been the focus of main attention of recent and as a result, techniques which applies electric field to desalinate water such as desalination batteries and capacitive deionization (CDI) have come to existence. These novel technologies operate by separating ions from water. Here, the ions are removed and because of this, it is specifically designed for desalination of low saline water (brackish water) thus making it an energy efficient technologies.

1.2 Capacitive Deionization Systems

Similar to ED, CDI is closely related to ED as it uses electrochemical water desalination technology for desalting brackish water. CDI selectively targets solutes in water making it energetically effective for moderate and low saline water. Unlike ED that operates by intercalation of IEMs for ions exclusion, CDI makes use of porous carbonaceous materials as solid electrodes in temporary storage of ions and the fact that it makes use of porous materials gives it an edge and enviable diversity in terms of functionalities and other applications over ED. CDI operates under low potential difference to polarize electrodes and as a result, the ions get separated by electrostatic attraction to oppositely charged poles, and stored/adsorbed in the pores of the electrodes [17]. When an external direct voltage (usually below 1.4 V) is applied onto a system containing saline solution (feed solution), the electric field created electrostatically drives the solvated ions in the solution into their different polarized poles where they are adsorbed in the pores of the electrodes and the process continues until the pores are saturated. Conversely, as soon as the external electric field is removed (short circuiting), the ions are desorbed from the pores of the electrodes (generating concentrate) hence leading to regeneration of saturated electrode materials [18].

The fact that the electrodes can store and easily dissipate charges when needed make them qualified as capacitors. When the charges are stored via a non-faradaic process (no redox peak

observed), the capacitor is considered as an electrical double layer (EDL) capacitor while it is considered as a pseudo-capacitor if the carbon material is in combination with transition metal oxides (TMOs) and charges are stored under faradaic condition making adsorption process occurs via redox reaction. Super-capacitors possess a high capacitive ability but the performances are limited by water electrolysis at high voltage (>1.4 V) leading to undesirable by-products. In literature, most of the super-capacitors in electrochemical water desalination are based on activated carbon (AC) electrodes. The main advantages of activated carbon are related to its high availability and versatility of structure/texture, low cost and highly developed surface area. Carbon based materials have extensively been studied as source of EDLCs due to their porosity, high surface area, adsorption ability, tunable surface oxygen-containing complexes, low cost, availability, non-toxicity etc., [5]. Super-capacitor devices are classified as electrode materials are shown in Figure 1.2

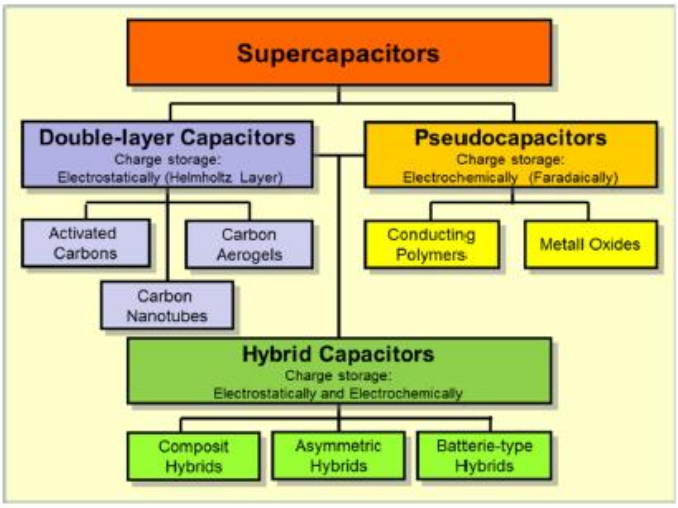

Fig 1.2 Synopsis of super-capacitor [19]

From an experimental point of view, capacitance of EDLCs could be evaluated via cyclic voltammetry (CV) and galvanostatic charge-discharge (GCD). In the absence of faradaic contributions and in galvanostatic mode, capacitance can be obtained directly from the cyclic voltammogram recorded at different sweep rate:

$$C = \int {}^{dq}/_{dV} = I \int {}^{dt}/_{dV} = {}^{I}/_{v} \quad (1)$$

where q = charge (C), V = potential difference (V), t = time (s), I = intensity (A), and v = sweep rate (Vs^{-1}). The behavior of electrode materials towards electro-adsorption could be directly obtained from resulting voltammograms.

1.2.1 Principle of Ion Adsorption

The phenomenon of ions adsorption lies on the principle of electrical double layer (EDL). EDL is an electrode–electrolyte interface that is responsible for ion adsorption. As proposed by Helmholtz in 1883 [20]; in EDLCs (Figure 1.3), distribution of charges at the double layer is governed by charge surface accumulation of one sign while the opposite charges are accumulated at the solution side. Helmholtz model predicted a constant capacitance that is independent of the charge density but depends on the dielectric constant of the electrolyte and the thickness of the double layer. The model offers good foundation of EDL but fails to consider factors including diffusion of ions in solution, the possibility of adsorption onto the surface and the interaction between solvent dipole moments and the electrode.

Gouy–Chapman-Stern model made significant improvements by introducing a model of the EDL. Based on the assumption of Gouy-Chapman-Stern model, the double layer can be divided into an 'inner' region and a 'diffusion' region. The inner region is referred to as the Helmholtz layer where ions covered directly onto the surface of electrode while the region farther from the surface is a diffusion layer called the Gouy–Chapman layer or model [21] in which the distribution of electric charge depends on the potential at the surface and as such, the capacitance of EDLCs is not a constant variable but depends on factors such as applied potential and ionic concentration of electrolytes. It is noteworthy to bear in mind that in CDI, since it operates by adsorption phenomenon, that ionic concentration is inversely proportional to double layer thickness thus the lower the ionic concentration, the greater the double layer thickness. With increasing ionic strength, the charge potential on electrode surface tends to decrease as proposed by Gouy–Chapman-Stern model. In concept, ions in the diffused electrical double layer reach the equilibrium between the diffusion and electrostatic force. Therefore, the electrical double layer thickness L is directly related to the electrostatic forces and diffusion. Since electrical double layer thickness is inversely proportional to the solution concentration with lower concentration, the electric field can extend to a longer distance since the solution is less effective in holding the charge

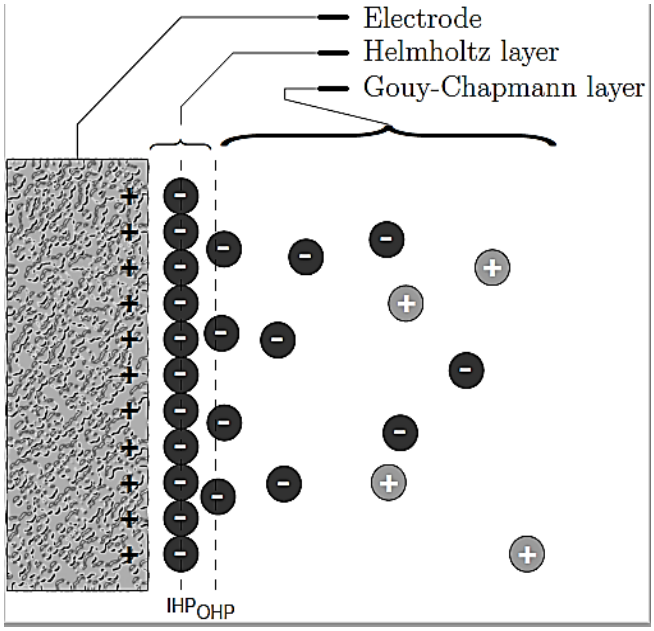

Fig 1.3. Distribution of charges as described by Gouy–Chapman

1.3. How does capacitive deionization (CDI) Work?

Simply, a saline feed solution is made to flow by a pair of electrodes that are separated by a spacer (non-conducting CDI spacer). For pseudo-capacitors, no redox reaction occurs (absence of Faradaic reaction) and the response is purely capacitive in nature. Potential difference is generated by an external source to the system enabling electrostatic attraction of ions to the oppositely charged electrodes (adsorbed) until the pores of the electrodes are saturated. Consequently, desorption occurs by the desorption of adsorbed ions which is made evident by the increase in ionic conductivity that is being monitored by a conductimeter. Figure 1.4 (a) shows a schematic laboratory CDI set up in which the potentiostat powers the cell. The current response in relation to electrosorption is made evident by the monitor of a computer that is connected to the potentiostat. The influent solution is fed in by a peristatic pump at a constant flow rate and the ionic conductivity change is monitored and recorded by a conductimeter. Figure 1.4 (b) shows the schematic representation of a laboratory CDI cell; it consisted of two parallel electrode sheets separated by a non-electrically conductive spacer of about 500 to 1200 microns thick. This prevents an electrical shortage and allows liquid to flow [17, 18].

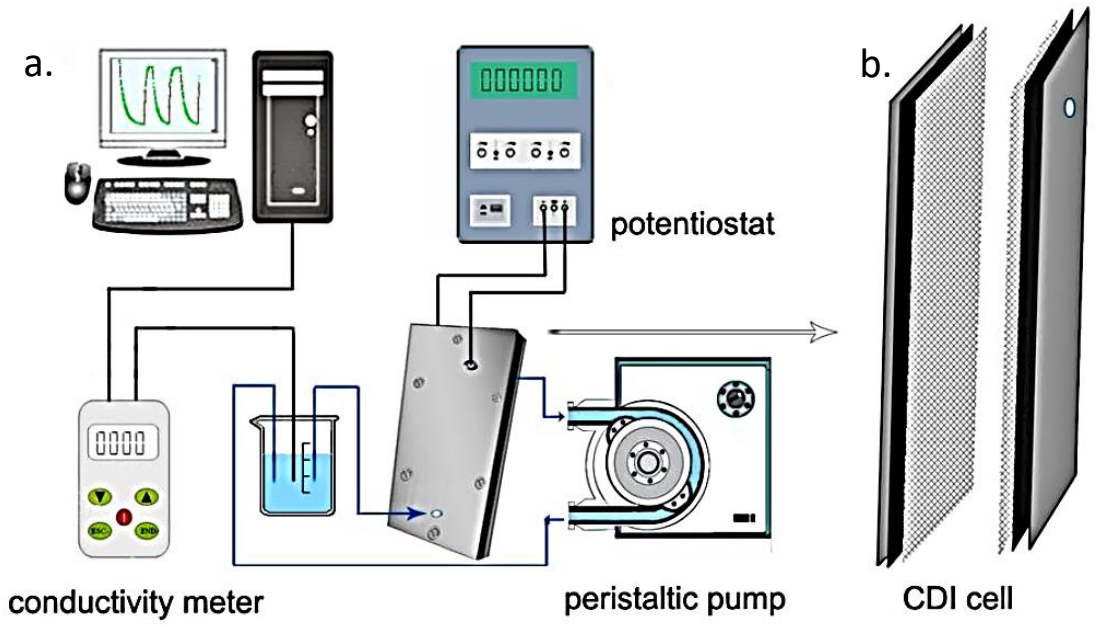

Fig 1.4. Schematic diagram of capacitive deionization (CDI) set-up

Schematic representation of fresh water and brine generation during adsorption and desorption processes is shown in Figure 1.5 (a), and 1.5 (b) respectively. In adsorption process as shown in Figure 1.5 (a), the solvated ions are electrostatically attracted to different polarized poles (electrodes) as a result of electric field created thus producing fresh water while in desorption process; Figure 1.5 (b), brine generation is produced due to the release of the ions from the pores of the electrodes once the electric field is cut off at zero volt (short-circuit). CDI is a deionization technique that does not require membrane. CDI however has a major challenge of co-ion adsorption as there is no means to screen off oppositely charged ions thus leading to low charge efficiency of the system. There is then a great interest to work on electrode materials to increase overall performance of the system. Additionally, it is an intermittent process—there is a lag of time as adsorption process is limited to the fixed and immobilized electrodes on the current collectors thus limiting adsorption rate. Biesheuvel *et al.* [22] described a thermodynamic model for the CDI charge efficiency improvement i.e. by increasing cell voltage or decreasing the ionic strength of the solution being treated.

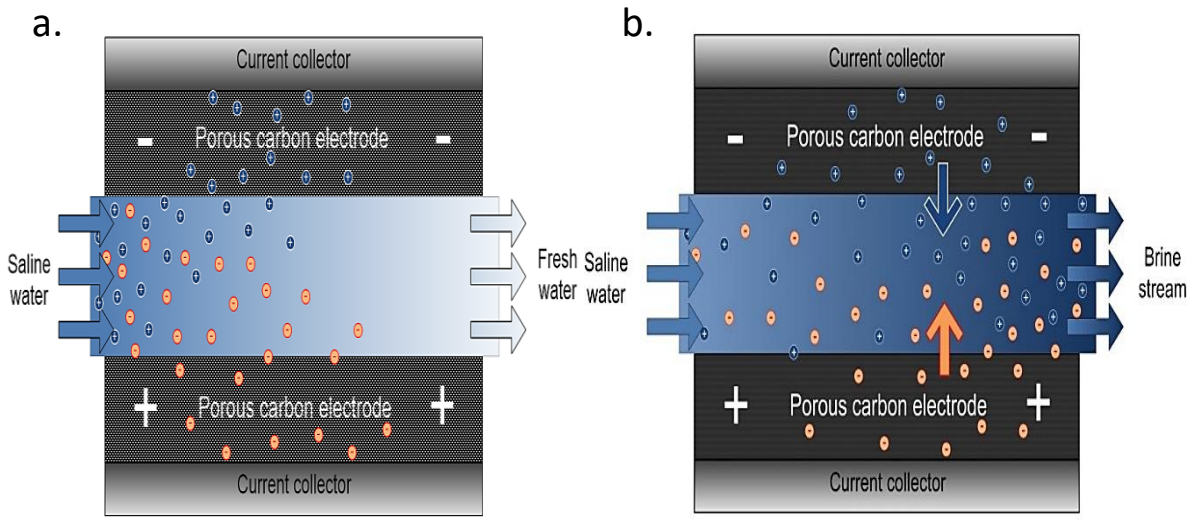

Fig 1.5. Schematic representation of CDI during (**a**) adsorption and (**b**) desorption process at zero volt.

1.3.1 Why Capacitive Deionization?

Undoubtedly, RO, MSFD and ED are well established water technologies used for many decades in water desalination. As described above, CDI has the potential to deliver significant operational, infrastructure, and energetic advantages relative to RO. It is a simple technology that is easy to set up, simple cell geometries, cheap operational cost and in terms of energy; it consumes less for brackish water desalination compared to RO. CDI targets solutes (salt ions) from solvent thus requiring little energy of operation. In addition, it makes use of porous materials as electrodes that can be engineered or tailored to carry out specific tasks i.e., water remediation task or research. Figure 1.6 shows the growing interest in CDI related research published articles while table 1.1 shows the historical background of this technology as reported by Wang *et al.* [3].

Elimelech *et al.* [7] did comprehensive studies of the energetics of CDI and RO for brackish water. They found out that for RO system, as feed concentration decreases from 600 mM to 10 mM (approximately potable water), the energy requirements for RO asymptotes to 1 $kWhm^{-3}$. Thus, at 10 mM, the RO reversible energy requirement is only a small fraction of the total RO energy requirement, as the irreversible losses from pumping water through the RO membrane dominate. By contrast, CDI energy requirements decreases linearly with feed concentration, and so CDI becomes more energy efficient than RO below feeds concentrations of 41, 56, 86, and 207 mM. CDI is then an attractive desalination technique for

brackish water desalination especially in the United States where brackish water constitutes over 80 % of the yearly-desalinated water volume [3].

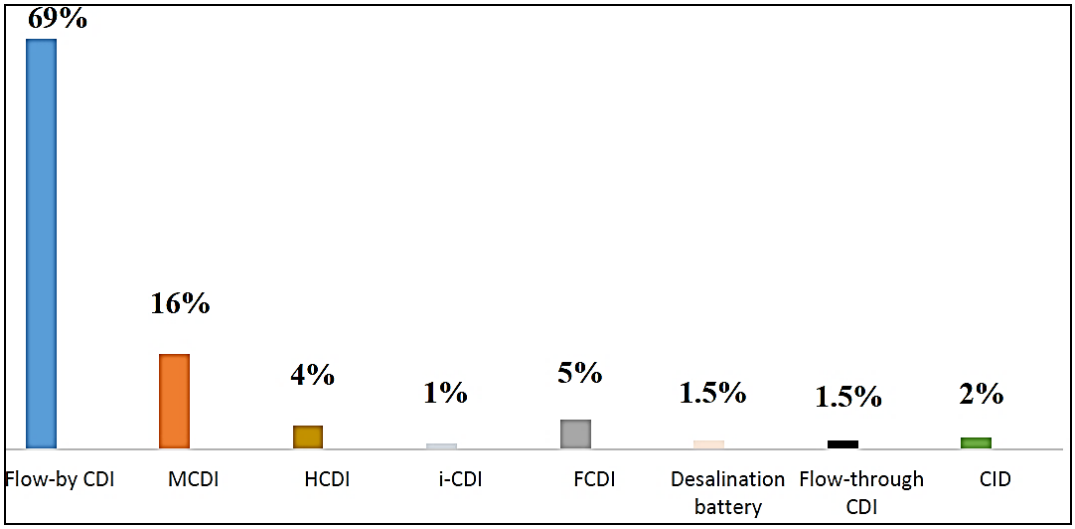

Fig 1.6. Percentage of research papers published per technology (electrochemical water desalination) [3]

Table 1.1: Progress in innovation in electrochemical water desalination [3]

Electrochemical Technology	Innovators	Year
Flow-by CDI	Bair and Murphy	1960
Flow through CDI	Johnson	1970
MCDI	Lee	2006
Battery desalination	Pasta	2012
Flow electrode CDI	Jeon	2013
Hybrid CDI	Lee	2014
Inverted CDI	Gao	2015
Cation intercalated desalination	Smith and Dimello	2016

In summary, membrane based desalination technologies such as RO are commonly used as water desalination techniques to obtain potable water for human consumption. Though RO is widely used yet it is not without some challenges. For instance, large pressure is needed to desalt seawater and this have a large footprint and high capital costs. Furthermore, biofouling is one the primary major challenges of reverse osmosis plants. Fouling greatly decreases

membrane permeability over time thus chemical pretreatments are used to mitigate membrane fouling in order to remove some organic material. However, this challenge still persists as a dominant issue. Due to these limitations, there was a need to develop a simple and environmentally friendly technology that could overcome some of the challenges of RO and can operate in smaller, portable units with lower pressures. This led to the invention of electrochemical water desalination (Capacitive deionization, CDI). CDI, in contrast to these known technologies leverage electric fields to desalinate water by extracting solutes from solvent. However, CDI cannot still effectively compete with established membrane based desalination techniques but it augments the drawbacks of known technologies by effectively desalting brackish water at a minimal energy level.

1.4 Research objectives

This thesis focuses on the development of novel carbon based electrode materials for the improvement of electrochemical water desalination through capacitive deionization techniques by using commercially available activated carbon. In this thesis, activated carbon is chosen as a candidate of interest above other advanced carbon materials such as carbon aerogel, mesoporous carbon, nanoporous carbons etc., because of its readily and renewable available source (biomass), low cost and ease of production of huge quantity of the material. These advantages make the author believe in the realistic improvement of this material for industrial application as the cost of developing advanced carbon materials could be expensive and the process might be time consuming. However, commercial activated carbon is not without some challenges such as low hydrophilicity, low electrical conductivity, high resistance, low porosity etc. In the light of this, this thesis focuses on improving some of the challenges of commercial activated carbon by developing strategies necessary for its improvement by employing simple doping method.

Herein, the specific research objectives are outlined below:

The specific objectives of this study are as follows:

- To modify successfully AC by doping strategies. This enabled the author to improve the drawbacks of pristine AC by forming composite electrodes. The upgraded properties of fabricated electrodes were proved by physical as well as electrochemical characterizations.

- To achieve higher desalination efficiency by fabricating a laboratory scale flow capacitive deionization cell in order to overcome the drawbacks of a conventional CDI technique.
- To understand and tackle new challenges towards parameters such as carbon loading, viscosity, ion transport and characterize new materials that will be used as flow electrodes in the fabricated flow capacitive deionization cell (FCDI).

1.5 Scope of the dissertation

To attain the above objectives, the following topics were investigated:

In Chapter 2, recent development in material aspect of CDI was described and several models of capacitive deionization systems were analyzed. Material aspect of this technology is instrumental for improvement in desalination efficiency in CDI and so far, most research interest is geared towards different strategies of obtaining carbon materials of hierarchical structure and performance; of which the means of achieving these strategies are limited to laboratory scale and as a result, these limitations (as documented in chapter 2) has made the author to improvise and define precisely the objective of this thesis.

Chapter 3, presents all the materials and method that will be essential for realization of the previously defined objectives. To justify experimental observations and achieve the aim of chapter 4, physico-chemical characterizations such as Scanning electron microscope (SEM) was used to confirm the morphology of the commercial activated carbon and its modified forms. Low temperature nitrogen adsorption-desorption isotherm was used to reveal the textural properties and pore size distribution of the materials. This enabled the author to understand the type of physi-sorption and the region responsible for adsorption within the carbon structure. The influence of surface chemistry on adsorption by carbon materials were also justified by Fourier transform infra-red, FTIR (to ascertain the functional finger prints of the samples) and X-ray photoelectron spectroscopy, XPS (to verify the chemical moieties of the materials). Structural properties were studied by Raman spectroscopy and X-ray diffraction (XRD) was used to study the crystallinity of the materials. UV–VIS spectrophotometry measurement was conducted in order to ascertain the shift in the wavelength of absorption. Also, TGA was done to understand the stability of our carbon materials. Furthermore; electrochemical characterizations such as galvanostatic charge-discharge (GCD), cyclic voltammetry (CV), and electrochemical impedance spectroscopy

(EIS) was used to ascertain the reversibility, adsorption mechanism, capacitive nature and impedance (charge transfer resistance or interfacial resistance) of our materials.

Chapter 4, presents the physico-chemical and electrochemical characterizations of solid based electrodes in CDI. From the results of these characterizations, certain properties were improved and correlated with electrode electro-sorption effectiveness in chapter 5. Furthermore, a prototype fabrication and experimental characterization of a variant of CDI in terms of flow capacitive deionization (FCDI) was verified. FCDI was developed for carbon slurry utilization. It makes use of flow carbon instead of conventional solid electrode. Through this architecture, the author was able to demonstrate significant improvements in desalination time and salt removal efficiency. Also, the effect of surface chemistry, textural properties, clogging phenomenon, electrode charging rate and resistance in slurry electrodes was described

Chapter 5, presents the effect of modified electrodes on desalination application using both CDI and FCDI techniques on different salt concentrations. This help in providing spatially and temporally resolved measurements of salt concentration in a CDI/FCDI cell. The experimental results obtained were compared to results reported in literature in order to show the efficacy of our methods

Finally, **in Chapter 6**, Summary, important contributions of this thesis and recommendation for potential future research were discussed.

Chapter 2. Theory and literature Review

The write-up in this section has been published in *Membranes* **2020**, 10 (5), 96 as below:

Review on Capacitive Deoinization, Membrane Capacitive Deoinization and Flow Capacitive Deionization

Gbenro Folaranmi, Mikhael Bechelany, Philippe Sistat, Marc Cretin and Francois Zaviska

Institut Européen des Membranes, IEM, UMR-5635, University of Montpellier, ENSCM, CNRS, Place Eugène Bataillon, CEDEX 5, 34095 Montpellier, France; gbenro.folaranmi@etu.umontpellier.fr (G.F.); philippe.sistat@umontpellier.fr (P.S.); marc.cretin@umontpellier.fr (M.C.)

Abstract:

Electrochemical water desalination has been a major research area since the 1960s with the development of capacitive deionization technique. For the latter, its modus operandi lie in temporary salt ion adsorption when a simple potential difference (1.0–1.4 V) of about 1.2 V is supplied to the system to temporarily create an electric field that drives the ions to their different polarized poles and subsequently desorb these solvated ions when potential is switched off. Capacitive deionization targets/extracts the solutes instead of the solvent and thus consumes less energy and is highly effective for brackish water. This paper reviews Capacitive deionization (CDI), Membrane capacitive deionization (MCDI) and Flow capacitive deionization (FCDI) mechanism of operation, improvements and shortcomings.

Keywords: brackish water desalination; electro-sorption; carbonaceous electrode materials; process consideration; capacitive deionization configurations.

2.0 Introduction

Porous carbon electrodes are extensively used as capacitors in many applications, including energy storage (electric double layer, supercapacitors), energy generation, and water desalination [23, 24]. In desalination applications, charging the electrode pair removes significant amounts of salt ions from a liquid electrolyte (such as brackish water), and energy can be recovered when the ions are released into a brine stream [24, 25].

In porous electrode capacitor systems, the electrode pore structure consists largely of nanoscale pores in order to maximize ion storage capacity [26, 27]. However, such a pore

structure can limit charge and discharge kinetics by impeding ion transport [25-28]. High impedance to ion transport within the pore structure slows the temporal response, and so reduces device power density or increases time required for desalination. To prevent such transport limitations, several studies have proposed and analyzed electrode materials with a hierarchical pore structure [29, 30]. These electrodes typically contain larger diameter pore network for low-resistance ion transport (typically meso-scale pores). These larger pores connect to smaller diameter pores that provide high specific surface areas used for ion storage (typically micro- or meso-scale pores).

2.1 Electrode materials for CDI

One of the key factors influencing the overall efficiency of CDI technology is the electrode material aspect. Undoubtedly, electrode is considered suitable for CDI if conditions such as: high surface area, high porosity, good electrical conductivity, good stability, high capacitance, high hydrophilicity, and must be economically feasible for industrial upscale in terms of availability and cost. In light of this, carbon-based materials fit into all the properties but none of them single handedly possess all the criteria/properties needed as high performance CDI electrodes hence various methods are employed to influence the properties of carbon-based materials. Some of the improvements in the material aspect as found in literature are discussed below.

2.1.1 Carbon Electrodes with Various Morphologies and Porosities

Various forms of carbon have been exploited, some of which are: activated carbon (AC), activated carbon fiber (ACF), carbon aerogel (CA), activated carbon cloth (ACC), carbon nanotubes (CNT), graphene (Gr), carbon nanofibers (CNF) etc., [31-34]. In most cases, carbon-based materials are converted to electrodes by making them into dispersion solution and thereafter get deposited or immobilized on a support (current collector) via many methods such as spray coating [35], pressure pressing [36], blade coating and or electrophoretic deposition [37]. Some major limiting factors for instance in AC are in terms of wettability, low porosity, and electrical conductivity. In graphene for instance, its intrinsic property of restacking possesses a major drawback for its independent usage as electrodes. However, in order to improve their efficiencies and other shortcomings, they are often treated both physically and chemically for an efficient ion adsorption capacity. Physical treatments such as thermal application modifications under inert gases (N_2, Ar, CO_2, etc.) for pores expansion has been employed. Depending on the operating conditions during the thermal process, pore

volume and microporous or mesoporous regions of activated carbon are usually influenced under this method [38]. Under chemical treatment, a lot of modifications exist depending on the property to be improved. For instance, surface area can be improved by treating with KOH or NaOH after which it is subject to further thermal treatment [39, 40]. With respect to wettability, the introduction of oxygenated functional groups (OFGs) into the surface of activated carbon (increase of surface hydrophilicity) is done as reported in literature through oxidation by acid (i.e., nitric acid) [41] or oxidizing agents like potassium permanganate ($KMnO_4$) [42].

2.1.1.1 Hybrid Carbon-Based Electrodes

Hybrid composites of activated carbon with materials of higher performance have been reported in literature [43-46]. Transition metal oxides (TMOs) for instance have been used by many researchers to enhance carbon-based electrode stability, conductivity, and electrochemical performance. Advanced chemical methods like chemical vapor deposition (CVD), ice segregation isolated self-assembly (ISISA), and electrospinning are also being exploited to make 3D carbon of high porosity and conductivity [47].

2.1.1.2. Alternative Carbon Source-Based Electrodes

It is of interest to know that the intrinsic properties of carbon materials are based on their methods of preparation and precursors used. Recently, carbon derived carbide (CDC) [48] and metal organic framework (MOF) [49] as sacrificial precursors as well as carbon monoliths [50] have drawn the attention of researchers in CDI. They possess suitable characteristics needed for carbons to be used as electrodes in CDI i.e., high surface area, porosity, and wettability. The performance of resorcinol-based mesoporous carbon (MC) in comparison to that of carbon aerogel (CA) was studied by Tsouris *et al.* [51] using feed salinity concentration of 1000 mg L^{-1} and 35,000 mg L^{-1}, their findings showed that resorcinol-based MC (adsorption capacity of 15.2 mg g^{-1}) has higher adsorption capacity over CA (adsorption capacity of 5.8 mg g^{-1}). It was suggested that the polymer precursor and the method of synthesis employed conferred higher porosity on MC hence improving adsorption.

Alternative carbon source of high performance based on sacrificial materials i.e., carbon derived carbide (CDC) has attracted attention. CDC reported by Arulepp *et al.* [52] showed excellent volumetric capacitance of 90 F cm^{-2} for non-aqueous EDL capacitors over commercial AC. AC derived from Fe-MOF in combination with graphene oxide when

investigated by Wenhua *et al*. [53] generated a highly porous and electrical conducting carbon network enabling higher electrosorption (37.7 mg g^{-1} at feed salinity of 1000 mg L^{-1} NaCl). Precursory sacrificial MOFs for AC synthesis usually yields AC of high porosity and specific surface area though this depends on the crystallinity and porosity of the MOF used [54].

2.1.1.3 Carbon Electrodes Modified by Nitrogen Doping

The introduction of nitrogen into carbon i.e., nitrogen doped graphene (NG) has been reported in literature mainly due to the improvement of electrical conductivity as well as increase in specific surface area [55-57]. As further reported, NG tremendously recorded an improved specific capacitance in the range from 140 to 326 F g^{-1}, much higher than that of pristine graphene (PG) (135 F g^{-1}) [57]. Yang *et al.* [58] improved the cyclability rate of potassium ion battery by intercalation of nitrogen into carbon nanofibers.

Deriving the best compromise for fabricating suitable composite or hybrid electrodes is one of the challenges in CDI and as such, many hybrid electrodes are fabricated to target a particular obstacles or more in some cases. Table 2 below shows a good understanding of the problem for the best choice of material electrodes

Table 2. Some recent advances in electrode modifications for capacitive desalination.

Electrode Material	**Purpose**	**Compromise**	**Water Salinity (ppm NaCl)**	**Capacity (mg/g)**	**Operation Voltage (V)**	**Ref.**
NG-CNFs	Electrical conductivity improvement	Between electrical conductivity and porosity	1000	14.79	1.2	[59]
Graphene gel	Electrical conductivity improvement	Porosity challenges	500	49.34	2.0	[60]

3D Graphene modified with SWCNT	Electrical conductivity and porosity improvement	Wettability challenges	300	48.73	2.0	[61]
GO/resorcinol formaldehyde microsphere (GORFM)	Wettability and porosity improvement	Electrical conductivity challenges	800	35.52	1.8	[62]
rGO/TiO_2	Wettability and electrical conductivity improvement	Challenge of passivation and porosity	300	9.1	0.8	[63]
ZrO_2/GO	Wettability and stability improvement	Porosity and electrical conductivity challenges	50	4.55	0.8–1.2	[64]
PANI/AC	Capacitance and stability improvement	Porosity challenges	250	3.15	1.2	[65]
Flexible Graphene			300	18.43	1.4	[66]
3D Graphene grafted with amine-sulfonic functional group	Wettability, porosity and electrical conductivity improvement	Agglomeration challenges	500	13.72	1.4	[67]

	Wettability and electrical conductivity improvement	Porosity challenges				
GO-CNT/AC			800	21.3	0.3–1.5	[68]

2.2 Operation modes

2.2.1 Batch mode vs single-pass mode

The desalination performance of CDI/MCDI is evaluated via monitoring the ion concentration change over time. Figure 2 (a) and (b) shows the different modes of operation. In the continuous mode (a), water is pumped from a feed vessel and the ion concentration of the effluent is measured. Here, there is a drop in effluent salinity after applying the cell voltage and then increases steadily as the electrodes reach their adsorption capacity. The total amount of salt removed is then calculated by integrating the hatched area as shown in Figure 2 (a). In the batch mode, Figure 2 (b), there is effluent recycling and the ion concentration of the recycle reservoir is monitored. The difference between the initial and final concentrations determines the salt removal.

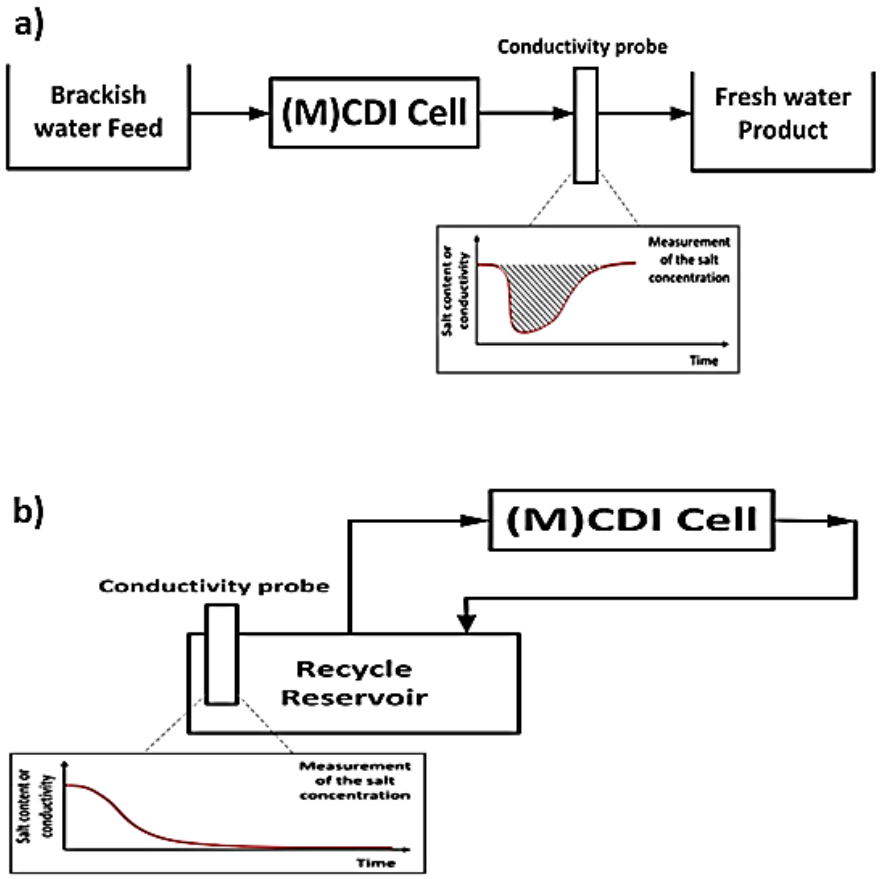

Fig 2. Schematic diagram of CDI/MCDI operational modes (a) Continuous mode, and (b) Batch mode [69].

2.2.1.1 CDI adsorption/desorption modes

As it is established that adsorption occurs when a constant voltage is applied to the CDI or MCDI cell. This approach is known as constant voltage (CV). An example is shown in Figure 2.1 (a) [66]. In the case of CV in continuous mode, by applying a certain voltage the ionic species are removed from the bulk stream, therefore, the effluent salt concentration falls. This adsorption also results in a high electrical current passing through the system. [5].
During the desorption period, by dropping the cell voltage to zero, the electrodes desorb the adsorbed ions. The rapid depletion of the adsorbed ions results in a sharp peak in effluent salt concentration and electrical current.

It is noteworthy that constant current (CC) approach has recently gained attention due to the fact that the effluent concentration can be adjusted to the desired level by controlling the flow

rate and the applied current Figure 2.1 (b). In CC mode, the electrodes are connected to a DC power supply set at a constant current. As a result of adsorption, the voltage increases and when the set maximum voltage is reached i.e. 1.4 V, desorption takes place. The regeneration step can be accomplished at zero voltage.

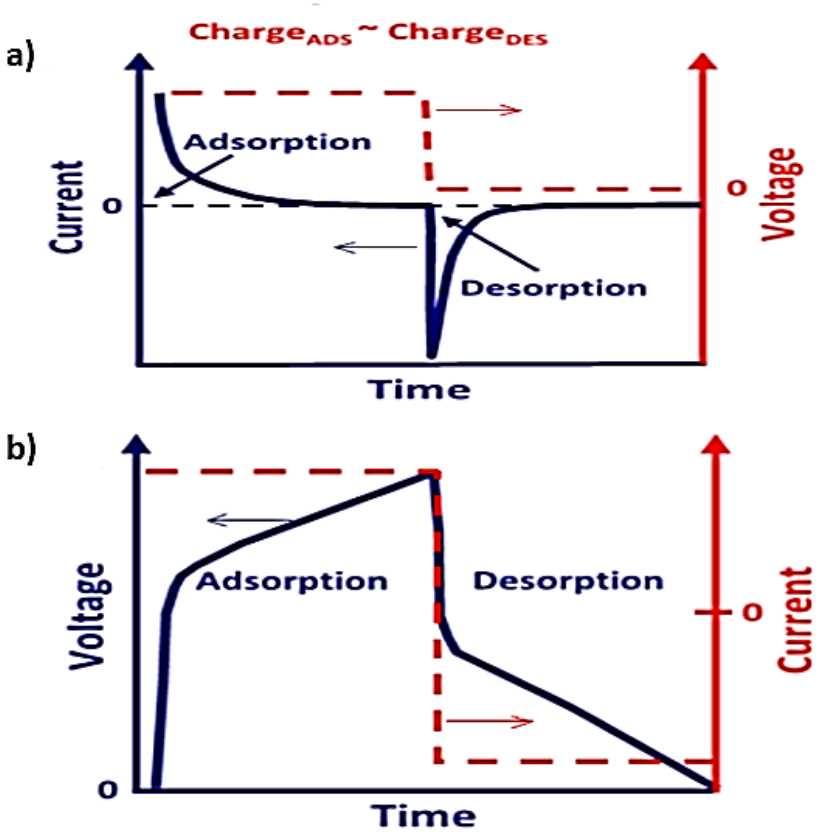

Fig 2.1. Cycle analysis of (a) Constant Voltage and (b) Constant current [69]

2.3 Properties affecting electrosorption in CDI

The three main operating parameters affecting CDI processes are the voltage (or the difference of electrical potential), the hydraulic retention time (HRT), and the hydrodynamics conditions.

2.3.1 Difference of Electrical Potential

In CDI process, the difference of electrical potential represents the driving force that moves ions from the bulk to the surface of the electrode (EDL). Hence, the higher the voltage, the faster the adsorption is. However, high voltage can cause faradaic reactions such as water

hydrolysis which are undesirable for desalination application and will decrease charge efficiency (CE). For instance, utilization of voltage above 1.4 V can lead to water splitting and the formation of undesirable by-products which can change the solution pH and leads to electrode oxidation. Basically, salt removal is achieved with increasing potential in the range of 0.8–1.4 V [38].

2.3.1.1 Hydraulic Retention Time (HRT)

Hydraulic retention time (HRT) is the residence time of feed solution (time spent by the influent inside the cell) which is for a given desalination objective (salt removal and fresh water production) and this is purely related to design aspect (cell sizing). HRT can be calculated by the volume of the cell (exclusively for water circulation) divided by the flow rate. The higher the HRT, the higher the salt removal will be (in conditions that the electrodes are not saturated).

2.3.1.2 Hydrodynamics

The flow configuration selected for a CDI system and the hydrodynamic condition associated are important parameters affecting the desalination performances due to their impact on ions transport from the bulk to the electrode surface. Mass transfer of ions from the feed solution onto the surface of the electrode is governed by electro-migration, diffusion, and advection phenomena. Considering the liquid/electrode interface with one dimensional analysis, three regions can be identified: the bulk or the middle channel, the porous electrode, and the stagnant diffusion layer (SDL) [70]. The thickness of the SDL also called Nernst layer is dependent on the convective mixing and turbulence of the bulk stream which affect the ions transport to/from the electrode surface during the adsorption and desorption phases.

2.4 Cell geometries, electrode configurations and structural state in CDI

Cell geometry/configuration is one of the many process factors that cannot be undermined in CDI aspect. In light of this, different geometries have been improvised and the two most conventional types of these geometries are highlighted below:

2.4.1 Flow-by CDI

In the conventional flow-by system, a small planar gap is left in between the electrodes (separated by a separator layer) through which water can flow along the electrodes placed parallel to one another. It affords high energy recovery and low energy consumption. The

limitation of this design is that it can only desalinate moderate brackish water and it requires long time of operation. In flow-by system, separator must be carefully optimized to minimize cell electrical resistance and volume while allowing sufficiently large area for efficient fluid flow.

2.4.2 Flow-through CDI

In contrast to flow-by CDI, instead of the feed water flowing in-between the parallel electrodes, it is possible to direct it straight through the porous electrodes and parallel to the applied electric field direction, this cell is named flow-through CDI. In this design the feed water is pumped perpendicular to the layered structure that is; straight through the larger pores in the electrodes. This system design offers increase in the kinetics of adsorption by promoting turbulence inside the pores canals and forcing ions to enter in contact with the charged electrode. Major pros and cons of the two geometries are presented in table 2.1

As reflected in Table 2.1 properties and performance of both flow-through and flow-by CDI geometries are related in part to the development of materials to achieve at the same time high capacity and kinetics for efficient desalination.

Table 2.1 Mains advantages and drawbacks of flow-by and flow-through CDI cells for desalination.

CDI Geometry	**Advantages**	**Drawbacks**
Flow-by	-Easy to design with low cost plate dense electrodes -High energy recovery -Low energy consumption	- Moderate water flow rate due to low electrodes interspace -Long times required for desalination due to quite low kinetics
Flow-through	-High ASAR due to high kinetics promoted by turbulence inside the pores of electrodes -High mSAC of the porous electrodes -High water flow rate due to low fluidic resistance of aerogel electrodes	-Higher CAPEX due to the cost of porous electrodes

ASAR: Average salt adsorption rate; mSAC: Maximum salt adsorption capacity; CAPEX: Capital cost

2.4.3 Electrode configuration in CDI

Electrode configuration in CDI can be divided into 2, namely; symmetric electrode and asymmetric electrode.

Symmetric electrode configuration

This simply refers to the process in which the same electrode material is used in both anode and cathode. Here, the composition of the electrode material in terms of structure, functionalities, textural properties etc., are the same. For comparison in electrode improvement after some modifications, both electrodes (pristine and modified forms) are used in CDI application. However, this configuration has tendency to lose electrochemical stability over a long period of time and also there is a challenge of co-ion adsorption leading to reduced charge efficiency.

Asymmetric electrode configuration

With this system of configuration, the electrode materials are of different composition in the anode and cathode. The difference could be in the surface chemistry, mass, functionalities etc., The significance of this configuration becomes positively effective over the former because it allows non-identical potential changes at both electrodes (cathode and anode) thus resulting in high ion removal capacity and charge efficiency. With this form of configuration, ion selectivity (another application of CDI) is improved.

2.4.3.1 Electrode Structural state

Morphology importance of electrode material in CDI has been considered as an important feature affecting the performance of ion transport within carbon structure. Here morphology refers to the shape or structure of the material. Due to this factor, there has been rational design of electrode materials of different shapes i.e., tubular like carbon (Carbon nanotubes), monolithic carbon (carbon aerogel), carbon fibers (fibrous morphology makes them to be very porous and due to their network interconnectivity, ions migration within the structure is enhanced) etc. For instance, carbon nanotubes offer tubular form of carbon (tubular carbon) composing mainly of a rolled graphene like sheets. Depending on the arrangement of the

carbon hexagonal rings, they could either be multi-walled or single walled nanotubes. Their structures afford high porosity and good electrical conductivity thus influencing positively the performance of CDI when used as electrodes. Carbon monoliths i.e., carbon aerogel have attracted significant attention as a potential candidate in CDI due to their structured microspheres morphology. They possess high specific surface area, good porosity and excellent electrical properties. The controlled morphology of this carbon material depends on the condition of precursory materials and conditions of operation. It has been recently shown that due to the nature of aerogel morphology, they exhibit higher tendency for ion adsorption for monovalent ions of smaller radii over multi-valent ions because of their pore size and shape.

2.5 Alternative to CDI

2.5.1 Membrane Capacitive Deionization (MCDI)

The inherent challenge of CDI (i.e. ion co-adsorption yielding low desalting efficiency) led to MCDI development. Here, co-ion adsorption refers to ions carrying the same charge as the electrode. In CDI, co-ions moved towards the corresponding electrodes, i.e. cations towards the positive electrode and anions towards the negative electrode, which then need to be repulsed. The consequent effect of this is low charge efficiency leading to low desalination and high energy consumption. Conventionally, capacitive deionization techniques (CDI, MCDI and flow capacitive deionization FCDI) operate via similar principle. The major difference comes in the cell configuration/set up. In the case of MCDI, introduction of ion exchange membranes (IEMs) intersect the migration of co-ions towards wrong electrodes i.e., cation-exchange membrane (CEM) and an anion-exchange membrane (AEM) are placed in front of the cathode and anode respectively as shown in Figure 2.2. IEM provides screening shield to the exclusion of undesired ions towards the electrodes thereby limiting co-ion adsorption to a great extent.

MCDI significantly increases the efficiency of CDI by improving parameters such as charge efficiency, ion adsorption etc.

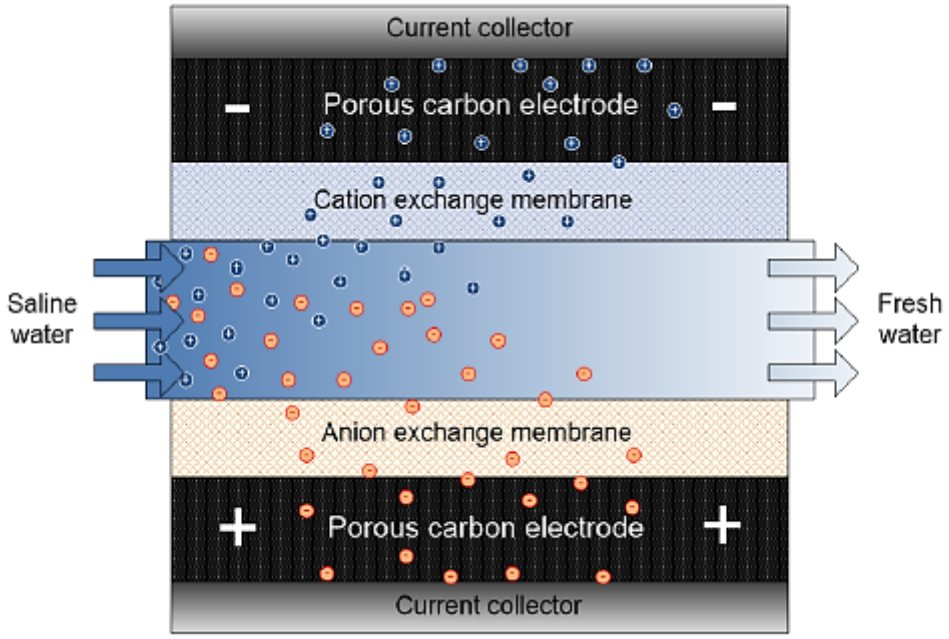

Fig 2.2. Schematic representation of membrane capacitive deionization (MCDI) system.

2.5.2 Flow Capacitive Deionization (FCDI)

The major challenge of CDI lies in its ion co-adsorption. This leads to low charge efficiency and low ion adsorption. By incorporating ion exchange membranes, this challenge was overcome and Membrane Capacitive deionization (MCDI) was developed. Nonetheless, solid electrodes employed in CDI/MCDI allow discontinuous electrosorption process (alternative process of adsorption/desorption phases). Additionally, the static mode of operation (as electrodes are deposited and fixed on a current collector) limits the utilization of availability of pores as electrodes need to be regenerated when saturation level is reached. Additionally, porosity of solid electrode material is compromised as the inclusion of a binder (usually PVDF polymer) drastically reduces available carbon pores and also affects the electrode electrochemical behavior. However, in order to bridge the gap of solid electrode usage and discontinuous mode of operation which apparently cannot be overcome by CDI process hence exploitation in the area of slurry electrodes has been of interest and that led to a new cell design with the name flow capacitive deionization (FCDI).

As invented in 2013, FCDI is based on the slight modification of MCDI by using carbon suspension as flow electrodes [71]. FCDI enables the major benefit relative to conventional

CDI in that it affords continuous mode of operation and desalination of high-salinity feed, as shown in Figure 2.3.

In principle, it entails the flowing of suspended carbon electrode (slurry) in a flow path carved on a current collector that is separated between two ion-exchange membranes (CEM and AEM) with salt water running through a spacer. Basically, the guiding principle of operation is the same as that of CDI.

The higher the carbon loading (slurry), the higher the adsorption rate as the network of interaction is increased within the active material thus promoting better electron transport within the carbon network. In FCDI, electrical field is created by the passage of voltage from an external source which drives the ions in the feed saline solution to migrate through the ion-exchange membrane, and is eventually adsorbed onto the pores of the suspended carbon slurry electrode. This method proffers a semi-continuous adsorption phase within the cell while desorption takes place outside of the cell (regeneration of the slurry electrode without short-circuiting the cell) [72].

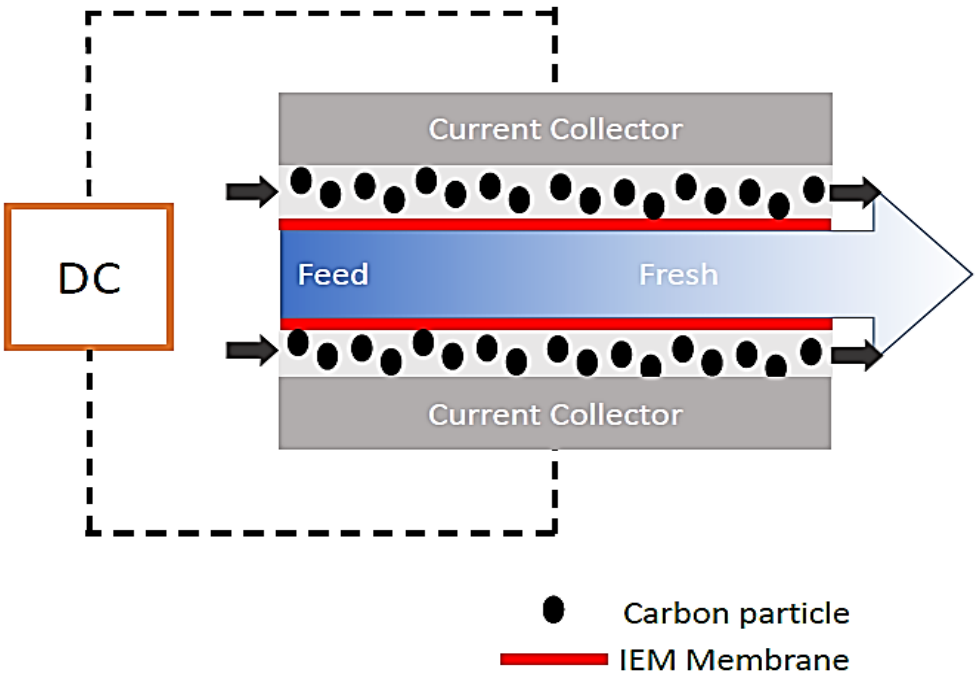

Fig 2.3. Schematic representation flow capacitive deionization (FCDI) system

In terms of comparison, a preferable amount of charge efficiency is improved in solid electrode as there is a high transfer of current by the current collector to the immobilized electrode unlike the slurry form. Indeed, the charge is slowly transferred to the flowing carbon slurry due to the limiting major component of the slurry (H_2O); although at high carbon loading, the carbon slurry electronic percolation or network can be increased to augment this shortcoming but at the expense of viscosity. The consequential effect of increase in the electrode slurry (at high carbon loading) can lead to increase in pressure loss and could lead to clogging of the carbon slurry and also dissipating pumping energy (mechanical) into thermal energy. Exploitation of carbon particles of low size (2–10 μm) and spherical carbons as application in slurry electrodes has also been reported to enable carbon loading and viscosity reduction [73-75]. The highest percentage of the slurry composition is water which is a poor electrolyte; hence to achieve a network of good electrical conductivity within the active material (carbon slurry), a compact interaction of electron percolation in flow electrode is desired. As found so far in literature, electrical improvement has been achieved with addition of NaCl [73], carbon black (CB) [74], carbon nanotubes (CNT) and functionalized carbon nanotubes additives (FCNT) [75].

Low resistance in flow electrode is a contributory factor in achieving better results in FCDI. Yang *et al.* [73] studied feed electrode containing high salt concentration and it was revealed that the high resistance created by water (major feed electrode component) was reduced by the addition of 2.44 wt. % of NaCl to the feed electrode hereby enhancing desalination. Effect of CB dosage on internal resistance and high voltage on charge efficiency was also studied by Peng et al. [74]. It was observed that at higher voltage (4.8 V), desalination rate 0.208 mg/(min·cm^2) was achieved while charge efficiency dropped from 92 % to 69.5 % due to Faradaic occurrence. Additionally, electrochemical impedance spectroscopy (EIS) revealed that the internal resistance of the FCDI decreased with increased CB dosage.

FCDI stacks has also been studied by Cheol *et al*. [76] revealing that FCDI with five unit cells shows a higher desalination rate compared to single FCDI unit cell. Using two FCDI modules, Gendel *et al.* [77] developed a continuous mode of electrosorption process in which 99 % desalination rate was achieved and 90 % water recovery was reported. A new FCDI without the use of IEMs has been demonstrated by Hatzell *et al.* [78] to desalt brackish and seawater.

Most FCDI systems are still in batch mode of operation. Report in the continuous mode is sparse in literature. FCDI continuous module employing two CDI set up offers recyclability of feed electrode. Figure 2.4 (a) and (b) shows a typical module of FCDI in a continuous

mode as developed by our group. Figure 2.4(a) offers the possibility of continuous operation in which FCDI cell is coupled with ultrafiltration technique. The feed electrode ions are recycled by ultrafiltration technique while in Figure 2.4 (b), two FCDI cells are present in which one serve as a desalination reactor while the other serves as concentrate generator. The possibility of continuous module could offer an upscale in desalination rate with the possibility of energy recovery as present in semi-continuous mode.

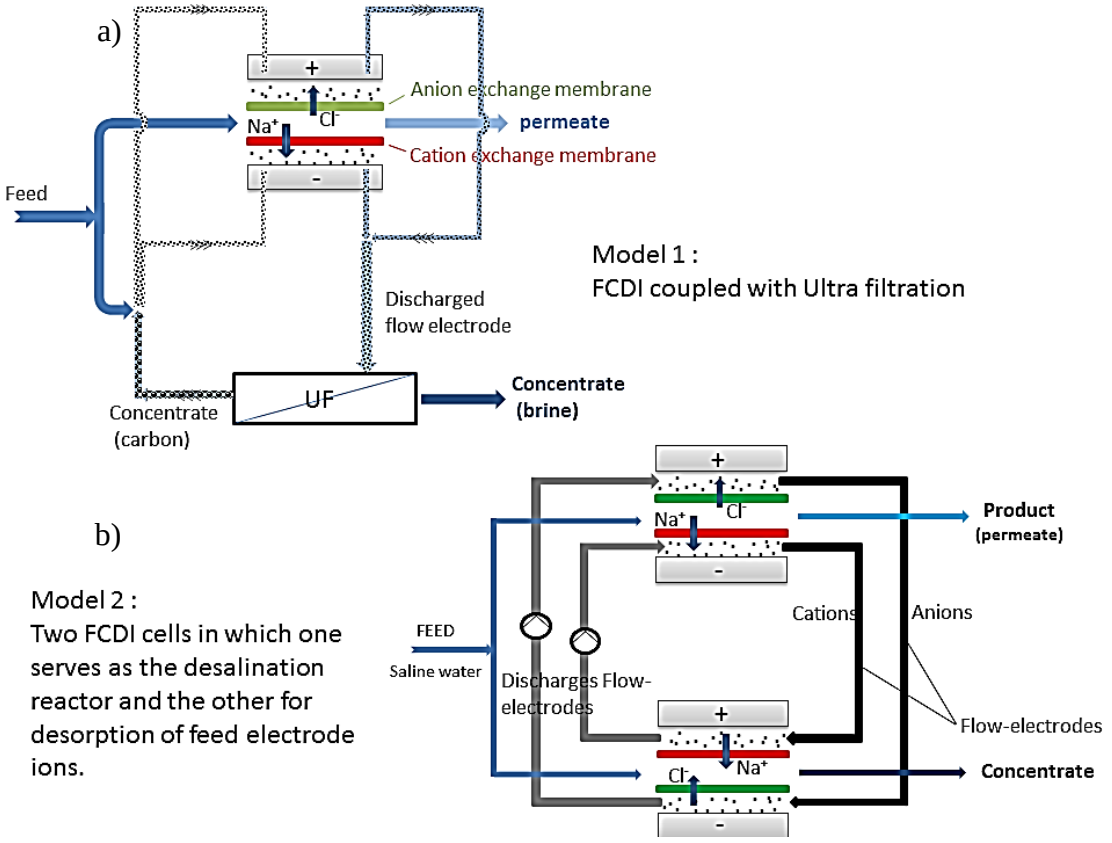

Fig 2.4. Schematic diagrams of FCDI in continuous mode via (**a**) FCDI coupled with ultrafiltration and (**b**) two FCDI cells.

2.6 Energy Recovery in CDI/FCDI

This is a fast developing and interesting aspect of CDI in which some of the energy used during deionization process can be recovered. Here, there is possibility of reusing the energy stored in capacitive cells once the deionization phase has finished. The regenerative use of energy in CDI technology consists of using the energy stored in the CDI cell once it is saturated (the deionization process is finished and the cleaning or desorption process begins) and transferring it to other cells that begin their deionization phase thus defining a cycle to produce clean water. In order to achieve this energy recovery process, electrical model and mathematical characterization of up/down DC/DC converter is used. This converter deals

with the voltage which is applied in each of the de-ionization modules. The main aim of the converter is to minimize the losses during the transference of energy between the stages. Undoubtedly, pumping of slurry in FCDI gives room for possibility of additional energy requirement [79]. Energy recovery up to 83 % in CDI [80] and 20 % in FCDI [81] have been reported in literature. However, Rommerkershin *et al.* [82] using continuous FCDI system was able to recover up to 36 % of applied energy. Junjun *et al.* [83] was able to recover maximum energy ratio of 7.6%. Additionally, Jeon *et al.* [81] incorporated salt to the flow electrode easing ionic resistance and confirmed electrical energy recovery of about 20 %. Studies by Lim *et al.* [84] confirmed that improving energy capacity in FCDI can be achieved by increasing the capacity of electrode slurry container and that the feed solution at high salt concentration (salt water) is advantageous in terms of higher capacity for both energy storage and generation compared with feed solution of low concentration (brackish water).

As found in literature, Table 2.2 summarizes the varied parametric conditions in terms of slurry composition, feed solution composition, and operating conditions in FCDI process.

Table 2.2. Summary of some recent advances in operating parameters for flow capacitive deionization systems as found in literature.

Slurry Electrodes				**Feed Solution**			
AC (Wt %)	**[NaCl] (mM)**	**Additive (Wt %)**	**Flow Rate (mLmin^{-1})**	**[NaCl]in Effluent (mM)**	**Flow Rate (mLmin^{-1})**	**Voltage (V)**	**Ref.**
0–16	60	-	0–175	60	2–13	1.2	[73]
20	11.1	CB 0.5-1.5	4	-	11	0.6–4.8	[74]
5	2.5	FCNT 0.25	25	-	3	1.2	[75]
10	0.016	CNT 1.5	15	9.01	15	-	[76]
5–35	2.5	-	25	3.5	3	1.2	[77]
5	-	-	60	17.1–256.4	9	1.2	[78]
5	1.7	-	1	3.42–598.3	1	1.2	[79]

5–23	10	-	5	5	-	-	[81]
8.3	20	-	0.5–1.5	20	0.5–1.5	1–1.91	[82]
9.1	100			-	-	1.2	[83]
25	17.1	-	-	-	-	1.2	[84]
25	2.5	-	-	3.5	-	1.2	[85]

2.7 CDI and FCDI performance metrics

In order to develop a cost effective CDI process, it is essential to identify and understand the effect of the main parameters affecting the electrochemical separation process. By this means we can improve the design aspect as well as operating conditions in order to reach a given objective of efficiency, best compromise in term of capital cost (CAPEX) and operational cost (OPEX). Also, it is essential to define the performance criteria of a CDI system which is briefly discussed below.

2.7.1 Maximum Salt Adsorption Capacity (mSAC)

The concept of this parameter was firstly introduced in 1972 by Sofer and Folman [37]. It is related to the mass of ions adsorbed as a function of adsorbent weight. The value of mSAC is expressed in mg of salt adsorbed per g of electrode material and it is calculated using Equation (2):

$$mSAC = \int_0^{tads} (Ci - Cf)\Phi_v \, dt \quad (2)$$

Where ϕ_v is the flow rate of solution in the CDI circuit, C_i is the initial concentration of the solute, C_f is the final solute concentration, and t_{ads} is the duration of the adsorption step. The maximum SAC is typically reported as the ratio of maximum weight of salt removal to the total weight of adsorbent, expressed in mg g^{-1}

of electrodes where mg is the amount of salt adsorbed, g is the weight of the adsorbent. It is important to note that the mSAC depends mainly on the intrinsic electrode properties (pore size, surface area, capacitance, surface physico-chemical properties etc.) but also on design consideration (i.e., electrode thickness) and on the electrochemical conditions (voltage, hydrodynamic, feed salinity, etc.). The mSAC can be determined from the evolution of the conductivity, when its variation in function of time becomes negligible. However, as long as

the adsorption phase is running, kinetics of salt adsorption becomes lower until reaching the equilibrium. In other word, in a practical point of view, it is not pertinent to reach the mSAC which will require a hydraulic retention time (HRT) that is too high, making the CDI process not favorable in terms of CAPEX.

In summary, mSAC is related to the storage capacity and represents one of the most important parameters for evaluating the performance of an electrode. Considering that CDI is an intermittent process alternating adsorption and desorption phases, the mSAC will directly determine the frequency of changing phases and will impact both CAPEX and OPEX.
For practicality and a general view of mSAC as an indicator index, we could consider that the typical value of mSAC often used as a reference is the one obtained from the AC electrode and it ranges between 3–5 mg g^{-1}. Such mSAC value is a bit too low for industrial application. mSAC values above 15 mg/g seems appropriate for CDI application [47,48].

2.7.2 Average Salt Adsorption Rate (ASAR)

Average Salt Adsorption Rate (ASAR) is a parameter related to the kinetics of the adsorption process, in other words, how fast ions can be adsorbed onto the electrode per unit of time of the adsorption process. It is defined as:

$$\frac{Q}{NAtads}\int_0^{tads}(Ci - Cf)\,dt \qquad (3)$$

The ASAR is expressed in mg/g/min where “min” is the average time in minute for the adsorption or desorption step. Unlike mSAC, ASAR depends on multiple external factors such as flow rate, applied potential, initial feed water concentration, and the cell architecture. Depending on the objective of treatment, there is a compromise to find in order to minimize the alternation of the adsorption/desorption phases (mSAC) and the ASAR. The most important parameter affecting ASAR is the driving force (difference of potential) but other parameters such as the physico-chemical properties, electrode design, as well as the operating conditions (hydrodynamics, feed solution salinity, etc.) affect desalination kinetics. There is no general reference value to assign for ASAR as it is dependent on factors like feed salinity, product salinity, etc.

2.7.3 Current Efficiency (CE)

The term charge efficiency or current efficiency (CE) was used the first time by Avraham in

2009 [91]. The charging efficiency of the system also called faradaic efficiency, is the ratio between the electrical charge that serve specifically to adsorbed ions on the total electrical charge applied between electrodes. In other words, CE corresponds to the fraction of current that was really used for desalination. The other fraction corresponds to the ohmnic losses and the current associated to the possible faradaic reactions if the voltage exceeds the potential of water hydrolysis (~1.4 V). CE is defined as follow:

$$CE = \frac{I_{min}}{I} = \frac{\mathrm{z \times F \times (Ci - Cf) \times Vs}}{\mathrm{M \times \int I dt}} \quad (4)$$

Where I_{min} is the minimum theoretical current necessary to remove a given amount of ions (in Amperes), I is the actual applied current, z is the elementary charge on ions, F is the number of Faraday constant (96485 C), C_i is the initial molar concentration of the solute, C_f is the final solute concentration, Vs is the volume of the solution, M is the molar mass of the solute, while $\int I dt$ is the recorded integral current with respect to time. Current efficiency is an important parameter for evaluating the performance of the CDI system. The higher charge efficiency leads to lower energy consumption. The maximum possible efficiency is the one which would occur when one ion is removed for each unit of charge deposited on the electrodes. Current efficiencies higher than 80% are desirable in order to minimize energy costs. Low current efficiencies indicate water splitting in the diluent or concentrate streams, or back-diffusion of ions from the concentrate to the diluent.

2.7.4. Specific Energy Consumption (SEC)

Energy consumption is one of the biggest hurdles desalination faces. Nowadays, in a worldwide energy crisis context, it seems not pertinent to talk about desalination performances without taking energy consumption into consideration.

SEC is often used to characterize the energy cost of a desalination process. SEC is expressed in $kWhm^{-3}$ and corresponds to the energy needed to produce one cubic meter of permeate at a desired water recovery. SEC in electrochemical processes can be expressed as the overall electrical power spent relative to one cubic meter produced.

$$\mathrm{SEC} = \frac{W_{CDI}}{V_{perm.}} = \frac{\int \mathcal{P}_{(t)}.dt}{V_{perm.}} \quad (5)$$

Where W_{CDI} is the energy supplied, $\mathcal{P}$ is the applied power, t is the time of treatment, and $V_{perm.}$ is the volume of desalinated water. The CDI process works usually at constant

electrical potential (to avoid parasitic faradaic reaction), letting the current varying over time with the degree of demineralization. Equation (5) can then be written as follows:

$$SEC = \frac{U. \int I(t).dt}{V_{perm.}} \quad (6)$$

Where I(t) is the actual applied current (amperes) at a given time, U is the electrical potential, and t is the time of treatment. SEC is also related to CE, Eq. (7)

$$SEC = \frac{U. \int I_{min}(t).dt}{CE. V_{perm.}} \quad (7)$$

However, because CDI (as well as ED) are focusing/targeting solute instead of the solvent, it seems more pertinent to expressed energy consumption on kWh/kg of salt removed instead of kWh/m^3. Indeed, in comparison to the other desalination processes, electro separation processes can modulate the desalination rate in function of the treatment efficiency. Just like ASAR, SEC is also dependent on factors like feed salinity, etc.

2.7.5 Electrode Stability (STAB)

Stable recyclability of a CDI electrode reveals the uncompromised electrode–electrolyte interaction over a long period of time which is critical for salt adsorption capacity. Electrosorption mechanism has to do with ion adsorption and desorption in which the latter leads to electrode regeneration. Various reports have been found in literature in improving electrode stability by incorporation of transition metal oxides to carbon-based materials [45] i.e. graphene-doped MnO_2 showed excellent recycling stability [86], ZnO doped AC shows stable electrode cyclability [87] and addition of carbon nanotube to ordered mesoporous carbon exhibited high reversibility and electrochemical stability during the Charge/discharge process [88].

Figure 2.5 summarizes the performance indicators related to a typical CDI process. Several Parameters/variables affect the performance of the process from either design or operating point of view. It is important to understand the way of how these parameters affect the performance criteria and how to contro them in order to develop and operate a cost effective desalination process based on electro-sorption. In a first instance, it is necessary to develop/select a good (performing) electrode material as it is at the heart of this technology then electrodes have to be shaped considering formulation (material, conductive additive, binder etc.), fabrication method, and sizing aspect (thickness, surface area etc.). Finally, in

addition to the design aspect, operate the process at its best condition is also essential to satisfy the most the treatment objectives. Treatment objective for water treatment processes refer to performance in terms of productivity (volume or flow rate) and quality (feed and product salinity) as well as investment and operating cost (CAPEX and OPEX).

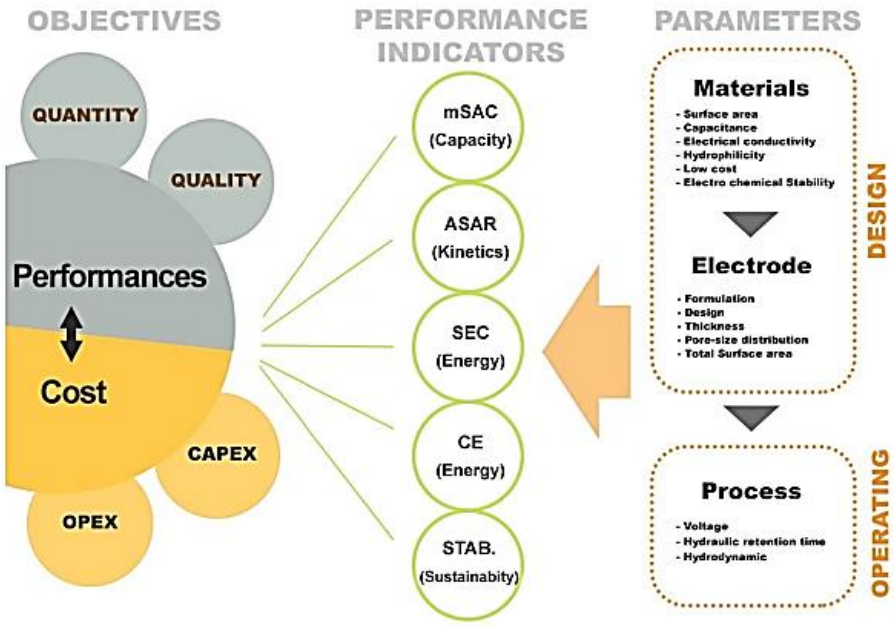

Fig 2.5. Schematic diagram of CDI performance indices

2.8. Conclusion

As reviewed in Chapter 2, material development and modifications of AC has provided vistas of opportunities into innovative hybrid electrode materials for electrochemical water desalination applications. Numerous modified or hybrid carbon electrodes with engineered structure and functionalities are constantly being developed and reported and the progress in material development offers a promising hope for CDI/FCDI upscale into industrial application. However, a key challenge abounds in CDI research field; this is in terms of compromise of material properties. The physico-chemical features of an engineered material could affect a potential functionality while trying to offset a particular drawback i.e., a well-controlled morphological material could offer high adsorption and lower viscosity but could be at the expense of electrical conductivity. Hence in this thesis, attempts have been made in the subsequent chapters to transform commercial AC into hybrid materials of well-tailored surface chemistry and advanced electrochemical properties for electrochemical water

desalination applications. The following chapter (chapter 3), reveals the technical know-how and the materials used to carry out various surface modifications of commercial AC to different modified electrode materials.

Chapter 3 Materials and method

3. Introduction

In this chapter, we intend introducing the basic background of the main instruments used for physico-chemical and electrochemical characterizations of our carbon electrodes and also the chemical reagents used in the modifications of carbon materials. Electrochemical techniques for evaluating the capacitive nature of both the pristine and modified electrode materials as well as the parameters to evaluate the electrodes are introduced. Furthermore, understanding of material properties (physico-chemical and electrochemical) and electro-sorption tests enabled us to better comprehend and interpret the results in relation to desalination application in the subsequent chapters.

3.1 Materials and method

3.2 Chemicals reagents

Activated carbon, Supelco Analytical (CAS no: 7440-44-0, France) and graphite powder (CAS no: 7782-42-5) were supplied by Sigma Aldrich (Steinheim, Germany). Carbon black (CAS no: 1333-86-4) was supplied by Alfa Aesar (Steinheim, Germany. Graphite foil (0.35 mm thick) was supplied by RMC Remacon (Bad Säckingen, Germany).

Polyvinylidenefluoride (PVDF) (CAS no: 24937-79-9), *N*-methyl-2-pyrrolidone (NMP) (CAS no 872-50-4, 99.7 %, M.W 99.13 g mol^{-1}), hydrochloric acid (HCl) (CAS no: 7647-01-0, 37 %), phosphoric acid (H_3PO_4 CAS no: 7664-38-2, 85 %) and potassium permanganate ($KMnO_4$) (CAS no: 7722-64-7, 98 %) were purchased from Alfa Aesar (Erlenbachweg 2, Germany). Sulfuric acid (H_2SO_4) was purchased from ACS Reagent (Belmont, CO, USA). Absolute ethanol (CAS no: 64-17-5, 99.8 %) and hydrogen peroxide (CAS no 7722-84-1, 7732-18-5 30 %) were purchased from VWR chemicals (Fontenay-sous-Bois, France). All chemicals were used as supplied.

Cationic and anionic exchange membranes were purchased from Membranes International Inc. (Ringwood, New Jersey, USA). Deionized water with electrical resistance of 1 MΩ cm^{-1} (Millipore) was used throughout in all the experiments.

3.3 Carbon based electrode/flow electrode preparation

To prepare solid based activated carbon (AC) electrodes for CDI, PVDF was first dissolved in NMP at room temperature and stirred for 2 h. Then activated carbon powder was added and the carbon slurry was stirred for 1 h and then sonicated for 45 min. The mass ratio of PVDF to AC was 1:8. The carbon slurry was cast by spray coating on to graphite sheet current collector/solid support with an average thickness of 0.357 mm. The coated electrode was dried in an oven at 80 °C for about 3-4 h. The operation is repeated until a mass difference between 0.75-0.85 g is reached which corresponds to the deposited mass of the electrode (carbon slurry).

Graphene Oxide (GO) was synthesized using Marcano's method. Briefly, a total of 5 g of graphite powder and 18 g of potassium permanganate was slowly added to a mixture of 40 mL of phosphoric acid and 360 mL of sulfuric acid. The solution was stirred for 18 h at room temperature, then 3 mL of H_2O_2 was added. The solution was then filtered and centrifuged (4000 rpm for 10 min) so the supernatant could be decanted away. The mixture was then washed multiple times with 30% HCl and then with distilled water. The obtained GO was placed in an oven for 4 h at 80 °C and GO electrode was made following the aforementioned procedure for AC electrode fabrication.

Regarding reduced graphene oxide synthesis (RGO), 3.7 g of as-prepared GO was mixed with 60 mL of 8 M KOH and sonicated for 2 h. After sonication, it was washed multiple times with distilled water under centrifugation and later dried in an oven at 80 ° C for 2-4 h. The obtained RGO was converted to an electrode following the aforementioned procedure for AC electrode fabrication.

For flow electrode preparation, activated AC of appropriate mass depending on the carbon loading is dissolved in a calculated volume of distilled water and then made to sonicated for 2-3 h. Thereafter, the slurry electrode is stirred on a magnetic stirrer for 1 h prior to desalination experiment in which it is also being stirred during the course of the experiment to keep the electrode wet.

3.4 Carbon electrodes characterization

To achieve the objectives of this thesis, the following physico-chemical and electrochemical characterizations were performed with the aid of the following techniques:

3.4.1. Scanning electron microscope (SEM)

SEM was done in order to understand the topographical features (surface morphology) of the pristine and modified AC electrodes. Briefly, SEM operates by using a focused electron beam under high vacuum to raster on the surface of the specimen line by line. The signals scattered from the surface of the sample are captured by electron detectors and the information is transferred to a computer for digitizing the image. In this research, all the electrode samples were first spray sputtered prior to imaging. This allows the materials to be conductive for image capturing. For SEM, a small amount of samples in a dried powder form are loaded onto one side of the double-sided carbon tape with the other side already taped on top of the sample stub. Then the sample stub is mounted onto the sample holder plate and introduced inside the vacuum chamber for further imaging. SEM images of the electrodes were obtained using Hitachi S4800 scanning electron microscope and the instrument was operated at 15 kV at a working distance of 10 mm. Figure 3 (a) shows the schematic representation of the working principle of a SEM machine while Figure 3 (b) shows the top view of a scanned AC material by SEM.

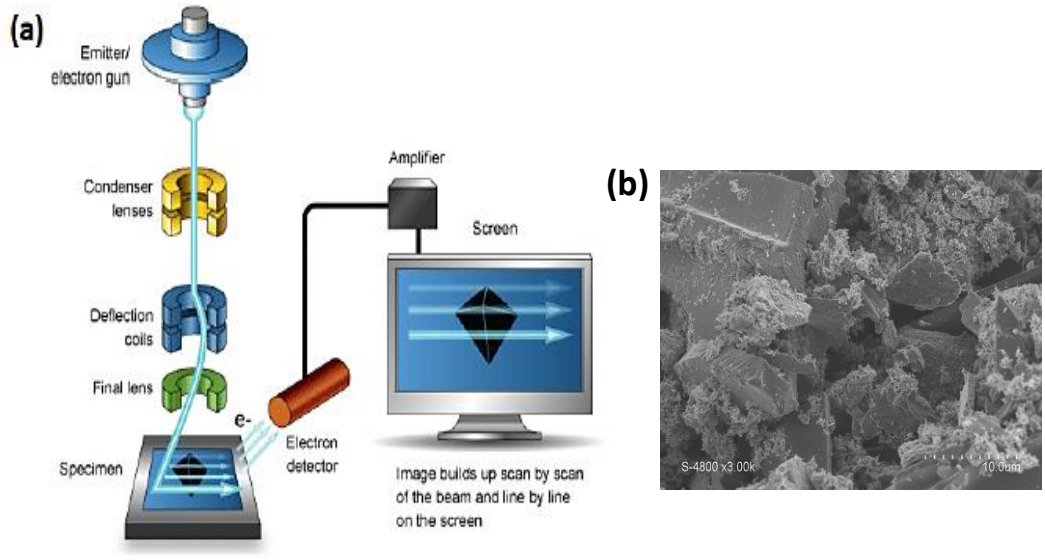

Fig 3 (a) SEM layout and working principle (b) Top view morphology of AC

3.4.2 Thermogravimetric Analysis (TGA)

TGA is a thermal analysis that measures the weight loss of a material as a function of increasing temperature. It also offers a scientific technique of monitoring the thermal stability and decomposition patterns of solid materials. In principle, it includes a sample pan that is hand down and supported by a precision balance, and a programmable furnace that can heat the sample at a controlled rate. The TGA instrument continuously weighs a sample as it is heated under the chosen atmosphere (e.g. air, Ar etc.). For sample analysis under TGA, the samples must be completely dried to avoid any interference of moisture at early stages of the test. Figure 3.1 shows the key units of TGA instrument while Figure 3.1 (b) gives the example of TG curve of a material. In this research, thermogravimetric analysis (Mettler Toledo TGA/SDTA 851) was performed by heating the powder sample in N_2 flow at room temperature to 1000 °C with a ramping rate of 10°C min^{-1}.

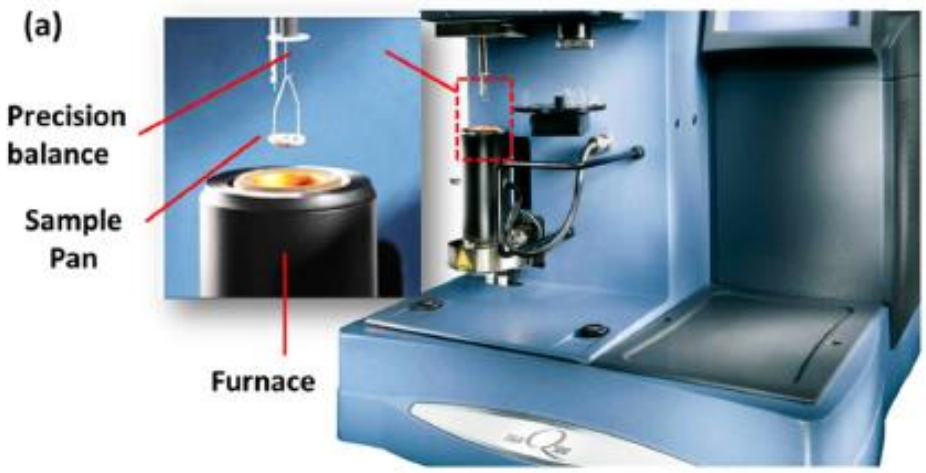

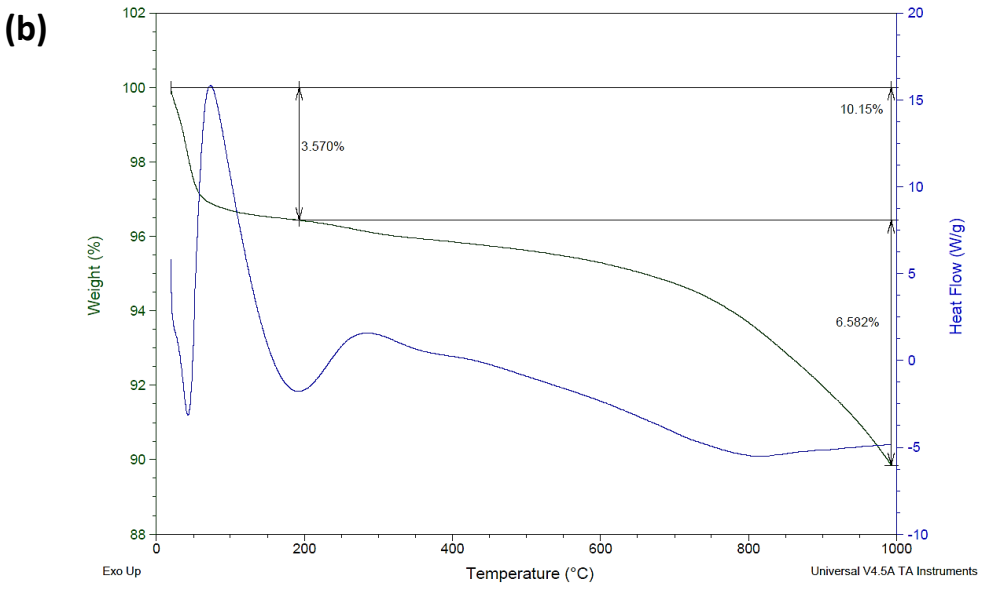

Fig 3.1 (a) Photo of TGA instrument showing the core units (b) Example of TGA curve of a carbon based material derived from polymer.

3.4.3 Nitrogen adsorption-desorption isotherms

Carbon based materials are known to have high surface area and porous structure. BET analysis is the most commonly used technique that determines the external surface area of the particles and provide insight into the open pores (e.g. pore size, pore volume, etc.) The measurement is based on BET theory where the exposed surface area of a material is determined by the amount of physical adsorption of a gas on the surface. In BET analysis, N_2 is typically used due to its strong interaction with solids and the availability in high purity. Before samples are measured, a degas process is necessary to remove the pre-adsorbed gases and vapors reside in the material. BET monitors the pressure change during the adsorption process. Once the surface of the sample is saturated with the adsorbed gas molecules, the sample is removed from N_2 and the adsorbed N_2 is released and quantified upon heating. The profile of the N_2 adsorption-desorption is presented in the form of a BET isotherm where the amount of gas adsorbed is plotted against relative pressure. According to IUPAC standard, pores of materials are classified into micropores (pore size below 2 nm), mesopores (pore size between 2 -50 nm) and macropore (pore size above 50 nm). Also, based on IUPAC classification, profile of N_2 adsorption-desorption isotherms is categorized into four types (type I-IV) as shown in Figure 3.2. Briefly, Type I typically refer to microporous material with the exposed surface area almost exclusively inside the pores; Type II are usually observed for materials of little porosity or macroporous solid; Type III refers to non-porous material with weak adsorbent-adsorbate interaction. Types IV with a hysteresis loop commonly associated with mesoporous material. Type V and VI isotherms are similar to Type III with weak adsorbent-adsorbate interaction except that the pores are mostly mesoporous. In this research, adsorption-desorption isotherms and specific surface area measurement was done under N_2 by using Brunauer–Emmett–Teller (BET) method (Micromeritics 2020 ASAP, Merignac, France). From the summary report of adsorption/desorption isotherms, the following parameters such as total pore volume (Vt) was calculated from the amount adsorbed at a relative pressure (P/P°) of 0.99, was the mesopore volume (V_{meso}) was calculated by the Barrett–Joyner–Halenda (BJH) model and the e specific surface area was obtained from the Brunauer-Emmett-Teller (BET) method at 77 K.

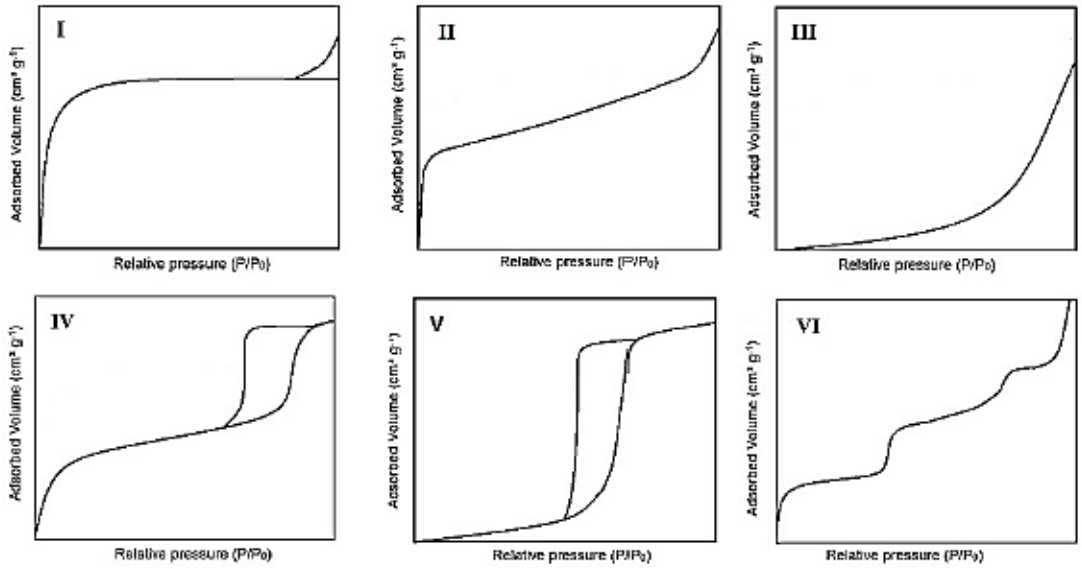

Fig 3.2. IUPAC classification of isotherms

3.4.4 Fourier Transform Infrared (FT-IR)

FTIR is a technique widely used to characterize the vibrational energy of materials. In principle, light consisting of a broadband in infra-red (IR) region is passed through the sample simultaneously. The light is then absorbed in different amount at distinct frequencies (i.e. vibrational frequency) by different bonds in the sample and get measured. The resulting spectrum provides a molecular fingerprint which correspond to the vibrations frequencies of different bonds in a sample. FTIR is suitable for characterizing graphitic carbon materials and in this research, all the FTIR characterizations were conducted using Thermo Nicolet Nexus 4700 ATR-FTIR (Thermo Electron Corporation, Quebec, Villebon Sur Yvette, Courtaboeuf Cedex, Canada) in order to verify the functional finger prints of the samples (AC and modified AC electrode materials) Briefly for the FTIR measurement, a few milligram of the powdered sample was placed on a doted red spot. Thereafter, it was made to have contact with the ATR detector by gentle pressing and the infrared transmittance was monitored and recorded on a computer using OMNIC software

3.4.5 UV-vis Spectrophotometry Measurement

UV-Vis is a spectroscopic technique that is widely used for the quantitative analysis of the analyte in a sample (mostly solution). During analysis under UV-Vis, incident light from UV-Vis is in the UV and visible range where molecules of the sample undergo electronic

transitions upon absorbing the energy. UV-Vis then measures the transition of electrons from the ground state to the excite state (i.e. the absorption). In a typical UV-Vis test, samples are typically placed in a cuvette, which are typically rectangular-shaped container with an internal width of 1 cm (i.e. path length L). Figure 3.3 (a) shows the four possible electronic transitions in a molecule under UV while Figure 3.3 (b) shows a typical example of UV spectrum. In this research, UV-vis spectrophotometry measurement was done using UV 2401PC SHIMADZU Corporation, Tokyo, Japan) in order to ascertain the shift in the wavelength of absorption

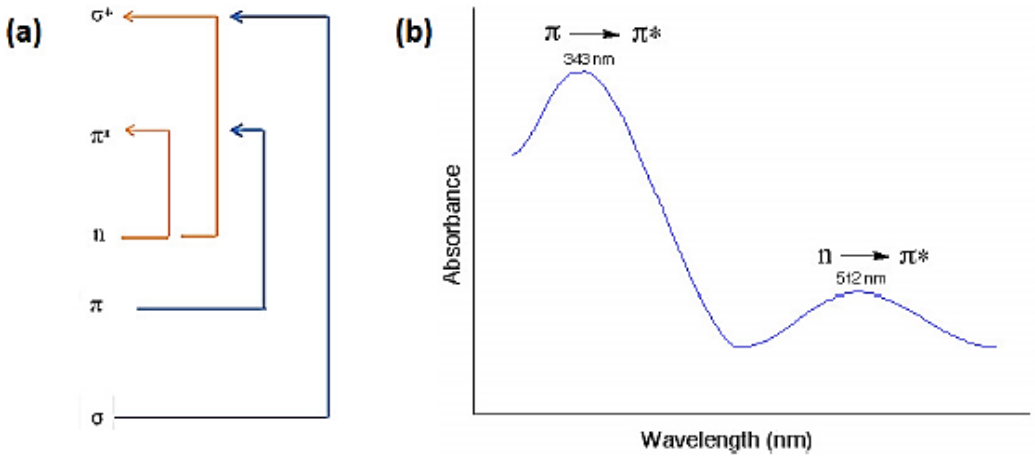

Fig 3.3. (a) Four types of electronic transitions in a molecule (b) Typical UV spectrum of a material undergoing two forms of transitions.

3.4.6 X-ray Photoelectron Spectroscopy (XPS)

XPS is a surface-sensitive quantitative spectroscopic technique employed to investigate the surface chemical composition of materials. The technique is based on the photoelectric effect where an incident X-ray photon hits the sample, interact with a core electron, and result in the ejection of the electron from the atom as shown in Figure 3.4 (a). The general layout of a XPS instrument is shown in Figure 3.4 (b) while Figure 3.4 (c) gives the XPS spectra of carbon based material. The sample is exposed to an incident X-ray beam and once the photoelectric effect causes electrons to escape from the atom, the kinetic energies of the emitted photoelectrons will be collected by the electron analyzer. Kinetic energy of the emitted electron is dependent on the incident dependent on the incident X-ray and binding energy of the atomic orbital from which it originated. XPS spectrum is usually given by intensity

(counts per second) as a function of binding energy and each photoelectron peak elucidate a certain chemical element that can be identified by its characteristic energy.

The chemical binding and chemical moieties of different functional groups of carbon based materials used in this research were determined by X-ray photoelectron spectroscopy (XPS ESCALAB 250 Thermo Electron, Strasbourg, France). For the XPS analysis, the excitation source is the monochromatic source Al line Kα with a photo energy observed at 1486.6 eV. The analyzed surface has a diameter of 500 µm. The photoelectron spectra are calibrated in terms of bond energy with respect to the energy of the C=C component of carbon C1 s at 284.4 eV.

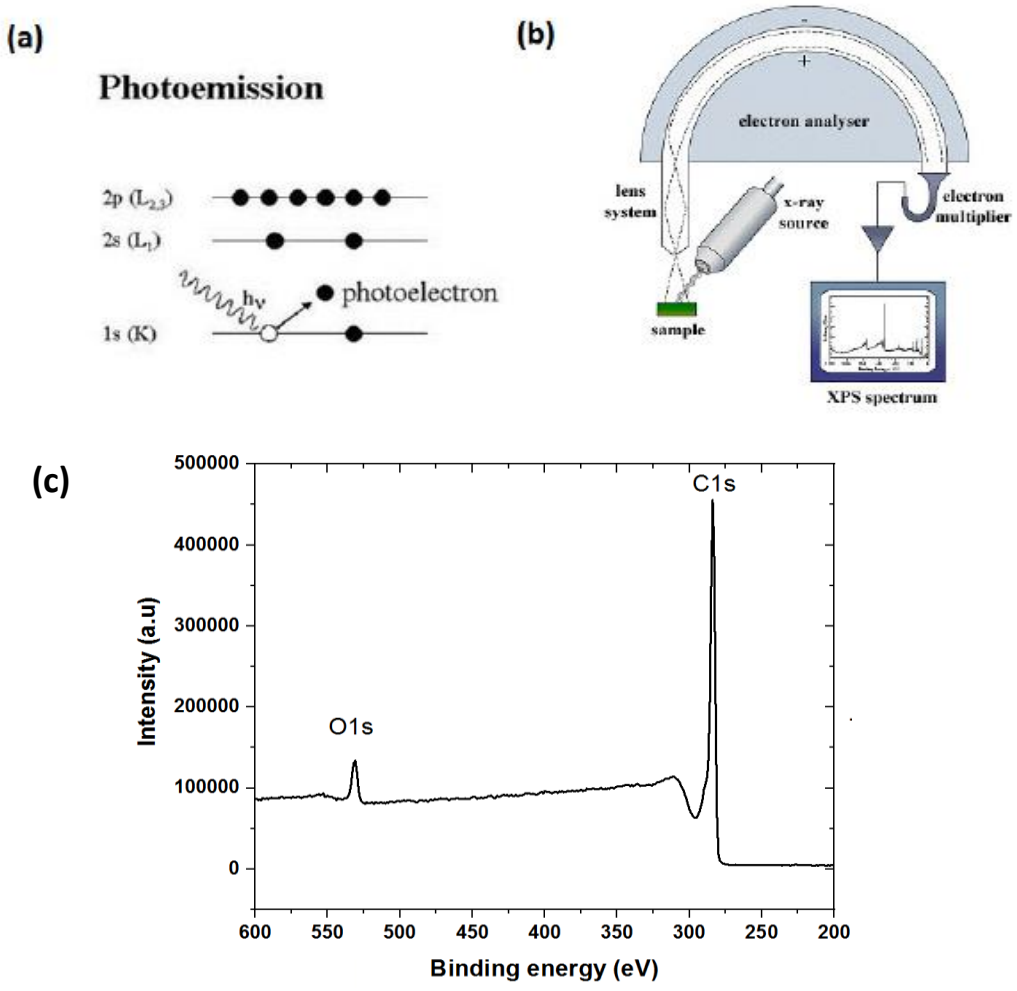

Fig 3.4 (a) Schematic representation of photoelectric effect (b) typical configuration of XPS instrument (c) XPS spectrum of a typical carbon based material

3.4.7 Energy Dispersive X-ray Spectroscopy (EDX)

EDX provides precise information regarding measurement for the weight percentage of carbon (C), oxygen (O) hydrogen (H) and other elements present in a sample. During elemental analysis, samples are exposed to a combustion process (up to 1800 °C) in an oxygen-rich atmosphere. As a result of the combustion, elements originally in the sample are converted to their combustion products: C to CO_2, H to H_2O, etc., then these products will go through a series of cells for separation and where their mass are measured individually to calculate the composition of the initial sample. Figure 3.5 shows the illustration of EDX elemental analyzer

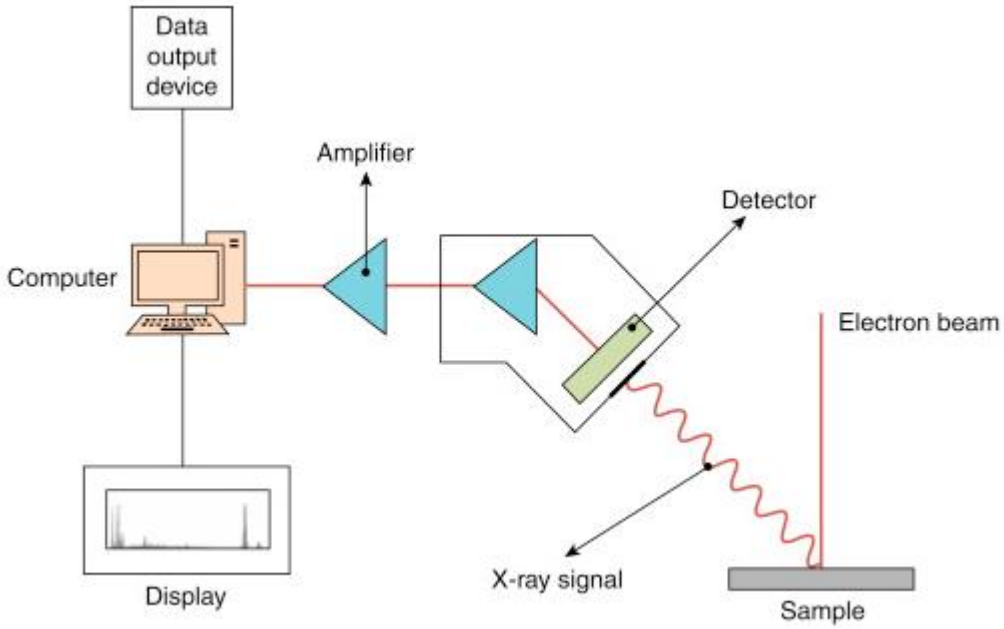

Fig 3.5. Schematic representation of a typical EDX elemental analyzer (Source: Chemical Engineering Department, Hacettepe University, Turkey)

3.4.8 X-ray Diffraction (XRD)

XRD is a technique commonly used to identify the crystallinity of materials. It functions by shooting a high energy electron beam to a metal plate to generate X-rays. Then the X-rays pass through a slit and hit the sample from a certain angle. During an XRD test, a series of angles will be tested by changing the X-ray arm and the scattered X-rays from the sample surface further hit a photographic film and get counted. For crystalline materials, some of the rays will pass through the lattice while others hit the atoms and get scattered. The structures of

crystals (e.g. lattice spacing) can thus been identified by this machine. X-ray diffractometer (XRD Pan Analytical X'pert Phillips, Lelyweg, EA Almelo Netherlands) with Cu Kα radiation λ = 0.15406 nm at 40 kV and 30 mA) was used to study the crystallinity and graphitic layer development of the materials used in this research.

3.4.9 Raman Spectroscopy

The structural properties and defects detection in the electrode materials were studied by Raman spectroscopy using a 532.4 nm laser (HORIBA Xplora, Minami-ku, Kyoto, Japan). Briefly for Raman analysis, few milligrams of carbon electrode (in powdered form) were deposited on a glass slide and then gently flattened on the surface using another glass slide. This is thereafter placed under Raman microscope for detection and focusing. After, laser light is passed on to the detected carbon under microscope and thereafter set into Raman mode for defect detection. In all cases, Raman wavelength was fixed between the range of 800-2000 cm^{-1}

3.4.10 Viscosity

Rotational tests for dynamic viscosity of the slurry materials were carried out with rheometer. First, applied velocity was presented via rotational speed or shear rate. This simulates processes that are dependent on flow velocity. Then dynamic viscosity which reveals the the flow behavior of the slurry materials under shear rate at constant temperature is presented as a Non-Newtonian fluid in which the viscosity decreases as a function of increasing shear rate (shear thinning behavior) as shown in Figure 3.6. The rheometry property (dynamic viscosity) was studied by Anton Paar rheometer France. Dynamic viscosity of the flow electrodes was measured using Anton Paar Rheometer Physica MCR 301 (Anton Paar GmbH, Graz, Austria).

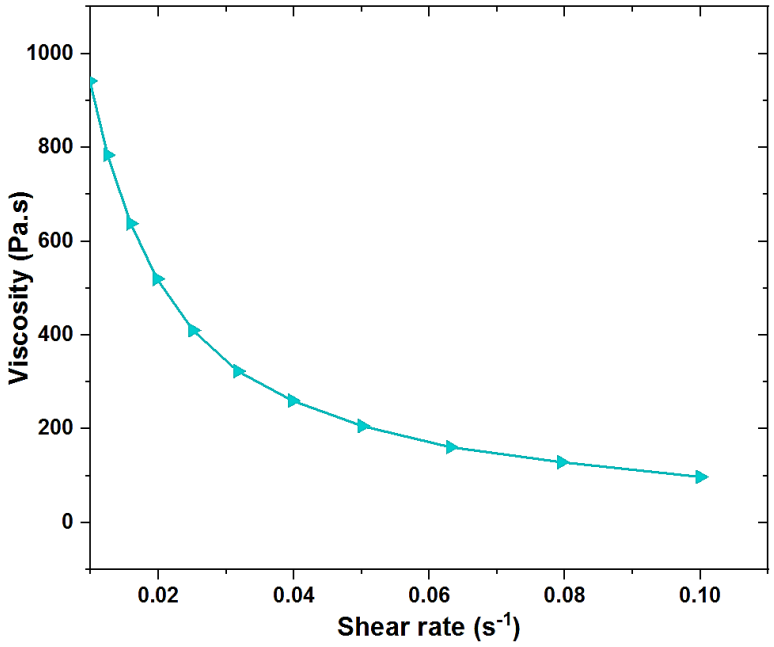

Fig 3.6. Dynamic viscosity measurement of a typical carbon slurry

3.4.11 Particle size determination

For this determination, dynamic light scattering technique was used. In principle, it works on the concept that when a beam of light is scattered by a group of particles, the angle of light scattering is inversely proportional to particle size (i.e. the smaller the particle size, the larger the angle of light scattering). For the carbon materials in this research, the average size of their particles was measured by Anton Paar litesizer (Anton Paar GmbH, Graz, Austria).

3.4.12 Zeta Potential

Zeta potential reveals the property of particles in suspension or dispersion in terms of their stability. Also, it is a key parameter that gives information about the level or magnitude of electrostatic repulsion or attraction between particles in suspension or dispersion under electric field. Based on electric double layer theory, charged particles in a suspension will attract a lay of tightly bounded counter-ions and another layer of loosely bounded ions forming the diffuse layer. An example of a negatively charged particle in a suspension is shown in Figure 3.7. The diffuse layer has certain ionic mobility and travels with the particle and those outside remain stationary and the boundary in between is the so called slipping plane. Zeta potential measures the potential difference between the particle surface to the slipping plane. In this research, zeta potential of slurry electrodes is determined in liquid media using Anton Paar litesizer (Anton Paar GmbH, Graz, Austria). Briefly for the zeta

potential measurement, few drops of slurry electrode suspension is placed in a cuvette and then inserted inside the machine. After, the machine is programmed to operate under electric field and zeta potential reading is recorded.

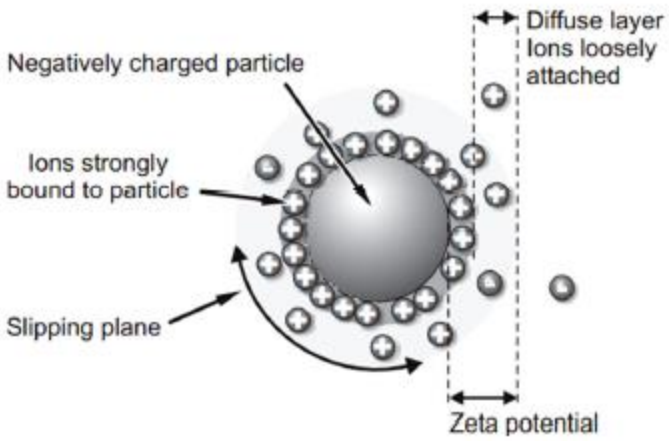

Fig 3.7. Schematic diagram showing zeta potential of a negatively charged particle in suspension (Source: Anton Paar zeta potential user manual)

3.4.13 Water Contact Angle (WCA)

Water contact angle was performed to reveal the surface interaction of the solid electrode. For WCA measurement, carbon electrode already deposited on a support was placed under a micro-syringe for water injection or droplet. Few drops of distilled water (DI) was dropped on the surface of the electrode for few seconds and immediately captured by a camera as it spreads. The capture images were treated with a software Image J for WCA reading

3.4.14 Cyclic Voltammetry (CV)

CV is a type of electrochemical technique commonly applied for the investigation of capacitive materials or various electrochemical reactions. In CV test, the potential of working electrode experiences a linear ramp within a certain time, and the ramp is reversed back to the initial potential within the same time period. During the process, the response current is measured and plotted against the applied potential, forming a closed curve as shown in Figure 3.8. In this research, electrochemical performance of the AC and modified AC electrodes was investigated with cyclic voltammetry (CV) using Origalys Potentiostat (OGF01A, Origalys

Electrochem SAS, Les Verchères 2, Rillieux-la-Pape, France) in a three electrode system at an operating window from -0.2 to 0.2 V / -0.4 to 0.6 V *vs.* ref in 0.5/1.0 M NaCl at the scan rate of 2-10mVs $^{-1}$. CV was conducted using carbon electrode deposited on graphite supporting sheet (exposed surface area of 1cm^2), platinum mesh and 3 M KCl, Ag/AgCl as the working, counter and reference electrodes respectively.

The double-layer capacitance was determined using cyclic voltammetry at different scan rates by considering the open circuit potential (OCP 0.1 V *vs.* ref) of the charging and discharging currents. The determined double-layer capacitance of the system is the average of the absolute value of the slope of the linear plot of the charging and discharging regions fitted to the data. C as the specific capacitance (F g^{-1}) was then determined considering the mass (g) of the active material on the electrode surface (1 cm^2) using Eq (1)

$$i = \upsilon C_{DL.} \qquad (8)$$

For an ideal capacitor Q = CV, thus by differentiation i = C υ, where υ is the scan rate.
The double-layer charging current i is equal to the product of the scan rate υ, and the electrochemical double-layer capacitance $C_{DL.}$

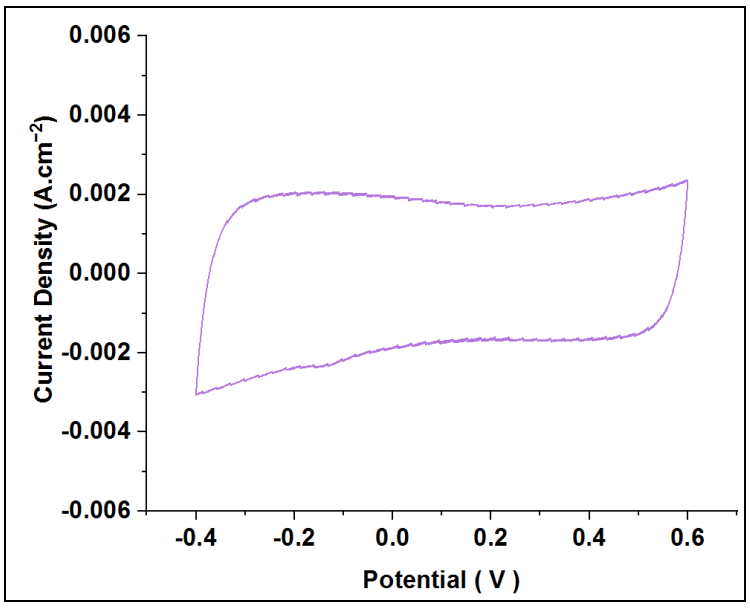

Fig 3.8. Cyclic voltammetry curve of a typical carbon based material at the scan rate of 2 mVs^{-1}

3.4.15 Electrochemical Impedance Spectroscopy (EIS)

EIS is an electrochemical tool that reveals the intrinsic resistance of a material when in contact with an electrolyte. Result emanating from EIS consists of a real and an imaginary part. When the real part is plotted as the X-axis and the imaginary part is plotted as the Y-axis of a chart; it is called "Nyquist Plot". An example of a Nyquist plot is shown in Figure 3.7 (a), the x-intercept represents the series resistance and the region of the semi-circle represents the charge transfer resistance. After the semicircle follows the 45-degree curve, known as Warburg diffusion regime, which occurred at lower frequencies. This region is closely related to the transition diffusion resistance. In order to extract the detailed information from EIS result, the shape of the EIS curve is often simulated using a software to fit an equivalent circuit model for the cell as shown in Figure 3.9 (b). The electrochemical impedance spectroscopy (EIS) in this research was done in the frequency range of 5000 KHz to 10 mHz was used at the sine wave amplitude of 5 mV. It was conducted by a carbon electrode deposited on a graphite sheet (1cm^2 surface area), platinum mesh and 3 M KCl, Ag/AgCl as the working, counter and reference electrodes respectively. It was performed using Origalys Potentiostat (OGF01A, Origalys Electrochem SAS, Les Verchères 2, Rillieux-la-Pape, France)

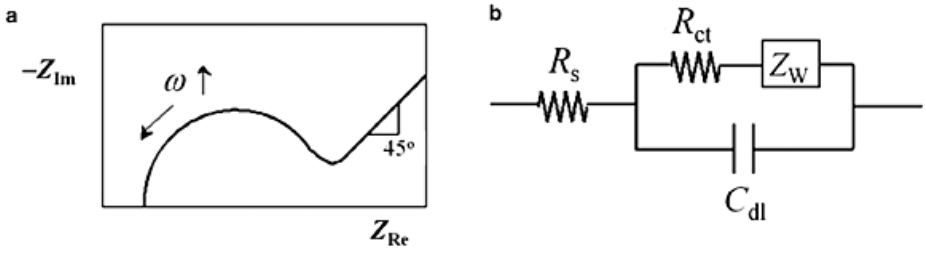

Fig 3.9 (a) Typical shape of Nyquist plot from EIS test and (b) Equivalent circuit fitting from EIS simulation

3.4.16 Galvanostatic Charge-Discharge (GCD)

GCD is another technique that can be used to determine the capacitive nature of a material and it is also used for cycling stability test. In GCD test, charge and discharge are performed by applying a constant current until a certain set voltage is reached. The capacitive nature of the materials can then be determined from the emanating curves from this process. In this research, GCD was performed at a constant current density of 0.1 A. g^{-1} within a potential

window of 0–2.5 V. It was conducted by a carbon electrode deposited on a graphite sheet (1cm^2 surface area), platinum mesh and 3 M KCl, Ag/AgCl as the working, counter and reference electrodes respectively. It was performed using Origalys Potentiostat (OGF01A, Origalys Electrochem SAS, Les Verchères 2, Rillieux-la-Pape, France)

3.4.17 Four Point Probe Conductivity Measurement (Electron Mobility Measurement)

This is one of the most important techniques to verify the conductivity of semiconducting or conducting materials. The four-point probe method is one of a most efficient and accurate way of measuring the bulk conductivity of materials. As shown in Figure 3.10, the apparatus consists of four equally placed tungsten metal tips as electrodes that made to contact the surface of the sample during the test. A current is then passed through the outer two probes and the voltage across the inner two probes is measured. For measuring the bulk conductivity of the materials used in this research. Hall effect for electron mobility was performed on four-point conductivity probes system using Bio-Rad HL5500PC (Hall Polaron, Germany). The four-point probe measurement was done following the procedure: Briefly, the carbon electrode deposited on a graphite sheet with an area of 1 cm^2 was placed on a white plastic sample support. Before this, the difference in thickness of the graphite was measured before and after sample deposition in order to ascertain the thickness of the sample deposited. Thereafter, the four probes were set and fixed at a particular position to maintain regular contact when placed upon the sample support and the Hall effect software was launched in order to take the resistivity values. After this, electron mobility measurement was carried out by replacing the four probes with hall probe (a giant bar made to focus on the sample support for few seconds approximately 30–40 s) to create magnetic field on the sample. As this is going on, the corresponding current and Hall voltage are recorded by a software after which the electron mobility value is displayed

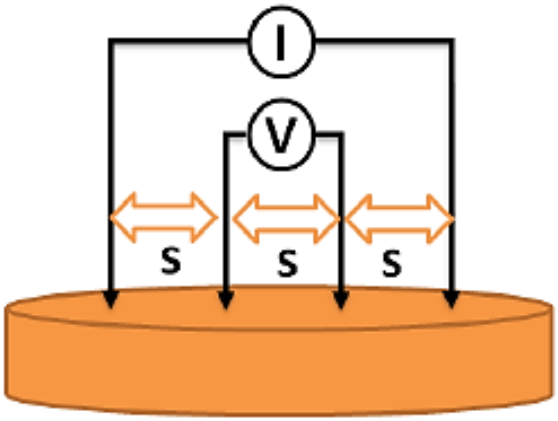

Fig 3.10. Schematic diagram of a four-point probe conductivity measurement

3.5 CDI and FCDI experiments

3.5.1 CDI

The CDI experiments were carried out in a batch mode as shown in Figure 3.11 In batch mode operation, the conductivity probe monitors the changes in the ion conductivity of the recycle reservoir. For each experiment, conductivity data is converted to salt concentration and adsorption per mass of carbon is calculated.

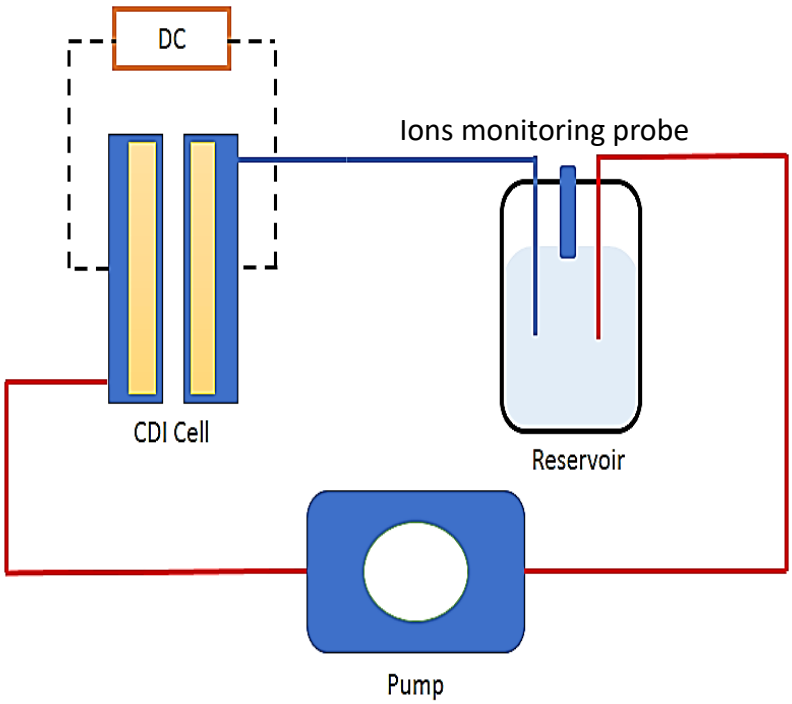

Fig 3.11. Schematic diagram of CDI in batch mode.

Figure 3.12 shows the laboratory setup while Figure 3.13 shows the constructed CDI cell; it consisted of two parallel electrode sheets separated by a non-electrically conductive spacer (0.99 mm thick), as displayed in Figure 3.13. The electrode materials were directly attached to the current collector, which was subsequently connected to an external power source (potentiostat). The CDI electrodes have an area of 6 × 10 cm^2 and brine solution (400 and 1200 mg L^{-1} NaCl) was continually pumped into the CDI cell at a constant rate of 25 mL min^{-1}. The conductivity changes of the brine solution (feed solution) was monitored at room temperature. The CDI tests were conducted at potential differences of 1.0 V and 1.4 V. Current response (chrono-amperometry profile) as a function of time of the CDI experiment is shown in Figure 3.14

Fig 3.12 Picture of laboratory setup of CDI experiment.

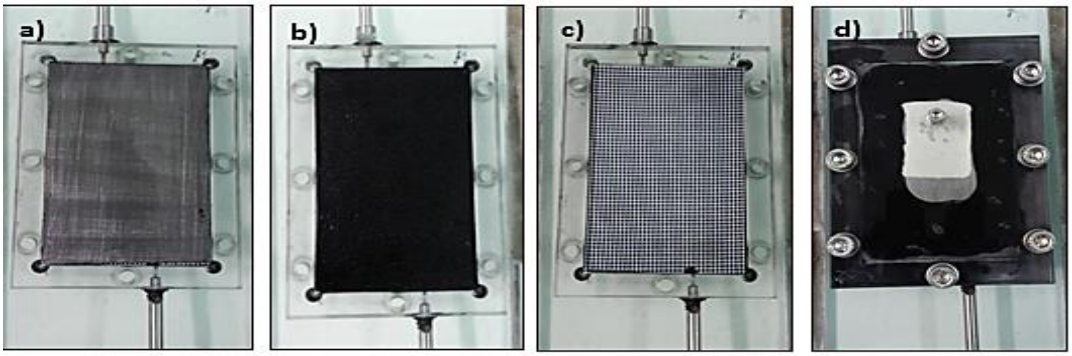

Figure 3.13. CDI, (a) Open cell with a current collector, **(b**) current collector with electrode, (**c**) solid electrode with a separator, (d) closed cell

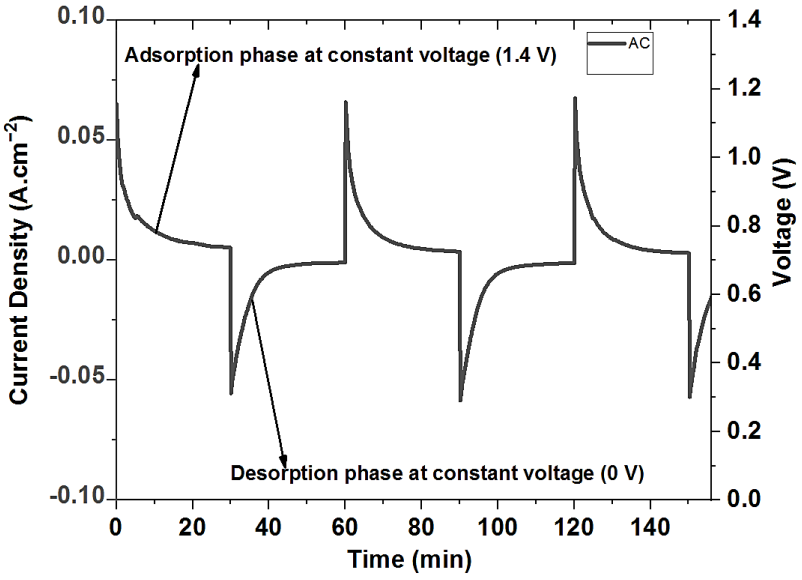

Fig 3.14 Current profile of pristine AC CDI experiment at constant potential difference of 1.4 V (adsorption phase) and 0 V during desorption phase.

3.5.2 FCDI

Flow capacitive deionization (FCDI) experiments were conducted in semi-continuous mode in which the cell configuration is in short circuited close cycle (SCC) as shown in Figure 3.15. It consisted of electrochemical cell, peristaltic pumps, a potentiostat as an external power supply and a conductivity meter. The cell is powered by a potentiostat and the feed solution (FS) was made to pass through a spacer sandwiched in between cation and anion exchange membranes. The feed electrodes (FE) stored in a reservoir were made to pass (by pumping) through flow channels and as they exit the channels, they are fed back to the reservoir and then re-circulated. During this process, the conductivity of the FS was monitored by ion conductivity meter (Hanna Instruments SRL, Nusfalau, Str. Hanna, 457260 Jud. Salaj - Romania). Figure 3.16 shows experimental setup used in this work while Figure 3.6 shows the breakdown of the FCDI electrochemical cell. Figure 3.17 comprises 2 carved stainless-steel current collectors which also serves as passages for FE. Between these 2 current collectors the cell contains a nylon spacer sandwiched between a cation exchange membrane and an anion exchange membrane. These parts were held together using stainless steel plates. The stack of stainless-steel plates, current collectors, ion exchange membranes, and the spacer

was very well compressed with screws to assure there is no leakage of the feed solution or of the feed electrode out of the cell during the experiment as displayed in Figure 3.18. A feed saline solution of 5 g L^{-1} NaCl solution (86.5mM, 70 mL) was made to flow through the spacer sandwiched between the two ion exchange membranes at a constant flow rate of 5 mL min^{-1}. The flow feed electrode (77.8 mL) which consisted of 10 wt. % AC (Darco, Sigma Aldrich) flows along the flow path carved on the current collector at a flow rate of 30 mL min^{-1} and was circulated in a closed cycle method in which both the anionic and cationic electrodes are being re-circulated in a reservoir (for regeneration); this allows co-mixing of charged ions outside the cell. The initial electrical conductivity of the salt solution and that of the effluent was monitored every 1 min at room temperature by ion conductivity meter (Hanna Instruments SRL, Nusfalau, Str. Hanna, 457260 Jud. Salaj - Romania) inserted into this feed solution during the course of the experiment. A constant potential difference of 1.2 V was applied to the FCDI cell using an Origalys potentiostat for desalting experiments. Short circuited close cycle (SCC) configuration was used in this study. Current profile (chrono amperometry) as a function of time of the FCDI experiment is shown in Figure 3.19 in which a steady current is maintained after few minutes during adsorption process and the current is made to a sharp drop once the reaction time is complete.

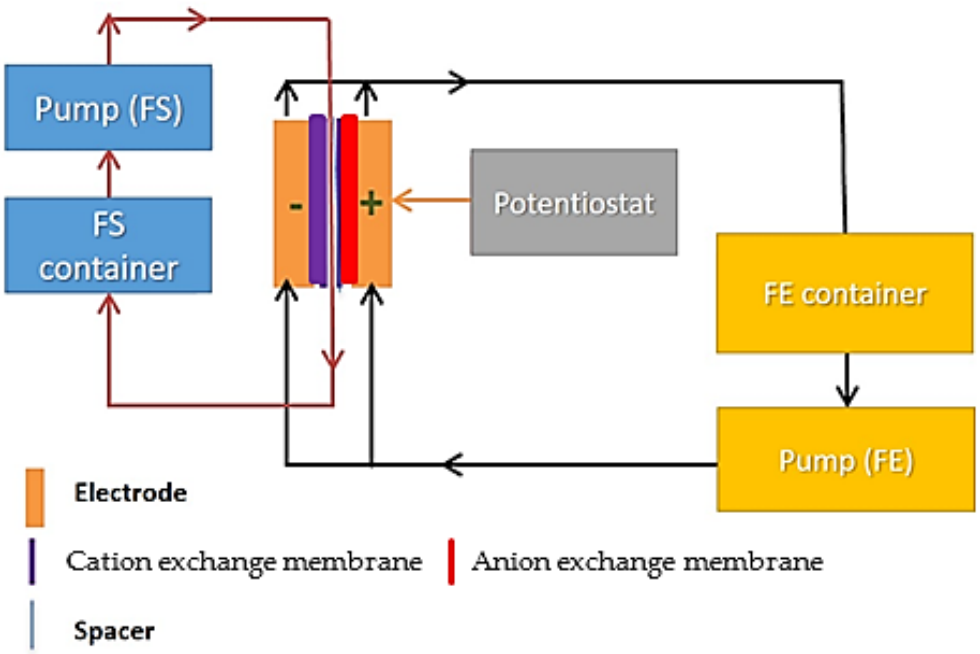

Fig 3.15. Schematic diagram of FCDI in a semi-continuous mode.

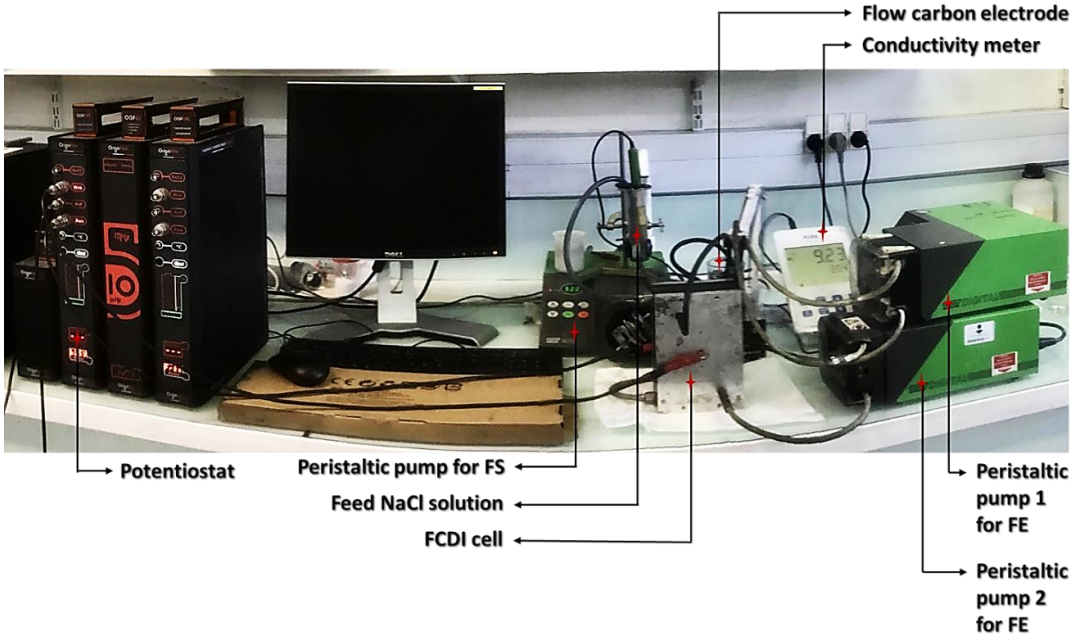

Fig 3.16 Picture of laboratory scale of FCDI in a semi-continuous mode.

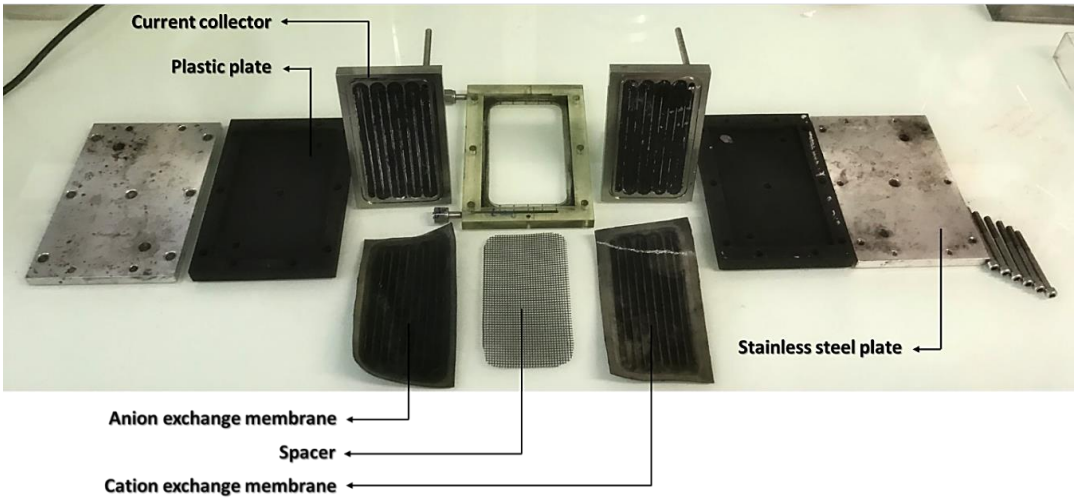

Fig 3.17. Different parts of FCDI electrochemical cell

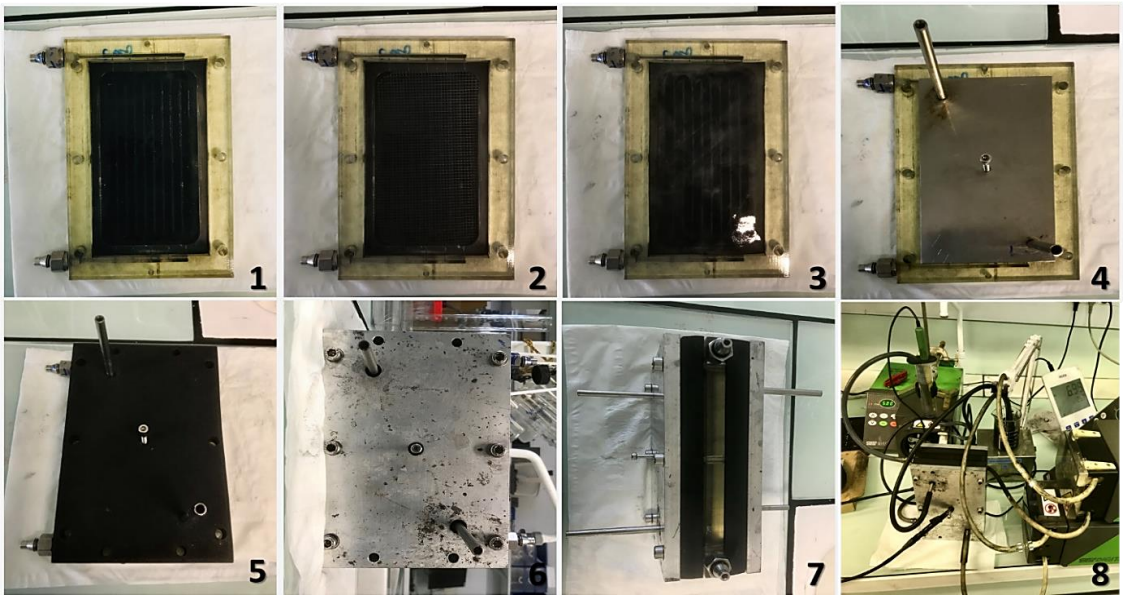

Fig 3.18. FCDI cell assembly. Anion exchange membrane (1), spacer (2), cation exchange membrane (3), current collector (4), plastic plate (5), stainless steel plate (6), assembled FCDI cell (7), and FCDI cell in the experimental setup (8)

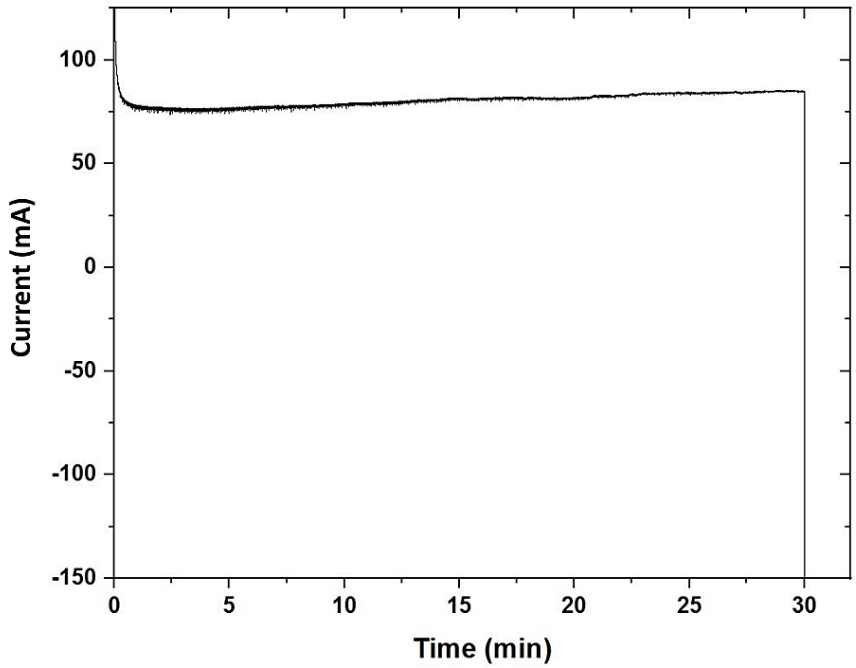

Fig 3.19 Current profile as a function of time of FCDI experiment

3.6 FCDI Performance indicators

In general, the performance matrices of FCDI for each experimental run are assessed in terms of the following performance indices:

In FCDI, the salt removal rate (SRR), is defined as the amount of salt adsorbed (in mg) per feed solution – feed electrode contact area (A in cm^2), per unit time (in min), and was calculated by Eq. (8):

$$SRR = \frac{(Co-Ce)\times V}{A\times t} \quad (8)$$

Where SRR ($mg/min.cm^{-1}$) is the salt removal rate, Co and Ce are the initial and final equilibrium conductivity of the feed solution in mg L^{-1}, V is the volume of the feed solution (L), A is the area (cm^2), and t is the duration of the FCDI experiment (min).

Desalination efficiency (%) was calculated using Eq. (9):

$$Desalination\ \ efficiency = \frac{Co-Ce}{Co} \times 100 \quad (9)$$

Maximum salt adsorption capacity mSAC, Q (mg g^{-1}) is defined by the mass of salt removed or abstracted to the deposited total mass of electrodes including binder (PVDF) and addictive (RGO) and it is expressed by equation (10).

$$Q = \frac{(Co - Ce)V}{m} \quad (10)$$

Where m is the total mass of the deposited electrode (g).

Charge efficiency (CE) is expressed as the ratio of moles of salt adsorbed to the coulomb of charge that is supplied to the system and was calculated according to Eq. (11):

$$CE = \frac{z\,(Co-Ce)\,V\,F}{\int Idt} \quad (11)$$

Where z is the equivalent charge of the ions (in our case, it is equal to 1), F is the Faradaic constant and $\int Idt$ is the integrated quantity of charge passed to the system as a function of time.

Energy consumption was calculated using the specific energy consumption (SEC) in $kWhm^{-3}$ which the energy is used in $kWhm^{-3}$ of desalinated water. SEC was calculated by Eq. (12):

$$SEC = \frac{E \times c}{V_{FS}} \quad (12)$$

Where E is the energy consumption (J) calculated using the equation $E = \int IVt$ where I is the current (A), V is the voltage (V) and t is time (s). c is energy conversion constant equals to 2.77778×10^{-7}, and V_{FS} is the volume of the feed saline solution in m^3.

Fluid behavior of our slurry in FCDI was investigated using Reynolds number which is inversely proportional to viscosity and it was calculated using Eq. (13):

$$R_e = \frac{\rho v D}{\eta} \quad (13)$$

Where ρ is the density of flow-electrode,1.06 gcm^{-3}; v is the velocity of flow-electrode in flow channel, 0.123 ms^{-1}; D is the hydraulic diameter of the flow channel, 2.6 mm; η is the coefficient of viscosity of flow-electrode which is a function of shear rate at 25 °C.

Average salt adsorption rate ASAR (mg g^{-1} min^{-1}) is defined as the ratio of maximum salt adsorbed to the time of adsorption. It is related by equation 4 below.

$$ASAR = \frac{Q}{t} \quad (14)$$

Where Q is in mg g^{-1} and t is the time in minute

3.7 Conclusion

In this chapter, we have shown the various instrumentation for carbon characterizations. The relevant techniques helped us in characterizing the effect of changes on the morphology, textural properties and electrochemical behavior of both the pristine and modified carbon

electrodes. Parameter evaluation from these characterizations better equipped us to understand and evaluate the obtained results in subsequent chapter 4.

Chapter 4. Characterisation of CDI

General Introduction

In this chapter, a well detailed information regarding the physico-chemical properties and electrochemical characterizations of the fabricated activated carbon electrodes and slurry electrodes are discussed.

In the first part of this section, we discussed in details the modifications made to solid based electrodes by improving the wettability and electrical conductivity challenges of commercial AC. To achieve this feat, we synthesized graphene oxide (GO) and reduced graphene oxide (RGO). The synthesized materials were characterized and used to modify pristine AC.

The second part is dedicated to slurry or flow electrodes using FCDI technique. Here, we verify the viability of pristine AC as flow electrode at moderate weight percentage and further tested its modified forms.

4.1 Overview of pristine AC modified with graphene oxide (GO)

This section discusses the physico-chemical properties and electrochemical characterizations of the fabricated activated carbon and modified activated carbon electrodes by graphene oxide. Here, various characterization analyses are used to evaluate the specific surface area, pore size distribution, surface functional groups, and specific capacitances of the pristine and modified carbon electrodes. Sequel to the analyses, the author was able to evaluate the properties of the electrodes in comparison to what is reported in literature. Furthermore, most of the knowledge garnered has been used in the subsequent chapter 5.

Some of the results provided in this section have been published in *Materials* **2020**, 13, 5185 as below:

Comparative Investigation of Activated Carbon Electrode and a Novel Activated Carbon/Graphene Oxide Composite Electrode for an Enhanced Capacitive Deionization

Gbenro Folaranmi, Mikhael Bechelany, Philippe Sistat, Marc Cretin and Francois Zaviska

Institut Européen des Membranes, IEM, UMR-5635, University of Montpellier, ENSCM, CNRS, Place Eugène Bataillon, CEDEX 5, 34095 Montpellier, France; gbenro.folaranmi@etu.umontpellier.fr (G.F.); philippe.sistat@umontpellier.fr (P.S.); marc.cretin@umontpellier.fr (M.C.)

4.1.1 Result and discussion

Physico-chemical and electrochemical characterizations of the pristine and modified carbon electrodes are discussed; effect of GO addition in relation to surface chemistry and electrochemical properties of pristine AC is discussed as shown below:

4.1.2 Characterisation of carbon based electrodes in CDI using GO

4.1.2.1 Scanning electron microscopy (SEM)

Figure 4. (a-c) shows the SEM images of the commercial AC electrodes fabricated through the procedure described in Section 3.3. As shown in Figure. 4. (a), carbon electrode deposited on a graphite sheet shows non uniform morphology with rough surfaces. Also, the composite electrodes show no significant difference in morphology when compared with that of pristine AC electrode probably due to the homogenous dispersion of the GO in the activated carbon. Both AC and its composites are of irregular shapes.

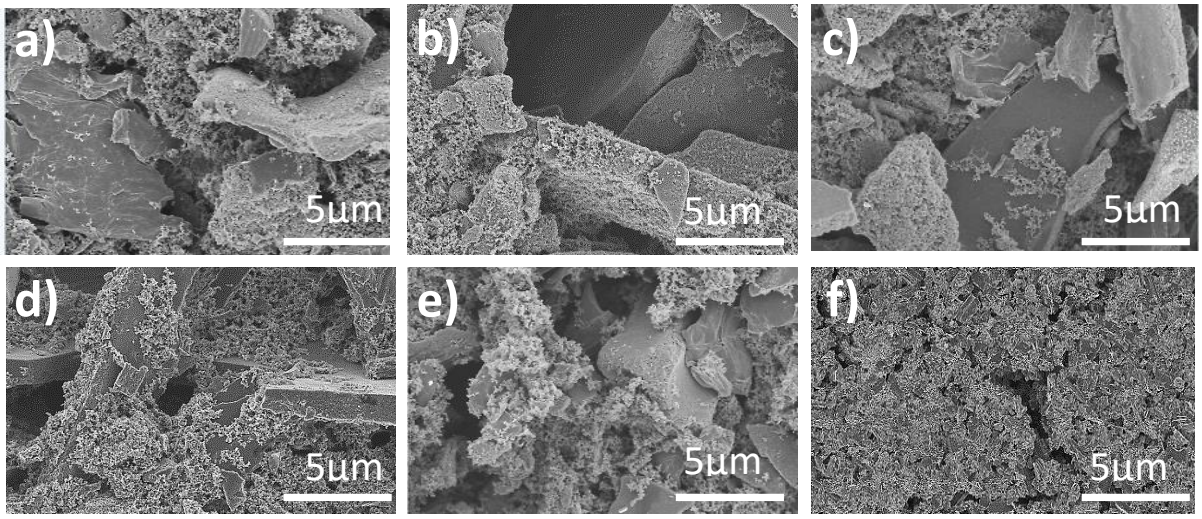

Fig 4. SEM of: a) AC (b) AC/GO-5 (c) AC/GO-10 (d) AC/GO-15 (e) AC/GO-20 and (f) GO-electrode.

4.1.2.2 Nitrogen adsorption-desorption isotherms

Specific surface area was carried out by Brunauer-Emmett-Teller (BET) method to investigate the adsorption nature of the materials under N_2, verify the pore size distribution of the

electrodes and the effect of the binder (PVDF) on the specific surface area. Adsorption behavior and pore size distribution of the pristine and modified electrodes were compared as shown in Figure 4.1 (a) and (b). There was a sharp decrease in the specific surface area of the activated carbon (AC) powder possibly due to the incorporation of both PVDF and graphene oxide (GO) as presented in table 4. From Figure 4.1 (a), it is evident that all isotherms are in the shape of typical IUPAC type II [89] as the hysteresis loops occurred between 0.4-0.8 P/P° relative pressures for all the materials. Pore size distribution as shown in Figure 4.1 (b) indicates the volume of pores accessible for a molecule or ions of particular size and shape. From 4.1.1 (b), it is clear that the available pores that were accessible for adsorption in our materials are within the mesopore region (greater than 20 Å). Parameters including the total pore volume, BET specific surface area, mesopore volume and average pore diameter of AC, and GO/AC-x are summarized in Table 4. It should be noted that there are no significant changes in the parameters V_t, and V_{MESO} the addition of GO.

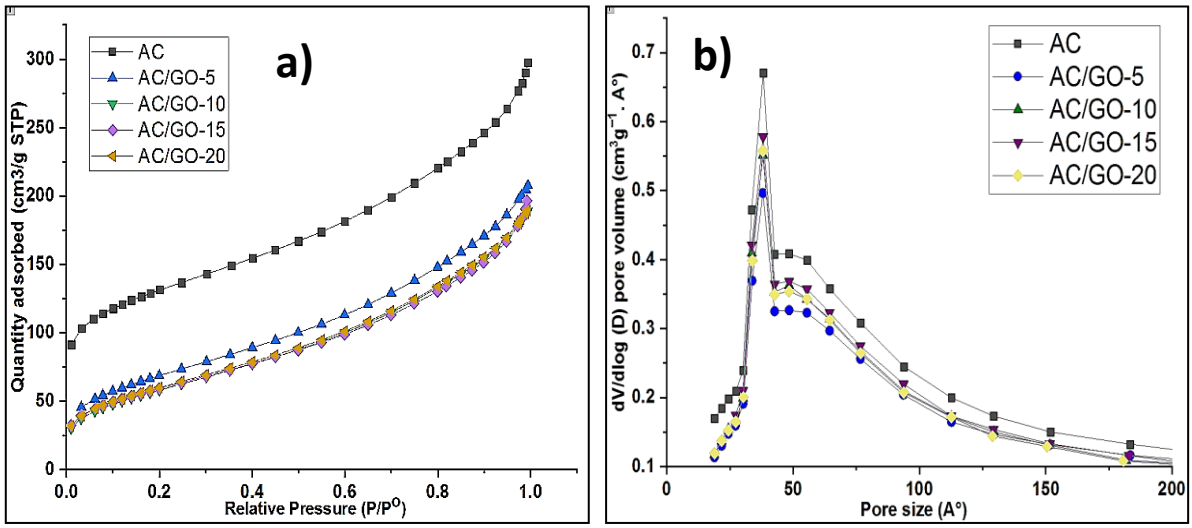

Fig 4.1: Nitrogen adsorption-desorption isotherm of (a) AC and AC/GO-x (b) Pore width distribution of AC and AC/GO-x.

Table 4 Textural parameters of Pure AC, AC electrode, GO and AC/GO-x

Sample	V_t (cm^3g^{-1})	S_{BET} (m^2g^{-1})	V_{MESO} (cm^3g^{-1})
Pure AC	0.82	1031±0.20	0.55
AC	0.33	467.05±0.15	0.35

GO	0.01	5.5±0.20	0.01
AC/GO-5	0.30	228.8±0.50	0.30
AC/GO-10	0.31	231.5±0.30	0.31
AC/GO-15	0.43	240.8±0.50	0.30
AC-GO-20	0.30	200.5±0.4	0.27

4.1.2.3 Water contact angle (WCA)

The Water Contact Angle (WCA) of the fabricated electrodes (AC and AC/GO-x) was measured to examine their wettability characteristics. Interestingly, all composites have an interesting hydrophilic property over the pristine AC electrode. This is possibly due to the addition of a graphene oxide (GO) that converts the highly hydrophobic PVDF binder (see Figure 4.1.1 a and b) into a less hydrophobic form that can be seen in Figure 4.1.1 (c–f), hence enabling more penetration of solvated ions into the pores of activated carbon. The addition of PVDF as an additive binder in AC electrode compromised its hydrophilicity; however, when graphene oxide was added to augment this compromise, the hydrophilic nature of the electrode was improved. It is somewhat difficult to capture all the WCA of the composites, as the water dropped on the surface of the materials spread rapidly when in contact with them, hence limited images were captured.

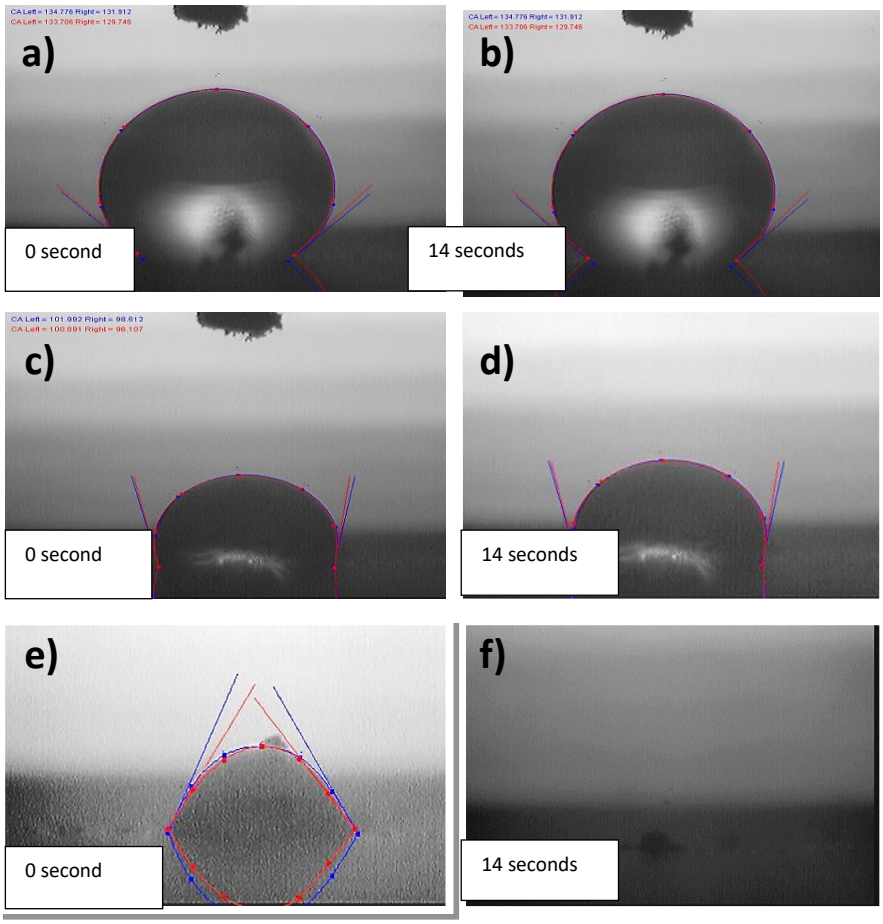

Fig 4.1.1: Water Contact Angle of (a,b) PVDF (c,d) AC electrode and (d,f) AC/GO-5 electrode.

4.1.2.4 Raman analysis and X-ray Diffraction (XRD) investigation

Raman analysis was performed in order to understand the defect that might have occurred on the lattice of pristine AC due to the addition of GO. As shown in Figure 4.1.2 (d), all the electrode materials conformed to the D-band at 1350 cm^{-1} due to the disordered graphite (out of plane vibration) and the G-band at 1580 cm^{-1} due to ordered graphite (in-plane vibration) [90]. Intensity ratio ($R = I_D/I_G$) in Raman gives us information of the level of defect present in any carbonaceous material. The intensity ratio of our pristine AC was 1.04 while that of GO is 1.25 (this intensity is high due to the effect of exfoliation process involved in making GO while that of AC might be due to industrial method of synthesis). A slight increase of defects was observed in the composite AC/GO-x (x = 5, 10, 15 and 20 wt. % GO) with a range of intensity ratio of 1.02–1.17, indicating a low degree of graphitization (a low level of graphitic domain) in all of the materials [91].

XRD was used to understand the amorphous or crystalline nature of AC and composite electrodes. For a typical crystalline carbon material, a sharp diffraction peak was observed at 2 θ = 25 and 45 ° corresponding to the 002 and 100/101 planes [92], respectively. As evident in Figure 4.1.2 (c), broad and diffuse diffraction peaks were observed for the as prepared AC and its corresponding composite electrodes, indicating a low degree of crystallinity and graphitic structure of the materials which corroborates with Raman analysis. The crystallinity of the AC in the composite was not enhanced by the addition of crystallized GO, which was made evident with a sharp diffraction peak at 10.0 ° (typical diffraction peak of a crystalline GO) [90]. No diffraction peak of GO was observed in all the composites due to its high dispersity [90].

The XRD peak of graphite was observed at 2 θ = 26.6 ° while after oxidation (exfoliation), new peak of GO at 2 θ = 10.0 ° was observed as shown in Figure 4.1.2 (b). Using Bragg's law ($n\lambda = 2d\sin\theta$), where n is 1, λ is X-ray diffraction (0.1541 nm), θ is the angle of diffraction in the degree and d is the inter-planar distance between graphite layers. The inter-planar distance of graphite and GO was calculated to be 0.3 nm and 0.9 nm respectively. This shows that there was an increase in the inter-layer spacing in the graphite layer due to the introduction of oxygenated functional groups via chemical oxidation [93]. There was no difference in the inter-layer spacing of pristine AC and its composites (d002 = 0.35 nm and d100/101 = 0.21 nm). In a typical carbonaceous material, i.e., graphite, the interlayer distance between two adjacent sheets as calculated was 0.33 nm [93] but that of our AC and its corresponding composites at 2 θ = 25 ° which corresponds to an interlayer distance (d002) is 0.35 nm suggesting a disordered carbonaceous interlayer graphitic material; a result corroborating Raman analysis. Figure 4.1.2 (a) shows the XRD pattern of pure PVDF binder but when dispersed in NMP (solvent), it became amorphous and could hardly be detected [94] (see Figure 4.1.2.2 b for further details), hence its peak was not observed in the diffractogram of the electrode, as shown in Figure 4.1.2 (c).

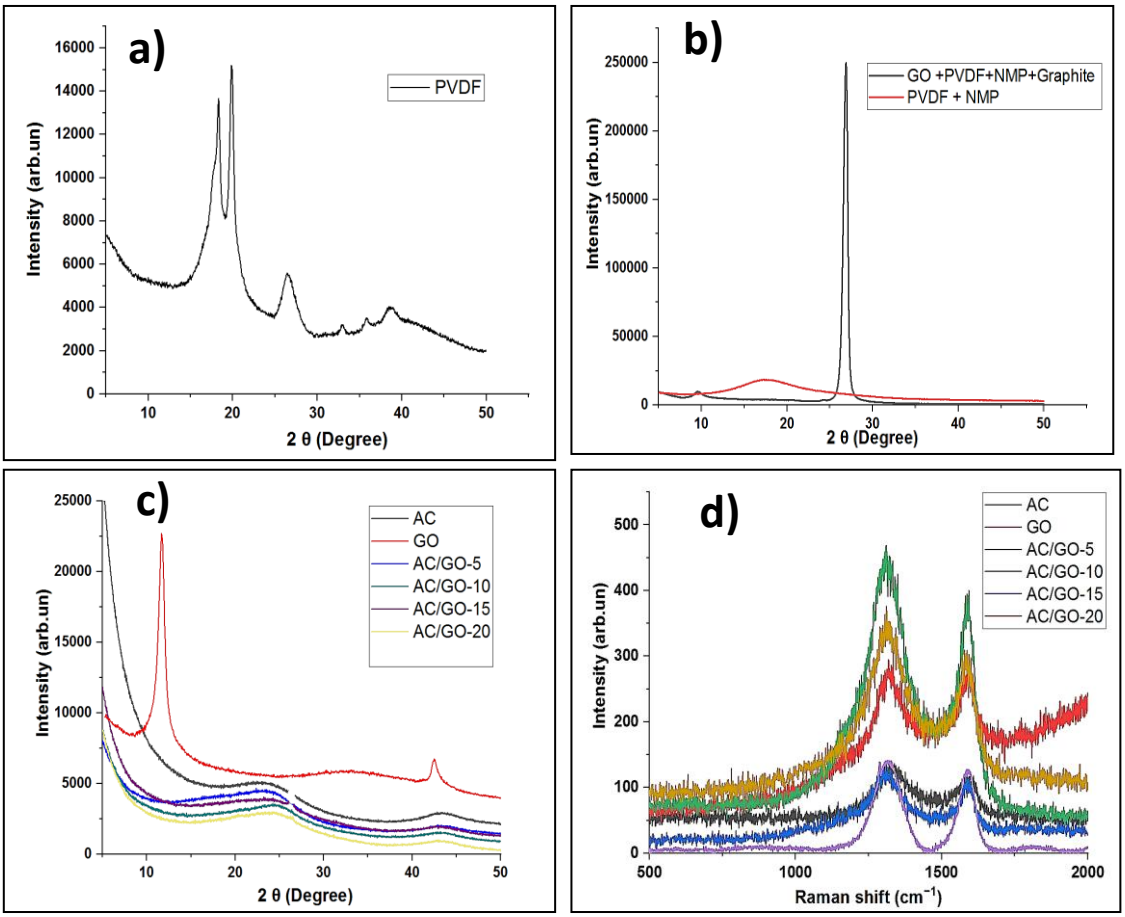

Figure 4.1.2 X-ray diffraction (XRD) of (**a**) Pure PVDF powder (**b**) PVDF dispersed in NMP solvent containing GO and graphite. (**c**) AC, GO and AC/GO-x electrodes. Raman spectroscopy of **(d)** AC, GO and AC/GO-x electrode

4.1.2.5 X-ray Photoelectron Spectroscopy (XPS)

Further investigation of GO influence on the surface chemistry of the composites was revealed by XPS analysis. For investigation one of the AC/GO-x was chosen and compared with pristine AC and the additive (GO).

Figure 4.1.3 (a)) shows the whole XPS spectra of AC, GO and AC/GO-15. From the spectra, it is obvious that the peak intensity of O element present in AC/GO-15 increased with addition of GO when compared with pristine AC. The oxygen content of the total element is 5.15 % in AC while for AC/GO-15 it is 9.51 % indicating that some oxygen containing functional groups have been added to the composite. Presence of oxygenated functional groups (OFGs) i.e. (C=O, COOH etc.) is beneficial for aiding electrochemical properties in

EDL capacitors due to surface chemistry improvement [95]. Figure 4.1.3 (b, c and d) shows the resolved C 1s spectrum of AC, AC/GO-15 and GO into their individual peaks. Binding energies of 284.5, 285.5, 287 and 288.5 eV present in the distribution of the peaks correspond to C=C, C-O, C=O and -COO- respectively [96]. Increase in the intensity band of some OFGs in the hybrid composite was observed as shown in Figure 4.1.3 (d) due to successful influence of GO.

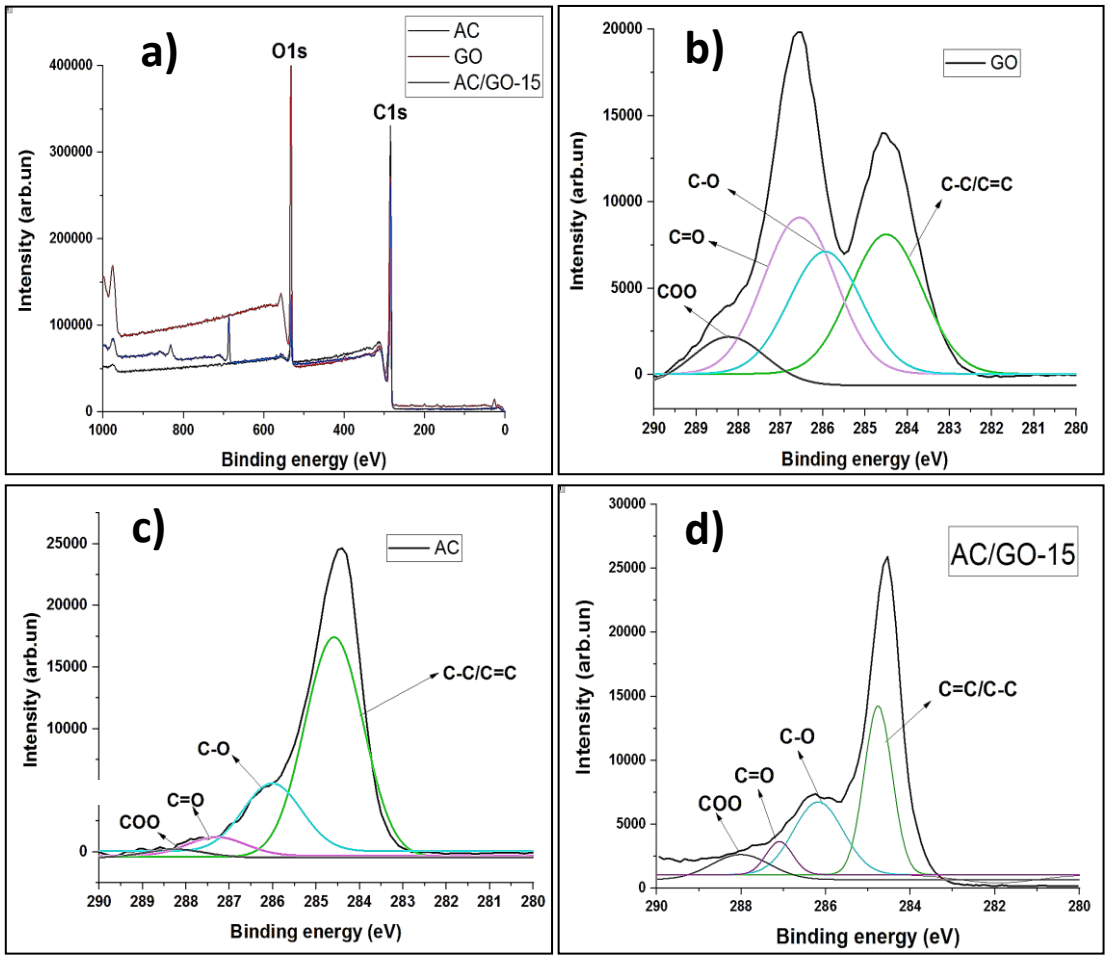

Fig 4.1.3: Whole XPS spectra of (a) AC, GO and AC/GO-x (where x is 15 wt. % GO). XPS spectra of C 1s peak of (b) GO (c) AC and (d) AC/GO-15.

4.1.2.6 Cyclic Voltammetry (CV)

Cyclic voltammetry (CV) curves of AC and its composite electrodes are shown in Figure 4.1.4 (a–c). At a low scan rate (2 mVs^{-1}), an almost rectangular shape was observed in both electrodes, indicating the capacitive nature of the electrodes (stable Electrical Double Layer formation at low scan rate) [97]. At a high scan rate of 200 mVs^{-1}, (Figure 4.1.4 c), an oval like or pseudo-rectangular shape is observed, which implies a high

instability of EDL and poor capacitive nature of the electrodes at high scan rate. Clearly, the AC/GO-15 composite electrode had a higher charging rate and faster ion transport than AC and its counter-part electrodes, possibly due to enhanced hydrophilicity that enables easier surface interaction, thus yielding low ion resistance and better reactivity of the electroactive species caused by the addition of GO at this proportion. Using Eq.1 (see chapter 3) and Figure 4.1.4 (d), calculated EDL capacitance and specific capacitance of all the electrodes are shown in Table 4.1. The calculated specific capacitance of the electrode is in the range of similar electrodes reported in literature [98].

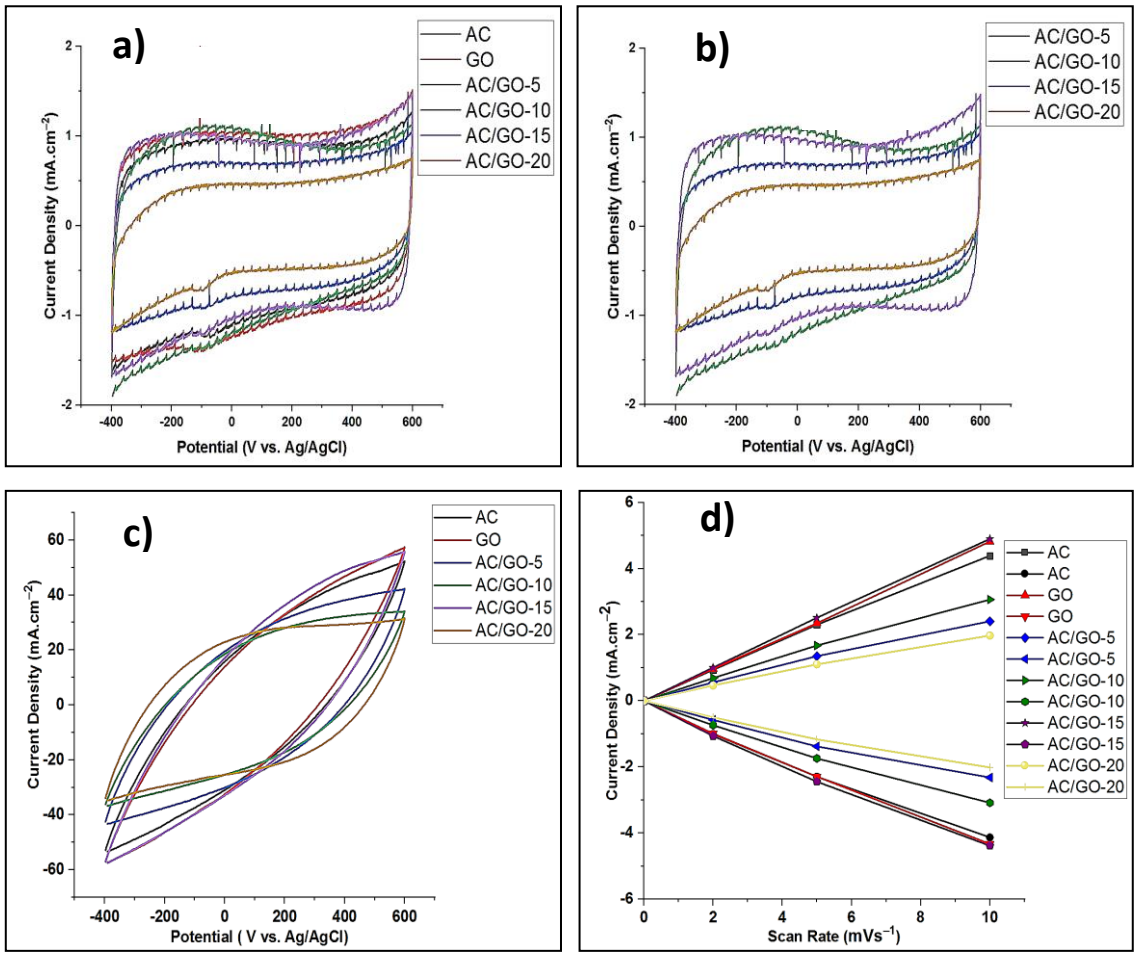

Fig 4.1.4: Cyclic voltammetry curve of (a) AC, GO and AC/GO-x composite electrodes at the scan rates of 2 mVs^{-1}; (b) AC/GO-x electrodes at scan rate of 2 mVs^{-1}; (**c**) AC, GO and AC/GO-x composite electrodes at the scan rate of 200 mVs^{-1}; (d) Double-layer capacitance measurements for AC, GO and AC/GO-x composite electrodes. Currents were measured in a non-Faradaic region of the voltammogram obtained in 0.5 M NaCl at low scan rates of 2–10 mVs^{-1}. The charging (ref current density above 0 $mA.cm^{-2}$) and discharging currents (ref current density below 0 $mA.cm^{-2}$) plotted as a function of scan

rate (mVs^{-1}). The determined double-layer capacitance of the system was taken as the average of the absolute value of the slope of the linear fits to the data [98].

Table 4.1 Electrical double layer capacitance (C_{EDL}) and specific capacitance ($C_{Specific}$) for AC and AC/GO-x electrodes.

Sample	AC	GO	AC/GO-5	AC/GO-10	AC/GO-15	AC/GO-20
C_{EDL}($F.cm^{-2}$)	0.92	0.58	0.62	0.94	1.61	0.47
Cspecific ($F.g^{-1}$)	56	157	43	66	75	33

4.1.3 Conclusion

As earlier discussed, graphene oxide was synthesized and subsequently combined with commercial AC to influence its surface chemistry. Based on our findings and according to XPS, increment in oxygenated functional groups (OFGs) of the modified electrodes was observed and a correlation between this factor and electrochemical properties of the modified electrodes was rationalized. Although, improvement in electrochemical properties was observed due to enhanced wettability that affords higher and easier surface interaction (electrode/electrolyte) thus promoting ions diffusion into the pores of the carbon electrodes but at the expense of porosity and specific surface area reduction.

4.2 Overview of pristine AC modified with reduced graphene oxide (RGO)

This section discusses the physico-chemical properties and electrochemical characterizations of the fabricated activated carbon and modified activated carbon electrodes by graphene oxide. Here, we fabricated hybrid of activated carbon composites by direct mechanical mixing with reduced graphene oxide (RGO). The effect of the additives at different combination ratio was verified. Evaluation of the physico-chemical and electrochemical properties of the as synthesized composites enabled the author to understand and rationalize the link of the additive ratios to ion transport within the carbon structure. Sequel to the analyses, the author was able to evaluate the properties of the electrodes in comparison to what is reported in literature. Furthermore, most of the knowledge garnered has been used in the subsequent chapter 5.

Some of the results provided in this section have been published in *Nanomaterials* **2021**, 13, 5185 as below:

Activated Carbon blended with Reduced Graphene Oxide Nanoflakes for Capacitive Deionization.

Gbenro Folaranmi, Mikhael Bechelany, Philippe Sistat, Marc Cretin and Francois Zaviska

Institut Européen des Membranes, IEM, UMR-5635, University of Montpellier, ENSCM, CNRS, Place Eugène Bataillon, CEDEX 5, 34095 Montpellier, France; gbenro.folaranmi@etu.umontpellier.fr (G.F.); philippe.sistat@umontpellier.fr (P.S.); marc.cretin@umontpellier.fr (M.C.)

4.2.1 Result and discussion

Physico-chemical and electrochemical characterizations of the pristine and hybrid carbon electrodes are discussed; effect of RGO addition on the porosity, morphological and textural properties of the hybrid electrodes in relation to their electrochemical properties is discussed as shown below:

4.2.2 Characterisation of carbon based electrodes in CDI using RGO

4.2.2.1 Scanning electron microscopy (SEM)

The morphology of AC and the composites containing RGO was examined by field emission scanning electron microscope (FESEM). The images are given in Figure 4.2 (a-f). Commercial AC shows an indefinite shape with no smooth surface (hill like surface). RGO observations prove that the rough surface of the RGO sheet tend to stack or agglomerate together showing very limited porosity and compacted structure. On the other hand, all the composites containing RGO show no significant difference in their morphology when compared to that of the pristine AC and no significant evolution concerning the texture of the materials can be ascertained by SEM.

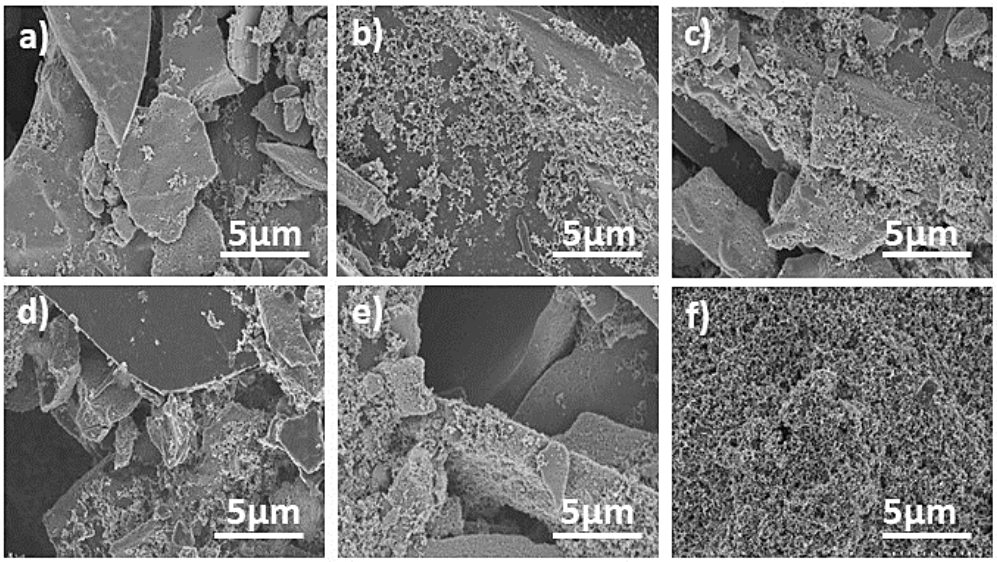

Fig 4.2 field emission scanning electron microscope (FESEM) images of (a) AC (b) AC/RGO-5 (c) AC/RGO-10 (d) AC/RGO-15 (e) AC/RGO-20 and (f) RGO electrodes

4.5.3 Structural properties of precursors

Structural properties were first investigated by X-ray diffraction. XRD patterns of GO, RGO and AC/RGO-x are shown in Figure 4.2.1 The XRD peak of graphene oxide was observed at 2 θ = 10.2° and a little sharp peak was also observed at 2 θ = 43 °; showing a turbostratic disorder of GO due to its incomplete oxidation [99] while after chemical reduction, a little broad peak at 2 θ = 25 ° was observed in RGO indicating a layer-to-layer sheet of RGO [99]. Using Bragg's law (nλ = 2dsin θ), where n is 1, λ is X-ray diffraction (0.1541 nm), θ is the angle of diffraction in degree and d is the inter-planar or layer spacing between graphite layers. The inter-layer spacing, i.e., the distance between the adjacent sheets or layers was calculated to be 0.9 nm for GO and 0.36 nm for RGO. This shows that after chemical reduction using KOH, there is a decrease in the inter-layer spacing in the graphitic layer of RGO due to the removal of most oxygenated functional groups in GO [100]. No significant difference was observed in the inter-layer spacing of pristine AC and its composites (*d*002 of 0.36 nm). The XRD pattern of AC/RGO-x composites exhibited combined characteristics with broad peaks at 2θ = 23.5–25.9 ° (002 plane) and 44.5 ° *(*10/101 plane). The 002 planes correspond to the graphitization of the organic component and nano-crystalline structure of the matrix, while the 10/101 plane reveals the formation of a 2D graphitic-like structure [101].

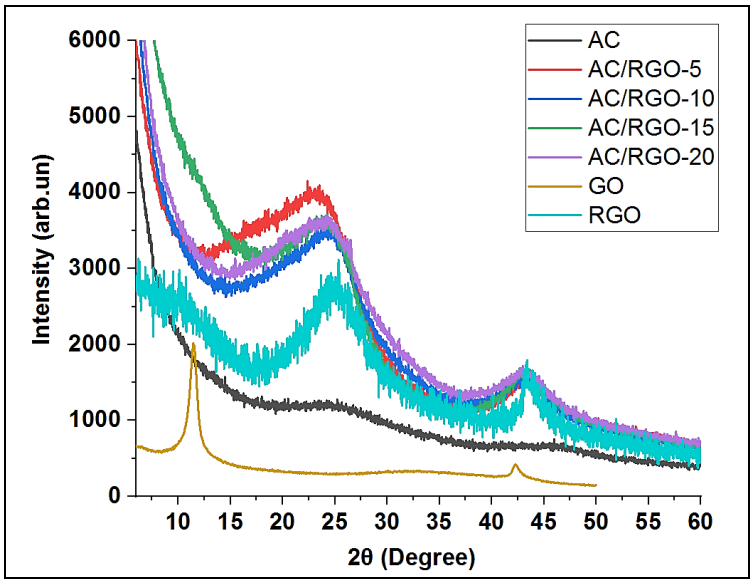

Fig 4.2.1: XRD patterns of AC, GO, RGO and AC/RGO-x (where x = 5, 10, 15 and 20 wt. % RGO)

Raman spectroscopy analysis was done to understand the level of defect and disorder in the materials. All of our materials possess characteristic features of graphitic carbon with Raman shift at 1350 cm^{-1} and 1590 cm^{-1} corresponding to D and G bands respectively (Figure 4.2.2 a). D band arises from a defect that is based on structural edge effect due to breathing mode of rings while D band relates to the first order scattering of E_2g phonon of Sp^2 C atoms or ordered structure of graphite crystals [101]. Intensity ratio I_D/I_G is an important parameter used to observe the level of disorder in carbonaceous materials. From the Raman spectra, GO possessed broad D band due to size reduction of sp^2 domains that is caused by distortion during oxidation [102]. However, as the proportion of additive increases, there is no increase or decrease in defects of the composites in comparison to pristine AC (1.10 ±0.13 in AC, 1.01-1.11 ±0.26 in AC/RGO-x)

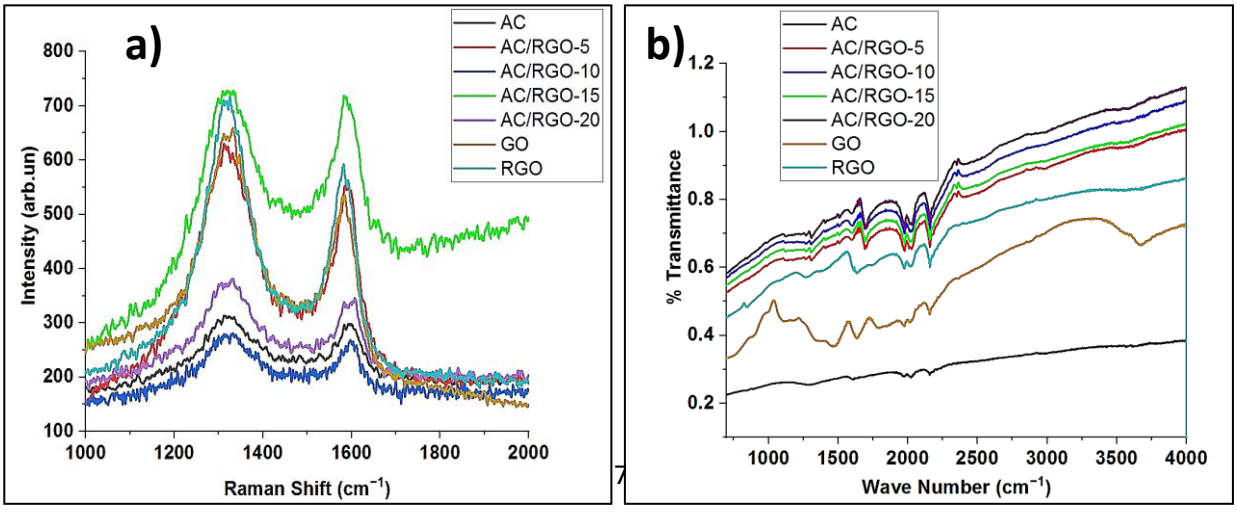

Fig 4.2.2 Raman spectra of precursors and AC/RGO-x composites b) FTIR spectra of precursors and AC/RGO-x composites.

Attempt to identify the functional groups of GO, RGO, AC and its composites were done via FTIR (Fig. 4.2.2 b). The peak at 3700 cm^{-1} is associated with the –OH stretching of alcohol/phenol [103, 104] which was significantly reduced in RGO on comparison with GO. The peaks present at 1720 cm^{-1} is due to C=O of carbonyl group and it's seen to be most pronounced in GO which is abundantly rich in oxygenated functional groups and also more obvious in all the composites than in AC. The peak at 1382 cm^{-1} is due to C–H stretching.

In Figure 4.2.3, the reduction of GO and RGO is further confirmed by UV-Vis absorption spectroscopy with GO having an absorption maximum at 205 nm while after reduction to RGO this absorption maximum is red shifted to 214 nm owing to the restoration of sp^2 carbon atoms [104].

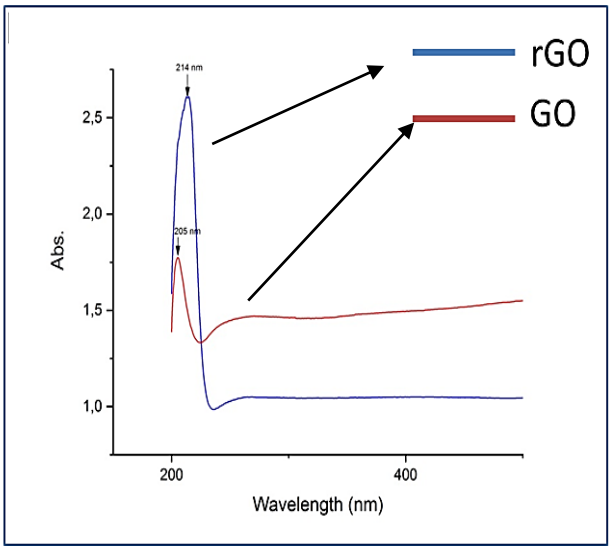

Fig 4.2.3: UV-Vis absorption spectroscopy shift of GO and RGO.

4.2.2.2 Thermogravimetric analysis (TGA)

To understand the stability of GO and RGO, thermogravimetric analysis (TGA) was done under nitrogen and GO in Figure 4.2.4 shows a significant weight loss (6.5 %) at 179.6 °C while little weight loss (1.2 %) is observed for RGO at this temperature. There is a probable evaporation of adsorbed water molecules at temperature below 180 °, leading to instability in the nature of GO. The significant weight loss between 179-300 °C is probably as a result of the decomposition of oxygenated functional groups (OFGs) to H_2O, CO_2 and CO gases [105].

The TGA of RGO shows a continuous weight loss with a relatively slow rate, revealing a higher stability compared to GO.

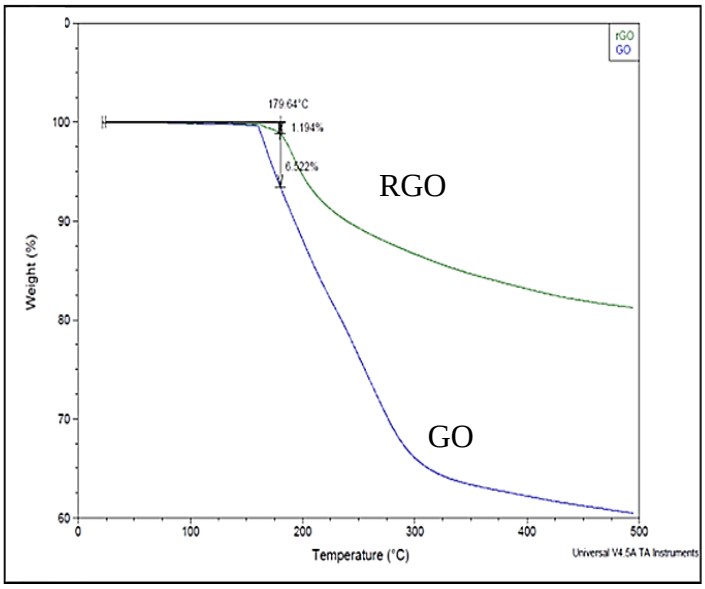

Fig 4.2.4: Thermogravimetric curves of GO and RGO.

4.2.2.3 X-ray photon spectroscopy (XPS)

Figure 4.2.5 (a) and (b) shows the deconvoluted XPS spectra of RGO and GO respectively. Binding energies of 284.5, 286.7, 287 and 288.5 eV present in the distribution of the peaks correspond to C=C, C-O, C=O and COO- functions respectively [106]. After chemical reduction of GO, there is peak reduction in the binding energies of the oxygenated functional groups of RGO as made obvious in Figure 4.2.5 (b). Figure 4.2.5 (c) shows the XPS spectra of GO and RGO. From the spectra, it is obvious that the peak intensity of O element present in RGO decreased having undergone chemical reduction on comparison with that of GO. After chemical reduction, the residual oxygen content of the total element is 23 % indicating that some oxygen containing functional groups are still present.

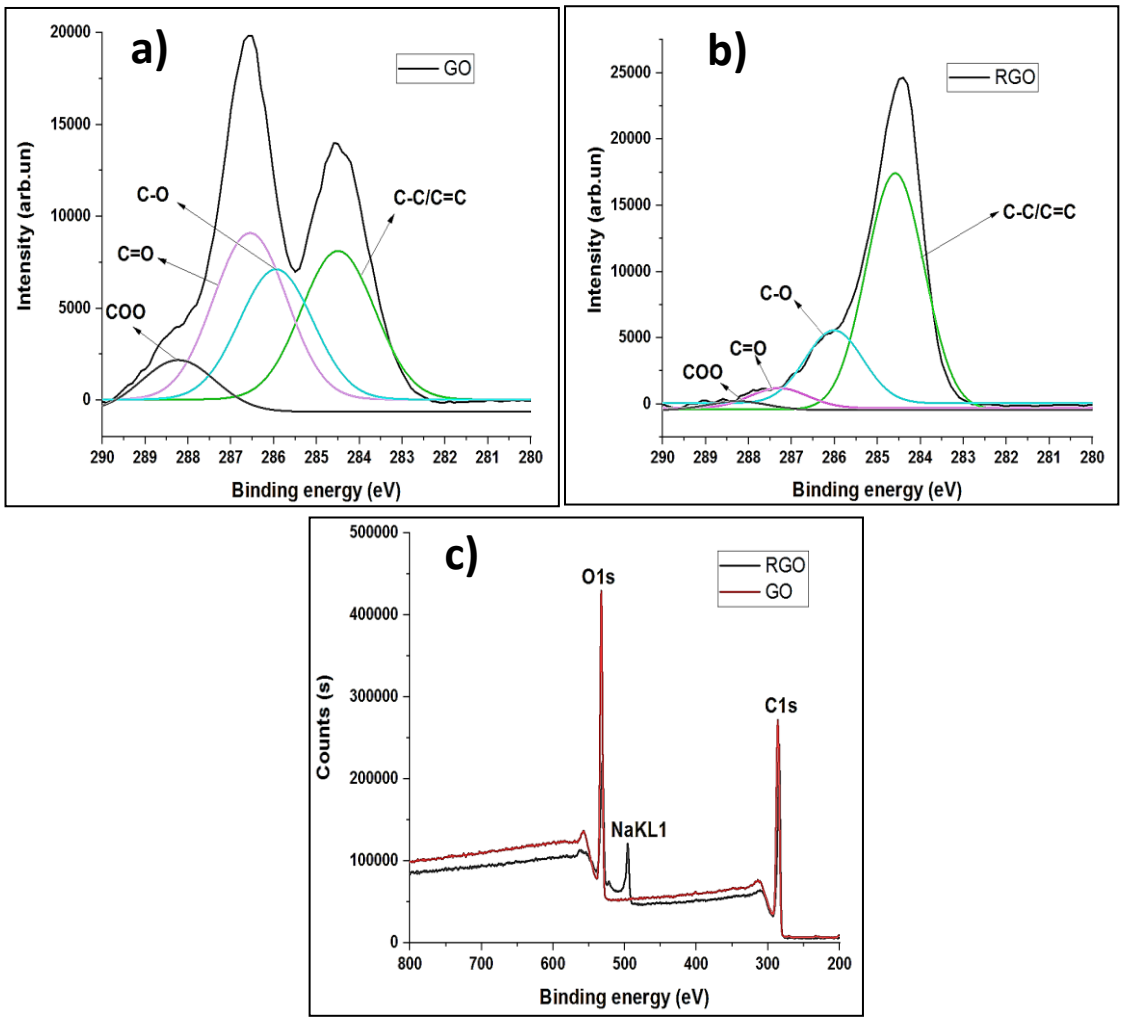

Fig 4.2.5: XPS spectra of C 1s peaks of (a) GO and (b) RGO (c) Whole spectra of GO and RGO

4.2.2.4 Textural properties of electrodes

In the present work, AC and AC/RGO-x (x = 5, 10, 15 and 20 wt. % of RGO) electrodes were synthesized for usage as active phases of CDI, and then there is a great interest to determine and compare their textural properties. Figure 4..2.6 gives the adsorption isotherms used to determine the main parameters expressed in table 4.2 The inclusion of PVDF in electrode synthesis possibly leads to a significant decrease in the specific surface area of AC from 1031±0.2 m^2 g^{-1} (initial value of AC used as precursor) to 474.6 ±0.2 m^2 g^{-1} for the electrode (table 4.2), On the other hand, the low specific surface area (SSA) or S_{BET} of GO and RGO is

due to the dense restacking of GO sheets as a result of van der Waal force between the layers and this factor consequently have negative effect on the effective surface area of RGO [106]

From Figure 4.2.6, AC and AC/RGO-x isotherms are similar to each other with a characteristic mesoporous property due to the sharp adsorption uptake between 0.1 and 1.0 relative pressure (P/P°) indicating a type II isotherm based on IUPAC classification [89, 107]. Also, based on the isotherm curves of the samples, a non-mutual curve arrangement was observed as shown in Figure 4.2.6; this could be due to additive effect on the textural properties of AC and this effect is independent on additive ratio. The textural parameters of AC and AC/RGO-x (different electrode values) collected are summarized in table 4.2 It is obvious that whatever is the RGO content in the composite, no significant effects on textural properties are observed. The synthesized RGO has a low specific surface area and a pore volume indicating its low porosity; a result in line with what is reported in literature [107]. The addition of additives at different proportion however do not have a significant reduction in the specific surface area of the pristine electrode; indicating good interaction that led to preservation of the specific surface area of AC by RGO sheets. Our result is in agreement with a study reported by Choi *et al*. [108]

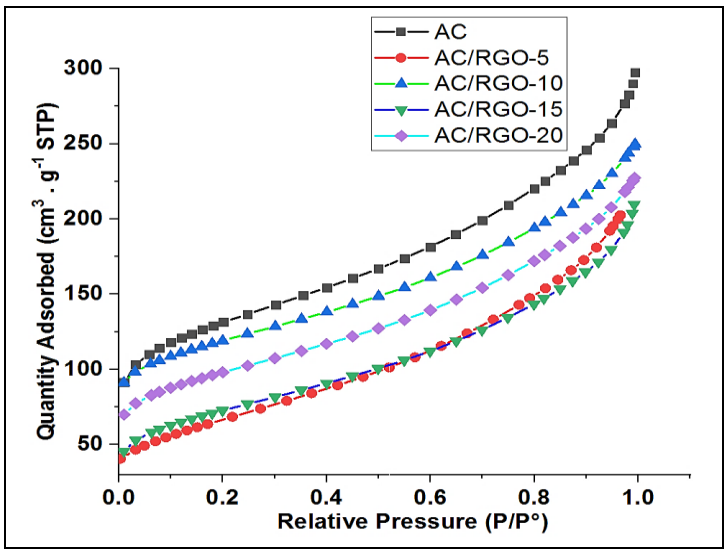

Fig 4.2.6: Isotherm linear plot of AC, and AC/RGO-x (where x = 5, 10, 15 and 20 wt. % RGO)

Table 4.2: Textural parameters of pure AC, AC electrode and AC/RGO-x (where x = 5, 10, 15, and 20 wt. % RGO) electrodes and the additive

Sample	**V_t ($cm^3 \cdot g^{-1}$)**	**S_{BET} ($m^2 \cdot g^{-1}$)**	**V_{MESO} ($cm^3 \cdot g^{-1}$)**
Pure AC	0.82	1031.03±0.20	0.55
AC electrode	0.46	474.6±0.20	0.40
GO	0.01	05.5±0.30	0.01
RGO	0.03	16.4±0.30	0.06
AC/RGO-5	0.41	374.4±0.20	0.30
AC/RGO-10	0.43	473.4±0.10	0.38
AC/RGO-15	0.40	434.1±0.20	0.33
AC/RGO-20	0.45	480.7±0.10	0.39

4.2.2.5 Electrochemical property

Electrochemical behavior of the pristine AC and composite electrodes were carried out using cyclic voltammetry (CV) at potential window of -0.4 – 0.6 V (to ensure electrochemical stability of the electrolyte and prevent water splitting i.e. oxygen and hydrogen evolution) and different scan rates in order to investigate the influence of the additive at different ratio. The experiment was conducted in 0.5 M NaCl aqueous solution. CV is an important technique carried out to understand the adsorption behavior and capacitive nature of carbon based materials.

CV curves show symmetrically pseudo-rectangular shapes with no obvious peaks indicating the capacitive behavior (Electrical double layer capacitors) [97]. By comparison of the CV curves of the composites with the pristine AC in Figure 4.2.7 (a), it is obvious that AC/RGO-5 exhibited largest area and current response. This shows that a little proportion of RGO (5 wt. %) is enough to improve the capacitive behavior of AC. The double layer capacitance was calculated from CV curves at different scan rates (2-10 mVs^{-1}) by taking into consideration

open circuit potential at 0.1 V vs. 3M KCl Ag/AgCl while specific capacitance of the materials was calculated by dividing the calculated double layer capacitance by the deposited mass of the electrode (Eq. 1, see chapter 3). Figure 4.2.7 (b) shows the linear plot of AC and the composites in which the positive and negative capacitive currents taken at 0.1 V vs. 3M KCl Ag/AgCl (OCP) is plotted against a range of scan rates (2-10 mV s^{-1}). The EDL capacitance (C_{DL}) is taken as the average of the absolute value of the slope of the linear plot of the charging and discharging currents fit to the data according to Eq. (1) (see chapter 3). The calculated EDL capacitance (C_{DL}) of all the electrodes is presented in Table 4.3. From the table, it can be seen that the dominating contribution of RGO at the ratio of 5 wt. % is more prominent in the electrochemical performance (highest C_{DL}) of AC/RGO-5 possibly due to the fact that the dopant level at this ratio offers a synergetic effect by creating a well interconnected network structure within the RGO sheets thus providing conductive bridge for AC that enables faster transport of ions to its pores. Although the specific surface area (SSA) of AC/RGO-5 is lower in comparison to other composites, yet its capacitance is higher; showing that SSA is not the only contributing factor for higher electrochemical performance.

Galvanostatic charge-discharge (GCD) was also performed to ascertain the reversibility nature of the electrodes. As shown in Figure 4.2.7 (c), the symmetrical triangular shapes of GCD without any form of deviation show clearly that the storage mechanism is dominantly EDL in nature and that all the electrodes are reversible. Additionally, the largest size of AC/RGO-5 under the curve corresponds or indicates its high specific capacitance [98].

In order to further understand the effect of the additive, electron mobility behavior of the electrodes was studied on a four probe system and in all cases, AC/RGO-5 possessed an overall electron mobility characteristic. The electron mobility values of AC, AC/RGO-5, AC/RGO-10, AC/RGO-15 and AC/RGO-20 are 48, 55.5, 44.10, 24.40 and 23.70 $cm^2/(V\text{-}s)$. Our result is similar to what is reported in literature [109, 110]. According to our result, AC/RGO-5 possessed a significant difference among its counterparts thus we opine that the dominating factor accounting for this electrochemical behavior might be due to the availability of electroactive species as a result of improved interconnectivity network structures at this ratio. Our result is in agreement with the report of Zhi *et al* [111].

Table 4.3: Calculated double layer capacitance (C_{DL}) and specific capacitance ($C_{Specific}$) for AC and AC/RGO-x electrodes

	AC	AC/RGO-5	AC/RGO-10	AC/RGO-15	AC/RGO-20
$\mathbf{C_{DL}}$ (F. cm^{-2})	0.29	0.89	0.74	0.49	0.65
$\mathbf{C_{Specific}}$($F.g^{-1}$)	32	74	48	29	50

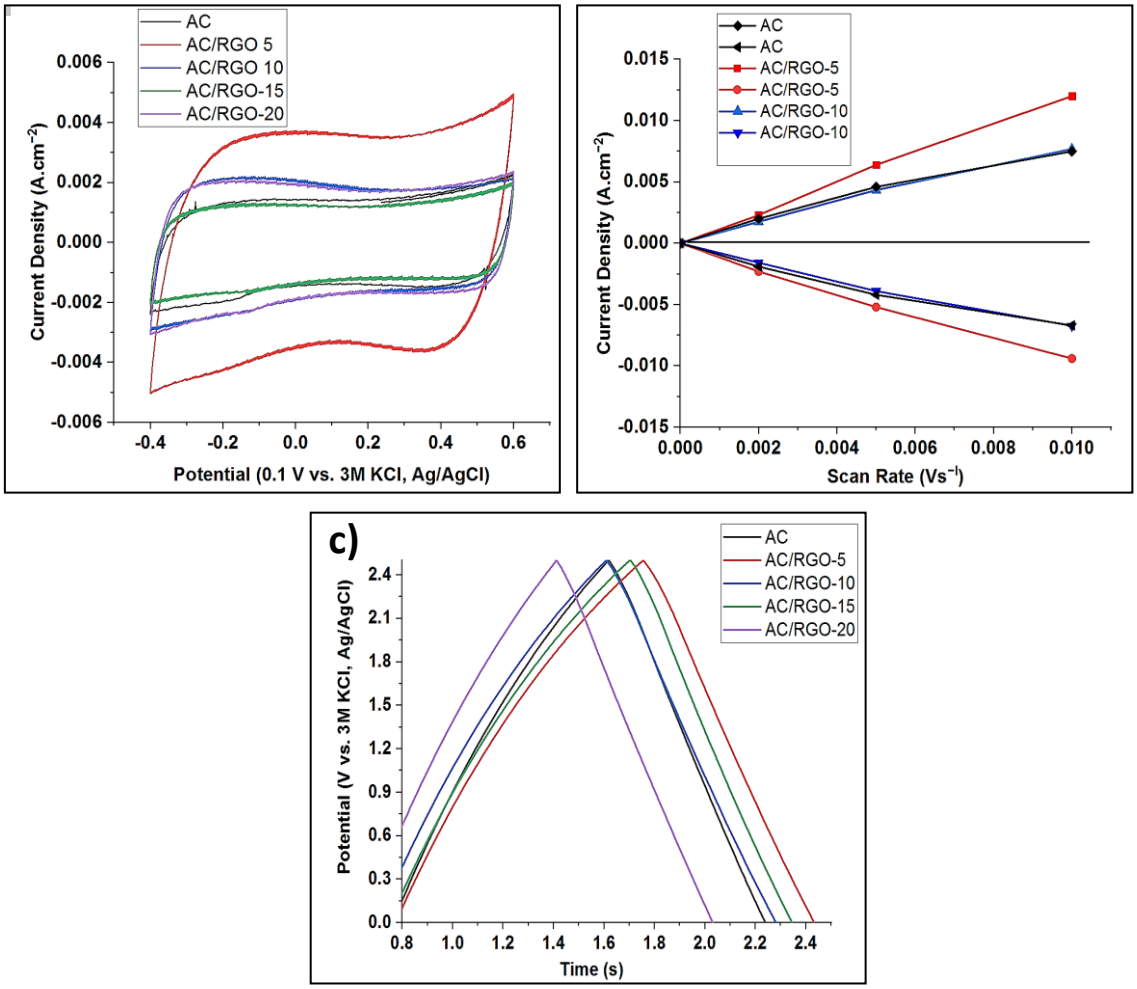

Fig 4.2.7: Cyclic voltammogram of (a) AC and AC/RGO-x at 2 mVs^{-1} (b) Plots of charging current (ref above 0 $A.cm^{-2}$) and discharging currents (ref below 0 $A.cm^{-2}$) against the scan rate (Vs^{-1}) for C_{DL} determination (c) Galvanostat charge-discharge (GCD) of AC and AC/RGO-x at 0.1 A**.** g^{-1}

AC/RGO composites of high specific capacitance using different approaches of RGO synthesis as against the method adopted by our group are found in literature [112-115]. Undoubtedly, the method of synthesis and thermal pre-treatment affect functionality (functional groups, textural and electrochemical properties) of carbon based materials [30]. Using thermally pre-treated AC, Lanshu *et al*. [112] reported electrochemical studies of free standing AC/RGO composites with an outstanding specific capacitance of 207 F g g^{-1}. Qiang *et al*. [113] synthesized a composite of ACF/RGO by electrospinning method and obtained specific capacitance of 193 F g^{-1} at the scan rate of 5 mV s^{-1}. Similar reports have been made by Haibo *et al.* [114] and Xin *et al.* [115].

4.2.3 Conclusion

As earlier discussed in this section, reduced graphene oxide (RGO) was synthesized and subsequently combined with commercial AC to influence its electrical properties. Based on the physico-chemical and electrochemical characterizations of the hybrid electrode materials, our findings showed that the conductance and electron mobility of the hybrid electrode at a particular ratio exhibited the most improved electrochemical properties. This behavior accounts for a synergetic effect of the additive in AC structure by creating a well interconnected network providing conductive bridge for AC thus enables faster transport of ions to its pores. However, the RGO tends to agglomerate due to the dense restacking of its sheets and as a result affects AC porosity and specific surface area but its presence nevertheless, offers improved electrical conductivity with AC structure at a certain level.

4.3 Introduction

As earlier explained in chapter 2, the inherent challenge of co-ion adsorption led to the invention of MCDI in which ion exchange membranes are aligned in front of each electrode to prevent undesirable attraction of ions carrying the same charge as the electrode. However, this variant technique did not overcome the fundamental challenge of discontinuous electrosorption process (alternative process of adsorption/desorption phases). Also, limitations of ions adsorption tend to arise as electrodes get easily saturated due to fixed surface area of contact between electrode and electrolyte. In order to overcome this challenges, flow electrode was improved in which carbon electrode is in constant flowing state thus allowing unlimited active sites for adsorption.

Although flow electrode offers unparalleled or exceptional desalination over conventional CDI/MCDI, the challenge of clogging at high carbon feed in the cell is a growing concern. As a result, most FCDI operation is limited to either low or moderate carbon loading. As a way of improving the adsorption capacity/salt removal rate of flow electrode at moderate loading (10 wt.% carbon electrode), we have for the first time verified the effect of ground commercial activated on its physico-chemical properties and tried to make a link on how this effect could improve its electrosorption. Also, we compared these properties with that of normal activated carbon.

4.3.1 Overview of superfine AC as viable flow electrode in FCDI

This section discusses the physico-chemical properties of superfine AC as a potential flow electrode. Here, we modified a bit the particle size of commercial activated carbon by ball milling process. This process enabled the grinding of large particles AC into generation of AC having smaller and finer particles hence the name superfine AC. The effect of mechanical grinding on the morphology, rheology, textural properties and other physical properties are discussed and most importantly, knowledge garnered in this aspect enabled us to evaluate the effect of this process on rheology in relation to desalination application is well detailed in the subsequent chapter 5.

Some of the results provided in this section will soon be been published in *desalination journal* **2021**, as below:

Investigation of superfine activated carbon as a viable flow electrode in capacitive deionization.

Gbenro Folaranmi, Myriam Tuak, Mikhael Bechelany, Philippe Sistat, Marc Cretin and Francois Zaviska

Institut Européen des Membranes, IEM, UMR-5635, University of Montpellier, ENSCM, CNRS, Place Eugène Bataillon, CEDEX 5, 34095 Montpellier, France ; gbenro.folaranmi@etu.umontpellier.fr (G.F.) ; philippe.sistat@umontpellier.fr (P.S.) ; marc.cretin@umontpellier.fr (M.C.)

4.3.2 Result and discussion

Physico-chemical properties of superfine AC and pristine or normal AC are discussed; effect of ball milling (grinding) on the particle size, morphology and textural properties of superfine AC in comparison to normal AC as flow electrodes is discussed as shown below:

4.3.3 Characterisation of superfine carbon electrodes in FCDI

4.3.3.1 Scanning electron microscopy (SEM)

The morphology of AC and superfine (SFAC) were examined by field emission scanning electron microscope (FESEM). As shown below in Figure 4.3 (a-d), the commercial AC is of no definite shape with presence of rough surfaces. Interestingly, there seem to be changes in the particle size of SFAC as its surface of SFAC becomes dominated with smoother particles as evident in Figure 4.3 (b) and (d). According to SEM, no significant observation can be seen concerning the texture of the materials.

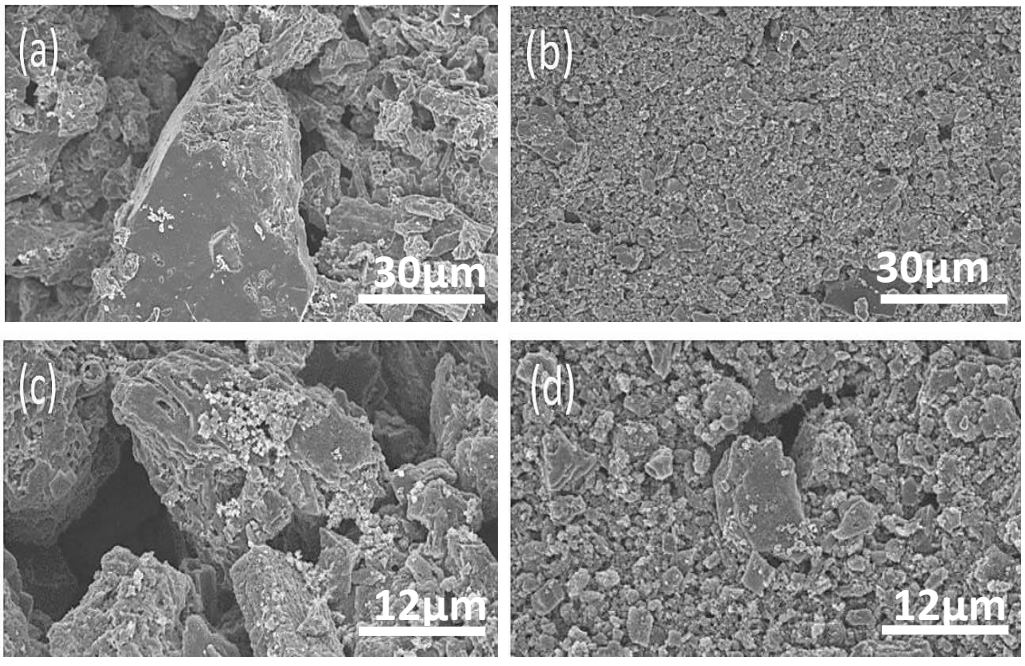

Fig 4.3: Field emission scanning electron microscope (FESEM) top view images of (a), (c) normal or pristine AC and (b), (d) superfine AC ground at 90 min.

Furthermore, the particle size of AC and SFAC was investigated by dynamic light scattering (DLS) at constant volume ratio to reveal the trend in particle size as grinding time increases. As shown in Figure 4.3.1, the result of DLS corroborates that of SEM in which pristine AC has largest particle size. From Figure 4.3.1, the particle diameter of AC and SFAC 30, 60 and 90 min was recorded to be 1.20, 0.70, 0.45 and 0.40 µm respectively

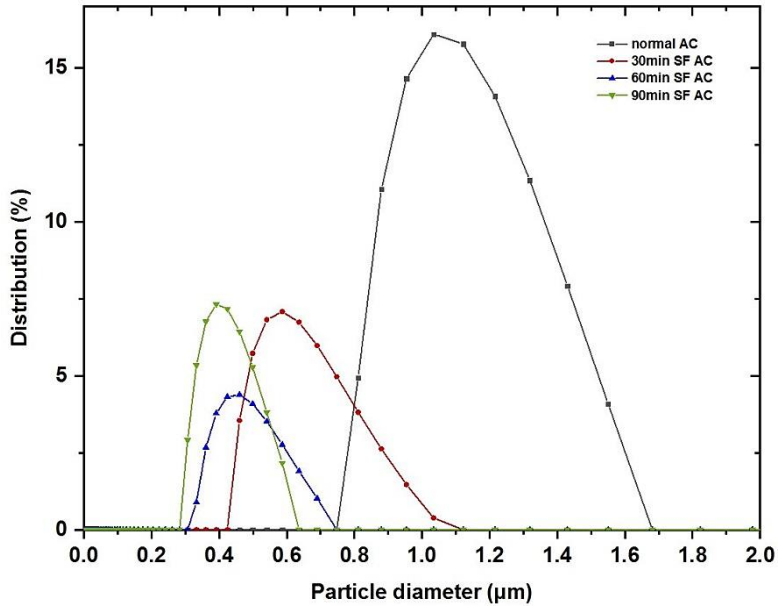

Figure 4.3.1: Particle size of AC and SFAC at 30, 60 and 90 min grinding respectively.

4.3.3.2 Structural properties

The structural properties of the samples were investigated by Raman and X-ray diffraction spectroscopy. Raman spectroscopy analysis was done to investigate the effect of grinding on the structure of the carbon lattice. All carbon materials have characteristics features at 1350 cm^{-1} and 1590 - 1610 cm^{-1} corresponding to D and G bands respectively. D band arises from a defect that is based on out of plane vibration structural while G band relates to the ordered structure of graphite crystals [89]. No Raman shift was observed in all cases as made evident in Figure 4.3.2 (a). Also, based on the values of intensity ratio ($R=I_D/I_G$)) which is used to observe the level of disorder in carbonaceous materials, SFAC showed no significant difference in defect on comparison with normal AC (SFAC, R = 1.2; normal AC, R = 1.0). This shows that grinding does not affect the structural arrangement in our carbon lattice.

XRD patterns of normal AC and superfine AC at all conditions do not show any significant change or shift in the interlayer spacing as shown in Figure 4.3.2 (b). They all demonstrated diffraction peaks of graphitic carbon at 2 Θ = 23 ° and 44 ° corresponding to 002 and 100 or 101 planes of graphite respectively. The sharp diffraction peaks at 002 indicates the presence of graphite microcrystalline structure [113]. No change was observed in the inter-planar distance of the materials; indicating that the integrity of the normal AC was preserved.

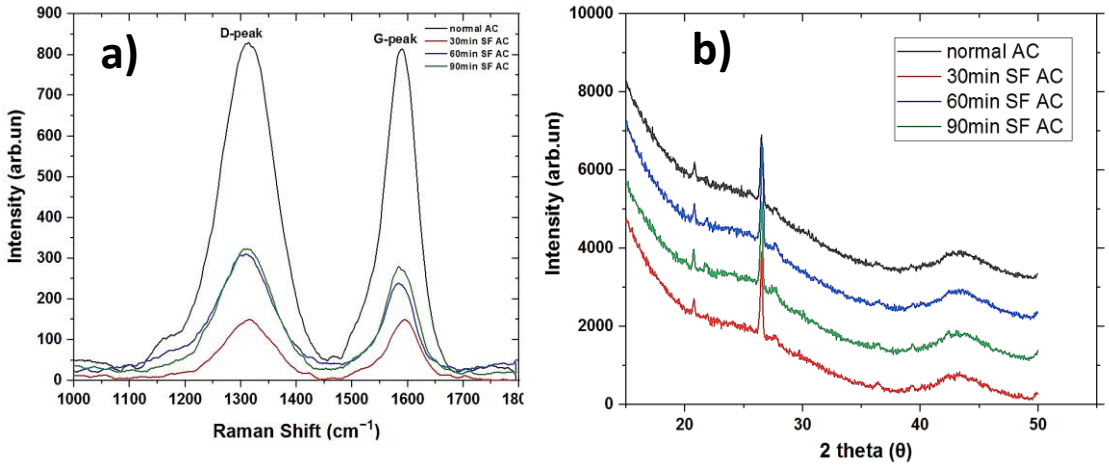

Fig 4.3.2: (a) Raman spectra and (b) XRD of AC and superfine AC at 30, 60 and 90 min respectively.

Also, chemical moieties or composition of AC and SFAC were investigated by FTIR and XPS. Figure 4.3.3 (a) shows the FTIR spectra of both normal AC and SFAC. The peak at 2925 cm^{-1} is associated with CH_3 bands [104] and the peak at 1490 cm^{-1} is due to the stretching of benzene ring [103]. The band at 2200 cm^{-1} can be assigned to N-N stretching [115, 116]. The peak at 1450 cm^{-1} is due to C–H stretching while the peak at 1022 cm^{-1} is associated with C–O bond from esters and ethers [117]. In all cases, there seem to be no obvious significant peak reduction in the functional groups of all the samples. This shows that the surface chemistry was preserved and grinding has no effect on it.

In the same vein, further probe by XPS showed no band reduction of the functional groups in SFAC on comparison to normal AC. Furthermore, and according to XPS analysis, the atomic percentage of both SFAC and PAC for C1s and O1s is the same (C1s = 94.80 %, O1s = 5.20 %). Figure 4.3.3 (b) shows the whole spectra of the samples while (c) and (d) shows the resolved C 1s spectrum of PAC and SFAC into their individual peaks respectively. Binding energies of 284.5, 285.8, 287 and 288 eV present in the distribution of the peaks corresponded to C=C, C-O, C=O and COO- respectively and no significant band reduction or increment was observed in the binding energies of the materials.

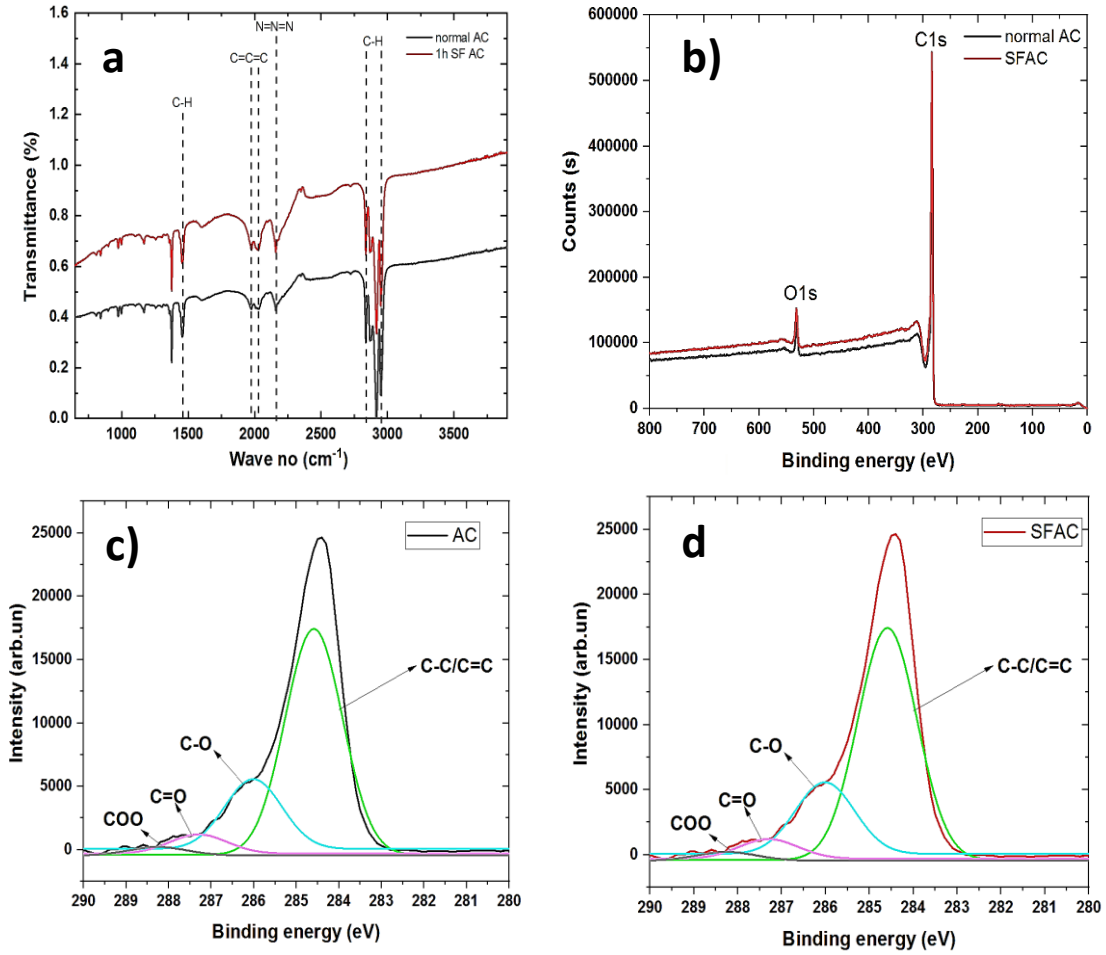

Fig 4.3.3: FT-IR spectra of (a) normal or pristine AC and superfine AC, (b) XI survey of pristine AC and superfine AC (c) and (d) Deconvoluted XPS spectra of C1s of normal AC and superfine AC respectively.

4.3.3.3. Textural Properties

The textural properties of AC and SFAC were verified and compared as presented in Table 4.4. No significant difference in effect of grinding was observed on the specific surface area of 30 and 60 min SFAC but at 90 min, an increase in the specific surface (SBET) of the material was observed. This could be due to the fact that greater percentage of less aggregated particles are present and making it more available for adsorption. Also, there could be generation of higher porosity at this grinding time. From Figure 4.3.4 (a), the isotherm curves of normal AC and SFAC are similar to each other with a sharp rise at above 0.1 and 0.8 relative pressure (P/P°); indicating a large presence of mesopores and typical type II isotherm based on IUPAC classification [90].

Pore size distribution which indicates the range of pores accessibility for a molecule or ions was used as shown in Figure 4.3.4 (b) to verify the region of ions adsorption in our carbon materials. Using BJH model and as indicated in Figure 4.3.4 (b); the pore size distribution of both AC and SFAC shows dominant adsorption characteristic at the mesopore region (2-50 nm).

Table 4.4. Textural parameters of AC and Superfine AC

Materiale	**V_t ($cm^3 \cdot g^{-1}$)**	**S_{BET} ($m^2 \cdot g^{-1}$)**	**V_{MESO} ($cm^3 \cdot g^{-1}$)**
Normal AC	0.67	839.3±0.40	0.47
30min SF AC	0.68	826.2±0.10	0.46
60min SF AC	0.66	817.3±0.10	0.47
90min SF AC	0.68	850.0±0.10	0.49

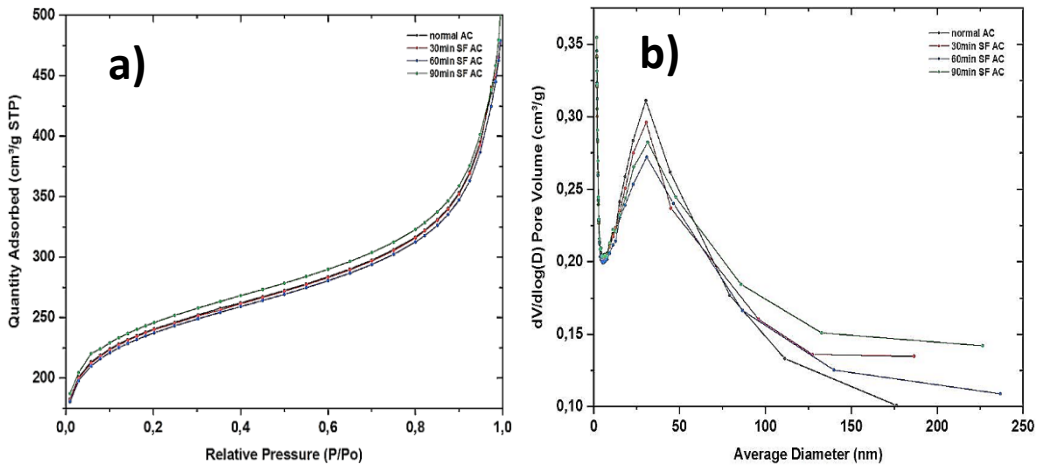

Fig 4.3.4: Nitrogen adsorption-desorption isotherm of (a) Normal AC and SFAC (b) Pore width distribution of normal AC and SFAC

4.3.3.4. Rheology properties and Zeta potential

Here we investigate the correlation between particle size, zeta potential and dynamic viscosity of the slurry. The dynamic viscosity of the slurry electrode was measured as a function of shear rate. Dynamic viscosity is the term used to describe resistance to flow of liquid while

shear rate describes the speed of deformation of the slurry under applied force. The dynamic viscosity was determined at a constant concentration of 10 wt. % carbon content in the slurry. From Figure 4.3.5 (a), it is obvious that the slurry follows the comportment of a non-Newtonian fluid (Shear Thinning effect) in which the viscosity of the slurry decreases with increasing shear rate [118]. Also, it can be concluded from Figure 4.3.5 (a) that viscosity of SFAC increases with increasing grinding. Reduction in particle size is associated with higher particle numbers thus with small particles, there tend to be increase in the number of intra-particle interactions and consequently an increase in resistance to flow; a dominating factor at low shear rate [119]. This effect becomes less significant as shear rate increases; intra-particle interactions become relatively less effective. Also, reducing particle size has a significant positive impact on surface area of contact between liquid and solid phases; resulting in additional energy dissipation due to friction hence increasing viscosity. As for normal AC, its lower viscosity is as a result of its high aggregation due to its large particle size. Also, viscosity decreases with increasing particle size distribution (PSD) [120] and as shown in Figure 4.3.1 normal AC exhibited the highest particle size distribution; this could account for its lower viscosity as grinding effect becomes more prominent. Particles possessing large distribution (high polydispersity) have high tendency to aggregate (pack) easily over the narrowly dispersed ones. This shows that suspension or dispersion with high poly-dispersed particles have free space for individual particle to move around with ease and as such, flow easily thus implying lower viscosity.

Zeta potential measurement is related to the charges of particles in dispersion or suspension. This factor is also associated with electrostatic repulsive forces between particles under the influence of electric field. An increase in this repulsive force (increase in zeta potential) prevents particles aggregation. Dispersion with high magnitude of zeta potential will induce a weak electrostatic attraction between particles and consequently a high viscosity of the slurry. Slurries prepared with low size particles are expected to have these characteristics as they are loosely bound (inter-particle interaction reduces as repulsive force increases; leading to increase in zeta potential). Furthermore, as the surface charge of particles increases due to increasing zeta potential, the thickness of the electric double layer (EDL) increases hence making room for higher ion adsorption (stable suspension with less aggregation) since the higher the thickness of the EDL, the higher the adsorption (assuming no pores blockage). Normal AC shows lowest potential due to aggregation as a result of large particle size; a result that is expected as shown in Figure 4.3.5 (b). For SFAC, as particle size decreases, the

dispersion slurries of these materials tend to be more stable due to increasing loosening of the particles thus there is high tendency of resistance to flow of particles and consequently yielding high zeta potential. This effect is predominantly more prevalent at lower shear rate which in turn leads to increase in viscosity.

In general, and from our experimental results, we can conclude that zeta potential increases with decrease in particle size and consequently, dispersion with lower particle size tend to be more stable as they are loosely bound thus leading to increase in viscosity and our result correlates with what is reported in literature [120-123].

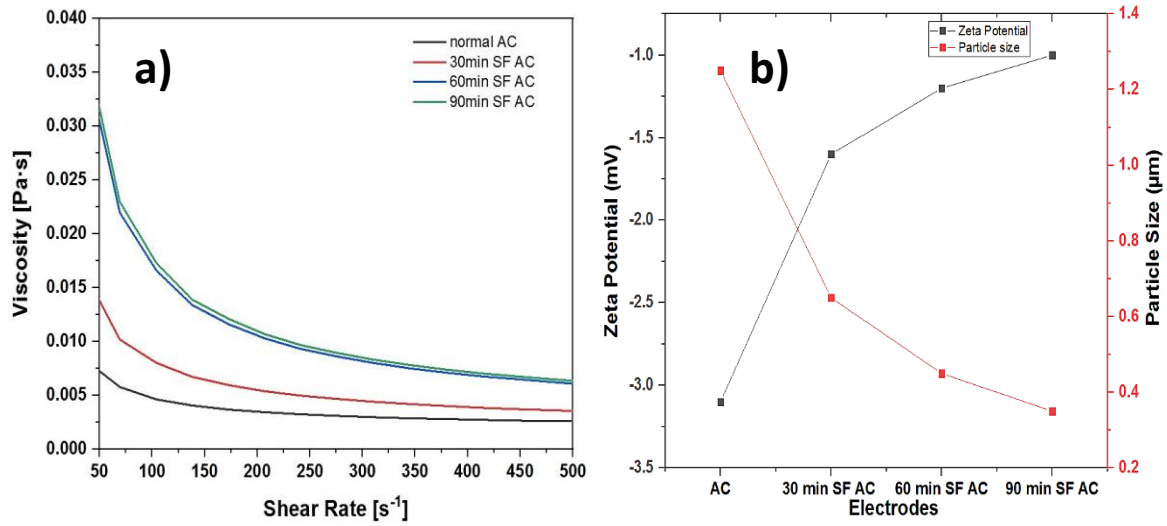

.

Fig 4.3.5: Rheological properties of AC and SF AC (b) Zeta potential of AC and SFAC

4.3.3.5. Reynolds number

The Reynolds number was calculated using equation (13) (see chapter 3) for the different slurry electrodes and the results are given in Table 4.5. The Reynolds number is observed to have been decreasing as from 60 min of grinding time for SFAC; a result that corroborates viscosity observation. From equation (6), lowest Reynolds number was calculated for 90 min SFAC, due to its lowest viscosity. In a similar study reported in literature by Peng *et al.* [73], the Reynolds number of their AC slurry at 20 wt. % was 0.122 while in our work, 10 wt. % was used and the Reynolds number is 0.07. Reynolds number relates to the level of flow pattern (turbulence or laminar) in fluid system. The calculated Reynolds numbers in all our carbon slurries as presented in Table 4.5. For a laminar flow, the Reynolds number is usually below 2,300 and when it is within the range of 2,300 and 4000; the pattern of flow is said to

be turbulent regardless of the nature of the fluid [74]. The Reynolds number, calculated using Eq (13, in chapter 3), shows that the prevalent flow pattern in our channel is laminar in nature thus implying that the carbon particles in the slurry flow along with the electrolyte solution in the flow channel of electrode compartment (no turbulence collision between carbon particles and current collector) thus we assume that the prevalent collision occurring in our system is Brownian motion; resulting in low charge transfer within the carbon slurry [74].

Table 4.5. Reynolds number of different feed electrode composition

Material	Reynold no
Normal AC	116.45
30min SF AC	84.59
60min SF AC	50.01
90min SF AC	47.99

4.3.4 Conclusion

In this section, the physico-chemical properties of superfine AC (SFAC) were verified by various characterization techniques. Grinding effect at different interval shows no significant change on the properties of SFAC and normal AC. However, a significant difference was observed in the dynamic viscosity of SFAC in comparison to normal AC. In furtherance for better understanding for this difference, zeta potential was done and a link between zeta potential and dynamic viscosity was established. As a result of this correlation, SFAC could offer a potential viability as a flow electrode but at the expense of viscosity. This is as a result of increase in zeta potential as force of repulsion existing among the particles increases thus making particles to separate further apart and consequently leads to increase in viscosity.

4.4 Overview on Activated carbon co-mixed electrospun titanium oxide nanofibers as flow electrode in capacitive deionization.

In this section, we intend verifying the stability of our slurry electrode/electric double layer capacitor (EDLC). For EDLCs and as earlier explained (in chapter 2), ions are stored in the EDL during adsorption phase in which significant amount of salty ions are removed when the electrodes are charged. Maximizing ion storage capacity of flow electrode is a key factor in overcoming resistance to ion transport. High impedance or resistance to ion movement within pore structure impedes or increase desalination time. To upgrade and prevent this limitation, it is necessary to develop hybrid flow electrodes relevant to facilitating ion transport through electrode/electrolyte interface. Here, we propose fabrication of hybrid flow electrodes through simple mixing with high surface charge additive to mitigate high resistance in flow electrode. These hybrid materials were evaluated through basic material characterizations and electrochemical techniques in order to understand and interpret the results in relation to capacitive improvement of the hybrid flow electrodes. Furthermore, the knowledge garnered from this study enabled the author to evaluate the effect of additive ratio on electrosorption behavior of the flow electrodes in the subsequent chapter 5.

Some of the results provided in this section is under review and will soon be published in *materials* as below:

Activated carbon co-mixed electrospun titanium oxide nanofibers as flow electrode in capacitive deionization.

Gbenro Folaranmi, Mikhael Bechelany, Philippe Sistat, Marc Cretin and Francois Zaviska

Institut Européen des Membranes, IEM, UMR-5635, University of Montpellier, ENSCM, CNRS, Place Eugène Bataillon, CEDEX 5, 34095 Montpellier, France; gbenro.folaranmi@etu.umontpellier.fr (G.F.); philippe.sistat@umontpellier.fr (P.S.); marc.cretin@umontpellier.fr (M.C.)

4.4.1 Result and discussion

In investigating the flow nanocomposites, the physico-chemical and electrochemical characterizations of the flow electrodes are discussed; effect of additive ratio on the morphology, dynamic viscosity and surface charge of the carbon electrode was verified and discussed as shown below:

4.4.2 Characterisation of carbon and nanocomposite carbon electrodes in FCDI

4.4.2.1 Scanning electron microscopy (SEM)

The morphology of as-synthesized titanium oxide nanofibers (TiO_2NFs), pristine AC and the composite electrodes ACTiO_2NFs-x are shown in Figure 4.4 (a-h) respectively. From Figure 4.4 (a), it is apparent that the electrospun TiO_2 showed fiber like morphology with no beads formation. This shows the successful nanofibrous morphology of TiO_2 formation by electrospinning process. Figure 4.4 (b) shows the morphology of pristine AC. It is clear that it has no defined shape with rough or uneven surface characteristics while Figure 4.4 (c-h) reveals the successful doping of TiO_2NFs on the surface of AC. It can also be seen that the nanofibers are well intercalated and anchored on the surface of AC especially from x=1.0.

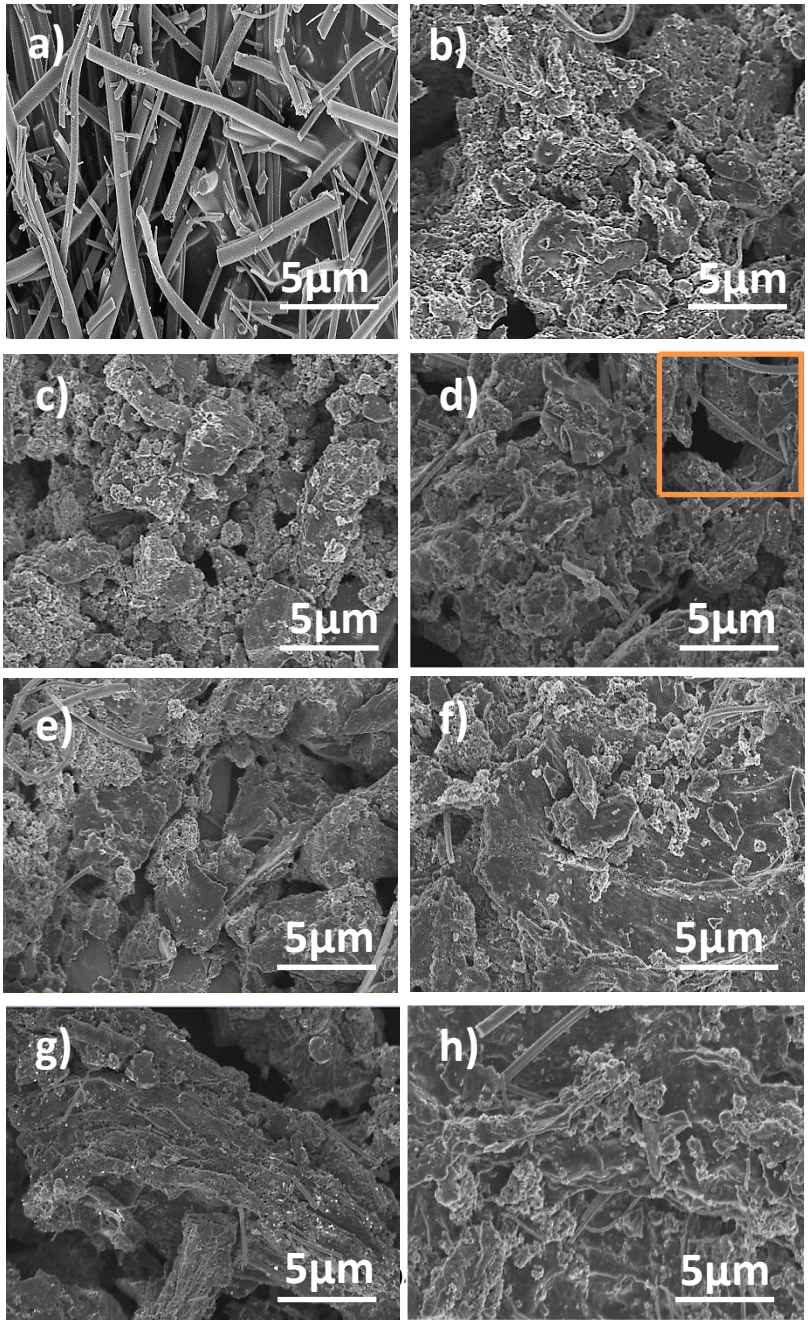

Fig 4.4: Field emission scanning electron microscope (FESEM) top view images of (a) TiO_2 NFs (b) AC (c-h) ACTiO_2NFs-x where (x = 0.5, 1.0, 1.5, 2.0, 2.5 and 5.0 wt. % TiO_2NFs) respectively.

4.4.2.2 Structural properties

Figure 4.4.1 (a) and (b) shows the Raman and XRD spectra of the TiO_2NFs, pristine AC and its composites respectively. The Raman spectra of the pristine AC and its nanocomposites in Figure 4.1.2.9 (a) conform to a typical graphitic carbon with distinguishable peaks at 1350 cm^{-1} and 1590 - 1610 cm^{-1} corresponding to D and G bands respectively [100]. D band arises from a defect that is based on out of plane vibration while G band relates to the ordered structure of graphite crystals [116]. For the as synthesized TiO_2NFs, Figure 4.1.2.9 (a), major peaks are observed at 142, 388, 516 and 638 cm^{-1} indicating anatase phase characteristics [124]. Distinguishable peaks of TiO_2NFs were observed in some of the composites especially for those with high percentage of TiO_2NFs as shown in Figure 4.1.2.9 (a). This indicates the successful intercalation of the nanofibers.

XRD investigation was carried out to understand the crystalline nature of the materials. Figure 4.4.1 (b) shows the XRD spectra of pure TiO_2NFs, pristine AC and its composites. The TiO_2NF crystals are predominantly dominated with definite and sharp diffraction peaks at 2 Θ = 25 ° 39 ° and 43.5 ° relating to 101, 004 and 200 planes of anatase phase respectively with presence of rutile phase at 2 Θ = 27.5 °, 36 ° and 41 ° relating to 110, 101 and 111 planes respectively [124]. Typical diffraction peaks of all graphite material is observed for pristine AC and its nanocomposites at 2 Θ = 26 ° and 43.5 ° corresponding to 002 and 100 or 101 planes of graphite respectively. The sharp diffraction peaks observed at 002 planes indicates the presence of graphite microcrystalline structure in the AC [116]. On comparison with pristine AC, peaks of TiO_2NFs were detected at 25 °, 27.5 ° and 48 ° diffraction peaks of TiO_2NFs in all the composites thus showing successful doping of the nanofibers in the AC. Furthermore, using Debye-Scherrer equation, ($D = K\lambda/\beta, \cos \Theta$) where K is the constant value of 0.9, λ is the radiation of the XRD machine (0.1541 nm), β is the full width at half maximum of the diffraction peak in radian and θ is the diffraction angle in radian, no changes were observed in the crystallite size of the as synthesized TiO_2 nanofibers, and the nanocomposites (10.21± 0.83 nm).

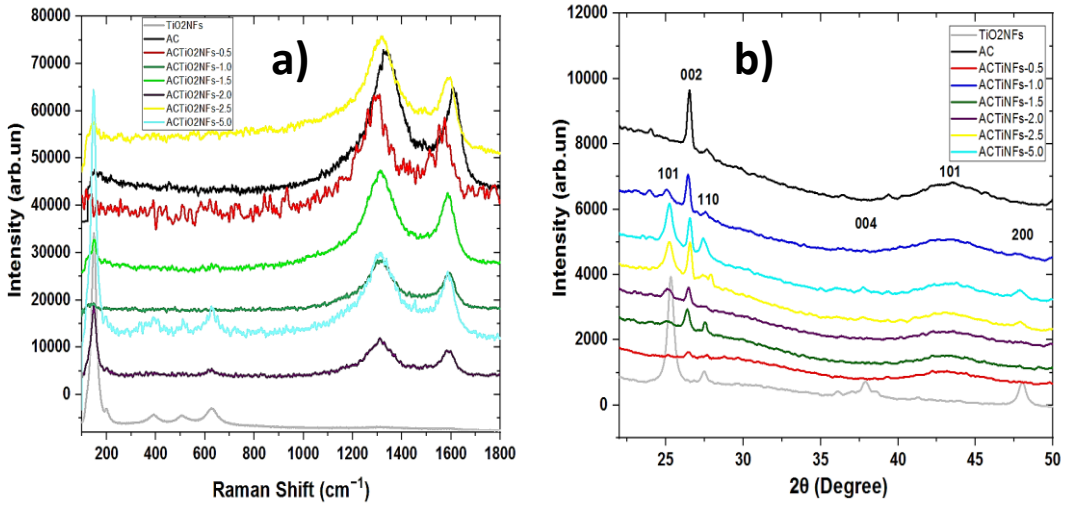

Fig 4.4.1: Raman spectra of a) Titanium oxide nanofibers TiO_2NFs and AC and its composites (ACTiO_2NFs-x) and X-ray Diffraction (XRD) of b) AC and its composites (ACTiO_2NFs-x)

4.4.2.3 EDX and XPS studies

Figure 4.4.2 (a) and (b) shows the energy dispersive X-ray spectroscopy (EDX) that was performed in order to identify the composition of the pristine AC and the composite electrode. Evidently from EDX, the elements detected at highest percentage in our materials are C and O. Titanium was detected among other elements in little quantity in the composite as shown in Figure 4.4.2 (b). The presence of Fluorine was also detected due to the addition of PVDF (binder) added in the course of electrode fabrication. Also, EDX mapping was further used to investigate the distribution of the additive in the nanocomposite structure. According to EDX mapping (appendix section), it can be seen that the additive distribution at lower concentration (1 wt. %) is homogenous (even dispersion) while at higher concentration (5 wt. %), its distribution is concentrated within a particular region. The results confirm the formation of well dispersed or good distribution of TiO_2NFs within the carbon structure at low percentage concentration.

Further investigation was carried out using X-ray photoelectron spectroscopy analysis in order to verify any change in the chemical composition of the pristine AC and its composites. Figure 4.4.2 (c) shows two prominent peaks at 458.69 and 464.44 eV belonging to to Ti $2P_{3/2}$ and Ti $2P_{1/2}$ respectively [125, 126]. From Figure 4.1.3 (c), it is shown that Ti (IV) is present in normal state in the composites due to the observed spin orbital splitting corresponding to 5.76 eV that is obtained between Ti $2p_{1/2}$ and Ti $2p_{3/2.}$ [126] As shown in Figure 4.1.3.3 (d), no Titanium was detected in the XPS spectra survey scan of the pristine AC on comparison

with ACTiO$_2$NFs; a complementary result with that of EDX. The O1s peak in the composite increased a little bit when compared to pristine AC due to the influence of oxygen content of the additive. According to XPS, the atomic composition of the ACTiO$_2$NFs-1.0 consisted of C1s 90.6±0.11 %, O1s 7.9±0.12 % while that of pristine AC is C1s 94 ±0.84 % and O1s 5±3.84 %.

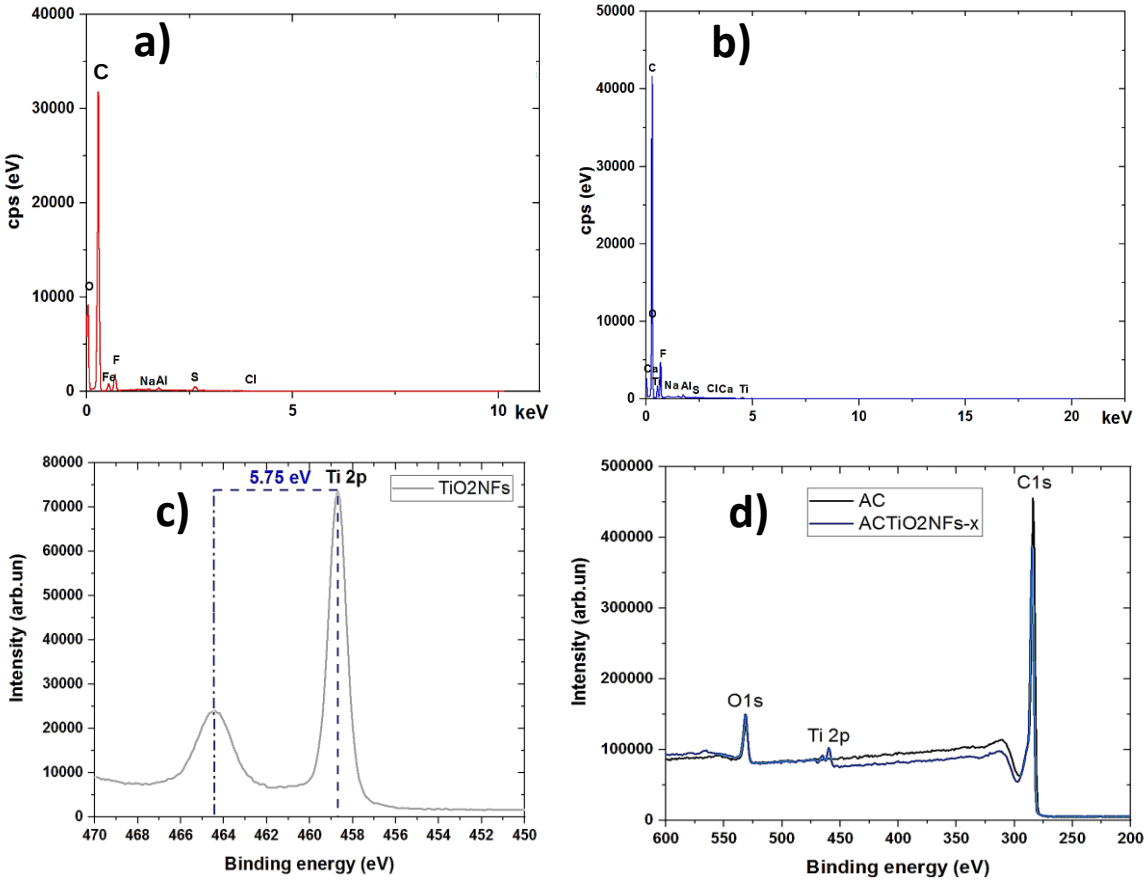

Fig 4.4.2: Energy Dispersive X-ray spectra of a) Pristine AC b) ACTiO$_2$NFs-x and X-ray photon electron spectroscopy of c) Ti 2p spectra of TiO$_2$NFs d) Spectra survey of the composite pristine AC and ACTiO$_2$NFs-.x where x = 1.0

4.4.2.4 Rheology study

Rheology property reveals the flow nature of the slurry used under applied force. The viscosity nature of the slurry electrode was measured as a function of shear rate. Here, rheology property is in terms of dynamic viscosity which is used to describe resistance to flow of liquid while shear rate describes the speed of deformation of the slurry under applied force. The viscosity of this experiment was carried out at a constant volume ratio of 10 wt. %. From

Figure 4.4.3 (a), it is obvious that the slurry follows a Non-Newtonian fluid (Shear Thinning effect) in which the viscosity of the slurries decreases with increasing shear rate [122]. To understand the effect of additive, the viscosities of both pristine AC and the nanocomposites were measured and compared. It is obvious from the rheogram curves that viscosity increases as the additive content increases in the composite. However, at low percentage of additive, there seems to be no significant difference in the viscosities of both the pristine AC and the composites but at i.e., TiO_2NFs ≥ 2.0 wt. %, a sharp increase in viscosity was observed. The increase in viscosity is possibly due to the factor of titanium nanofibers surface charge and concentration. The surface charge of the nanofibers (whether positive or negative) leads to creation of repulsive forces existing within the nanoparticles and as a result, they tend to move further apart due to strengthened force of repulsion; consequently, viscosity increases with increasing repulsive forces [121-123]. Therefore, as the concentration of the additive in the nanocomposite increases, a distinguishable jump in their viscosity was observed due to increase in force of repulsion as shown in Figure 4.4.3 (b). This implies that the presence of additive at high content level could lead to potential clogging of the feed electrodes in the cell.

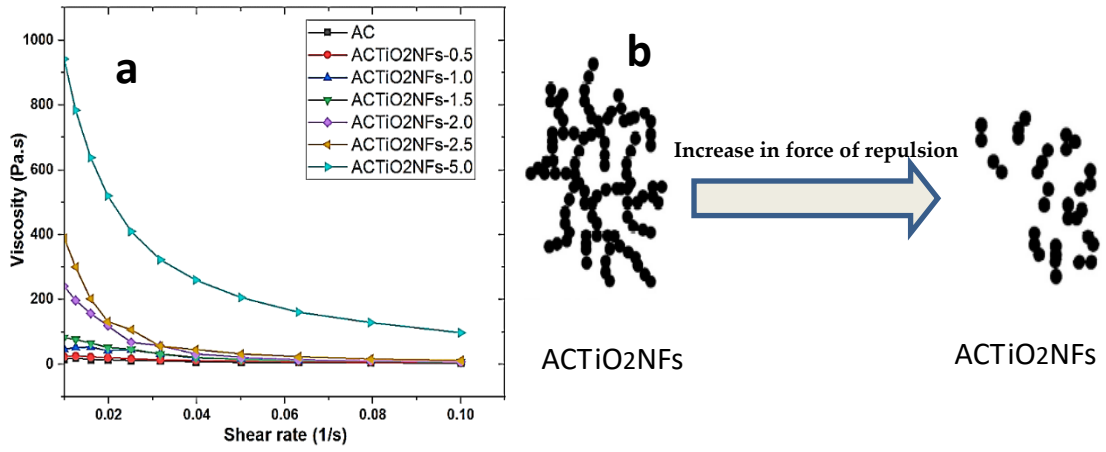

Fig 4.4.3 (a) Dynamic viscosities of pristine and nanocomposite flow-electrodes (b) schematic representation of effect of repulsive forces on the nanocomposite particles.

4.4.2.5. Electrochemical Properties

Electrochemical behavior of the pristine AC electrode and ACTiO_2NFs composite electrodes were carried out using cyclic voltammetry (CV) at potential window of -0.4 – 0.6 V (to ensure electrochemical stability of the electrolyte and prevent water splitting i.e. oxygen and hydrogen evolution) and different scan rates. The experiment was conducted in a solid state in 1 M NaCl aqueous solution to investigate the influence of the additive at different ratios.

Cyclic voltammetry (CV) is an important technique to probe the capacitive nature of EDLCs [97]. The CV curves of AC and ACTiO_2NFs-1.0 (see appendix for CV of other composites)) at 2 mVs^{-1} are shown in Figure 4.4.4 (a). At this scan rate, the composite (ACTiO_2NFs-1.0) exhibited obvious rectangular shape with no redox peak indicating ions adsorption phenomenon by electric double layer (EDL) formation. Also, the obvious rectangular shape at low scan rate further indicates the excellent capacitive behavior in which ions have enough time to migrate into the pores of the materials. However, as the additive content increases, (x $\geq$ 2.0 wt. % TiO_2NFs), there seem to be formation of pseudo-rectangular shape that is similar to that of pristine AC (as shown in appendix). This shows the poor capacitive nature of these composites even at low scan rate thus no significant improvement on the electrochemical behavior of the composites at high additive content. The effect of TiO_2NFs can also be seen in Figure 4.4.4 (a) in which ACTiO_2NFs-1.0 electrode demonstrated the largest area (charging and discharging area) under CV curve hence indicative of its outstanding electrochemical behavior. The CV results demonstrated an excellent reversibility in ion adsorption-desorption process. From the evolution of CV results, the optimum ratio of TiO_2NFs for AC doping is 1.0 %. From CV, it is observed that incorporating TiO_2NFs in low quantity into our carbon material enhances its double layer capacitance due to formation of uniform network distribution of TiO_2 nanofibers between AC particles. However, as the presence of TiO_2NFs increases in the composite, there seem to be exhibition of poor electrochemical behavior possibly due to increase in resistance to easy flow of ions into the pores of the electrode due to TiO_2NFs agglomeration. Our result correlate to the findings reported in literature [125-127]. Based on the average of the absolute value of the slopes of Figure 4.4.4 (b), the calculated EDL capacitance of the electrodes is shown in table 4.6. Furthermore, electrochemical impedance spectroscopy (EIS). was used to understand the interfacial resistance (impedance) that is developed during adsorption phase between the electrode and electrolyte. In EIS, solution resistance or ohmic resistance (Rs) is the beginning of the semicircle line at Z^i (at high frequency, intercept at real axis) and it is the resistance of the solution or electrolyte in use. The internal or intrinsic resistance (charge transfer resistance) of the electrode marks the end or termination of the semicircle (low frequency, intercept at Zi real axis). Warburg diffusion at middle frequency region relates to the ease of diffusion of ions into the pores of the electrode or material while the capacitive behavior of the material is represented at low frequency range [98]. As seen in Figure 4.4.4 (c), the lower ohmic resistance was observed for the nanocomposite to be 1.3. ± 0.31 Ω while pristine AC has 1.5 ± 0.20 Ω. Also, the nanocomposite possessed a smaller semi-circle diameter (interfacial

charge transfer) which reveals its lower interfacial resistance and consequently, leading to an efficient ions transport and faster diffusion into its pores thus its high capacitive behavior which is represented by its almost straight line in low frequency region. The EIS parameters obtained from constant phase element (CPE) equivalent circuit fitting of the Nyquist plot which is presented in table 4.6 shows that our materials do not exhibit the behavior of a pure capacitor due to its low phase change values (Q_2) unlike pure capacitor with a phase value of 1.0

Table 4.6. Electrical double layer capacitance (C_{DL}) of AC and $ACTiO_2NFs$-1.0 electrodes.

Material	C_{DL} ($F.cm^{-2}$)
AC	0.40
$ACTiO_2NFs$-1.0	0.96

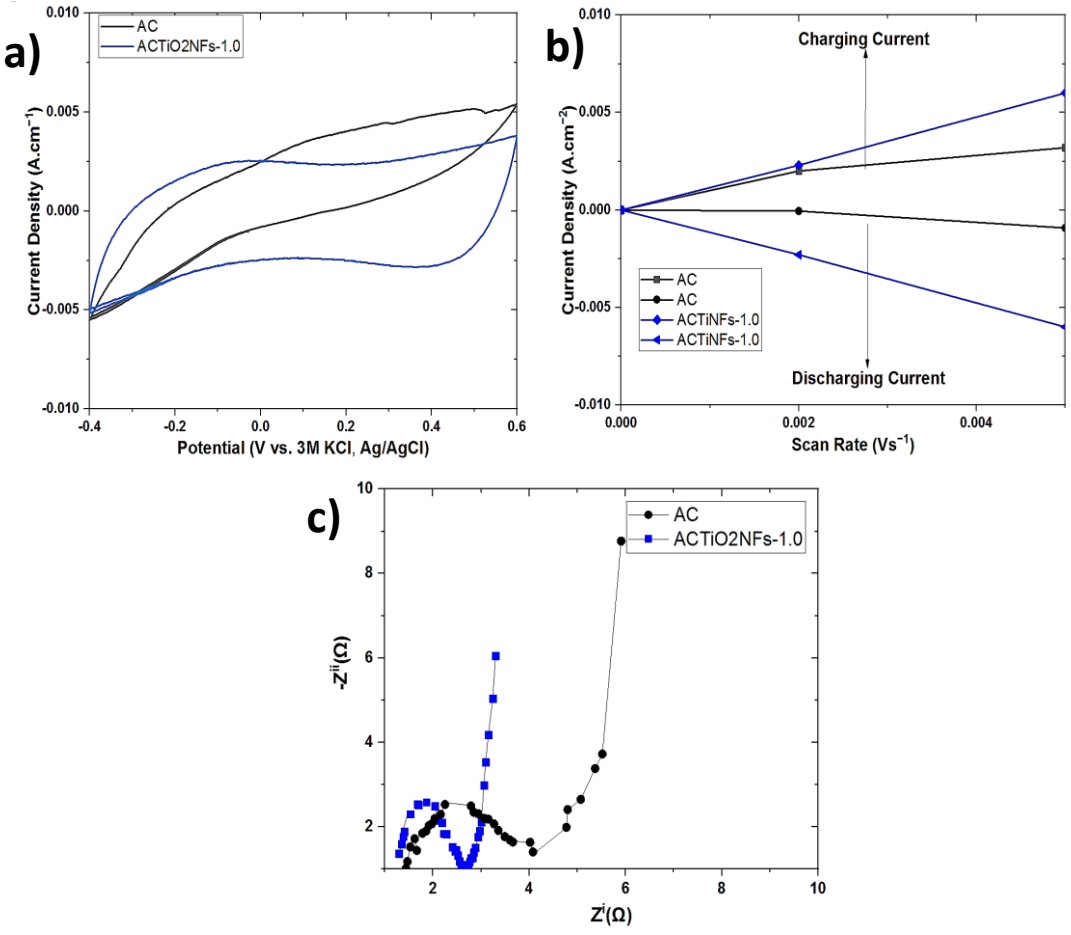

Fig 4.4.4: (a) Cyclic voltammetry curve of AC and ACTiO$_2$NFs-x composite electrodes at the scan rates of 2 mVs^{-1} (b) Double-layer capacitance voltammetry measurements for AC and ACTiO$_2$NFs-1.0 composite electrode. Cyclic voltammetry was measured in a non-Faradaic region (0.1 V) of the voltammogram at low scan rates of 2 mVs^{-1}. The charging current (ref current density above 0 A) and discharging currents (ref current density below 0 A) plotted as a function of scan rate (Vs^{-1}). The determined double-layer capacitance of the system was taken as the average of the absolute value of the slope of the linear fits to the data [97, 98] (c) Nyquist plot of AC and nanocomposite ACTiO$_2$NFs-1.0 in 1 M NaCl aqueous electrolyte.

Table 4.6. EIS parameters from Nyquist plots

Electrode material	R_1 (Ω)	R_2 (Ω)	W (mS)	Q_2 (mS)
AC	1.7±0.21	4.1±0.11	228.07±0.27	0.25±2.80
ACTiO$_2$NFs–1.0	1.5±0.17	2.60±0.22	255±0.18	0.38±1.10

R_1: Ohmic resistance, R_2: Charge transfer resistance, W: Warburg diffusion, Q_2: Phase change.

4.4.3 Conclusion

In this section, the physico-chemical and electrochemical properties of pristine AC and its hybrid nanocomposite electrodes were fabricated and characterized. From the characterizations of the materials, the presence of nanofibers at a low level on the surface of AC offers a network structure that reduces nanofibers particle agglomeration thus fast-tracking ion migration and impeding resistance in the carbon pores according to EIS characterization. Also, the high surface charge of the nanocomposites leads to high repulsion of the nanocomposite particle and consequently, leads to increased viscosity.

4.5 General Conclusion and Summary

Regarding the morphology of the commercial activated carbon, SEM observation shows that its pores is of no defined shape (neither rod like, cylindrical or bead shape) with a characteristic rough surface and from SEM evolution, its porosity cannot be ascertained. However, its textural properties such as the BET surface area of the carbon material, pore size distribution and total pore volumes were obtained through N_2 adsorption-desorption isotherms. From this investigation, it was observed that the material is mesoporous in nature

and this portion mainly accounts for the EDL development that is necessary for the temporary storage of ions in carbon pores. Also, a significant change in the BET surface area of the pristine AC was observed upon PVDF addition. A mass ratio of 1:8 (12.5 wt. % PVDF) of PVDF to AC was used in the CDI aspect of this work. Furthermore, the surface functional groups of the carbon and its hybrid forms were identified and the consequent of this is further elaborated in the following page (chapter 5).

A well detailed data collection regarding its structural properties were elucidated via RAMAN and XRD and in all cases, the carbon is of high level of defect and amorphous in nature with low graphitic development. Although, exhibit of micro-crystallinity is observed in commercial carbon (AC DARCO) that is used as electrodes in FCDI.

Cyclic voltammetry (CV) measurements at OCP (ref 0.1 V) region using aqueous electrolyte enabled us to calculate the specific and double layer capacitance of the carbon electrode and ascertained the reversibility of the non-Faradaic adsorption process. Also, electrochemical impedance spectroscopy (EIS) revealed the ohmnic and intrinsic resistance of our materials. The outcome of the electrochemical parameters is better explained in chapter 5.

To further improve the desalination performance of the carbon, FCDI architecture using flow electrode was employed. Reynolds numbers of the slurry electrodes were also calculated. It is believed that slurry electrode dispersion within the FCDI flow channel allows unlimited surface area of contact and positively affects desalination due to non-saturation of carbon pores for adsorption.

In summary, solid and flow carbon electrodes were fabricated and characterized by physico-chemical and electrochemical techniques. For solid electrodes, to overcome some challenges of low wettability in AC, it was combined with graphene oxide (GO). Regarding the properties of this composite electrode i.e., through low temperature N_2 adsorption desorption isotherms, the specific surface area of the carbon materials, pore size distribution and pore volumes were obtained and evaluated to show that GO addition has a profound effect on the specific surface area of AC (reduction in specific surface area) but through XPS, we verified that the attachment of oxygenated functional groups (OFGs) conferred on AC enabled easy transport of ions to the pores of AC and consequently offer stable and better EDL formation; this claim was ascertained through CV. More so, it was observed through XRD that the pristine AC is amorphous in nature and its crystallinity was not improved by addition of

crystalline GO. Also, the high wettability of the composites was verified through WCA measurement.

Furthermore, hybrid composites of AC combined with reduced graphene oxide (RGO) were fabricated and characterized. Pristine AC was combined with RGO in order to influence its electrical conductivity. RGO was used as an additive due to its high electrical conductivity. We synthesized the RGO through a simple reductive green method using KOH and it was thereafter characterized. It was observed through SEM and N_2 adsorption desorption isotherms that the synthesized RGO was of low porosity (low pore volume and specific surface area) and highly compacted in structure (agglomerated) possibly due to the dense restacking of GO sheets as a result of van der Waal force between the layers and this factor consequently have negative effect on the effective surface area of RGO. Comprehensive material characterizations i.e., FTIR and XRD of the composite electrodes revealed successful incorporation of RGO into AC. Also four-point probe data collection on the resistivity, conductance and electron mobility of the composites showed the influence of RGO on pristine AC in which the resistivity of the hybrid composites was reduced (conductance improvement) and electron mobility increased.

Regarding the prototype of CDI, we have designed a novel CDI cell called FCDI in which slurry carbon is used as flow electrodes. The properties of these flow electrodes are well studied and thereafter applied in desalination application. First, we validate a novel carbon material as flow electrode. This novel material called superfine AC (SFAC) was made by simple ball milling (grinding) of AC. Reduction in particle sizes of the superfine carbons were verified through dynamic light scattering technique (DLS particle analyzer) and the effect of particle size reduction on dynamic viscosity of these new materials was also confirmed. Furthermore, a link between dynamic viscosity and zeta potential was established. Also, SFAC flows as much as possible as pristine AC at moderate weight percentage. Physical characterizations such as XRD, Raman, XPS of this novel materials shown no significant change in comparison with pristine AC but according to SEM, surface of SFAC is smoother.

Lastly through electrospinning process, we synthesized titanium nanofibers (TiNFs) and mixed it with AC to fabricate hybrid flow electrode of high surface charge. TiNFs was co-mixed with pristine AC to influence ion mobility into its pores by reducing resistance. Water being a major component of flow electrode constitutes to its high resistivity and as such, we tried to reduce this phenomenon by TiNFs incorporation into AC network. Result by SEM

showed successful intercalation of TiNFs across AC structure. Also, Raman and XRD further revealed successful presence of the additive in AC. We further extend our investigation into the transport properties of these hybrid flow electrodes using CV and EIS. From be obtained results, it was observed that high affinity of ion permeability and diffusion into the pores of the hybrid flow electrodes increased for hybrid flow electrode with low percentage of TiNFs (at 1 wt. %).

In the subsequent chapter (chapter 5), we comprehensively elucidated the effect of the properties of both solid and flow electrodes on their application as desalination electrodes.

Chapter 5 Experimental investigation of Electrosorption in CDI/FCDI

5.1 General Introduction

CDI is a fast growing electrochemical water desalination technique which employs porous carbon electrodes (electric double layer capacitors, EDLCs) to extract salt ions from brackish solution. Conventionally, CDI comprises two porous carbon electrodes separated by a separator that is dielectric in nature. Potential difference of around 0.8-1.4 V is applied across the porous electrodes, causing ions to electrostatically migrate to the oppositely charged electrodes and be held at an interface developed between the electrode and electrolyte (EDL) in the pore surface.

In this chapter and for CDI experiments, the cell architecture of the CDI used is a flow-by architecture (see chapter 3, Figure 3.0) in which feed water (brackish solution) flows between the two charging porous electrodes and through the separator.

In this chapter, the desalination performance of Capacitive Deionization (CDI) and Flow Capacitive Deionization (FCDI) was studied for a wide range of salt compositions. The detailed data collection for simulated sodium chloride solution employed in this project enables the author to understand the electrosorption behavior of the state of the carbon electrodes (pristine and modified) in the different techniques (set-up). As expected, the modified electrodes showed salt adsorption improvement and charge efficiency in both CDI and more enhancement in FCDI. More so, the enhancement in the modified carbons and through FCDI shows significant importance of surface modification and effect of change of state of the electrodes with respect to ion transport. In all cases, a sharper drop in ion concentration curve is always observed during desalination process and this phenomenon can be attributed to the ease of transport of ions to the stable EDL formation in the carbon pores thus enabling better temporary storage of ions.

The first section of this chapter discusses the desalination performance of modified solid based electrodes in comparison to the pristine AC while the second section discusses a new form of AC as a viable flow electrode.

5.2 Overview on desalination performance of solid electrode using pristine AC modified with graphene oxide (GO) in CDI

To understand the effect of GO on AC and draw a link between its outstanding electrochemical performance and electrosorption, we have in this section tried to understand

the mechanism of ions capture in solid based electrodes by using CDI device to follow the progress of electrosorption behavior between commercial AC and its modified form. By correlating electrochemical measurements of the capacitance with measurements of electrode electrosorption, we hope to elucidate the relationship between the wettability nature of the electrode and its potential propensity for capacitive deionization.

Some of the results provided in this section have been published in *Materials* **2020**, 13, 5185 as below:

Comparative Investigation of Activated Carbon Electrode and a Novel Activated Carbon/Graphene Oxide Composite Electrode for an Enhanced Capacitive Deionization

Gbenro Folaranmi, Mikhael Bechelany, Philippe Sistat, Marc Cretin and Francois Zaviska

Institut Européen des Membranes, IEM, UMR-5635, University of Montpellier, ENSCM, CNRS, Place Eugène Bataillon, CEDEX 5, 34095 Montpellier, France; gbenro.folaranmi@etu.umontpellier.fr (G.F.); philippe.sistat@umontpellier.fr (P.S.); marc.cretin@umontpellier.fr (M.C.)

Abstract

Capacitive deionization is an emerging brackish water desalination technology whose principle lies in the utilization of porous electrodes (activated carbon materials) to temporarily store ions. Improving the properties of carbon material used as electrodes have been the focus of recent research, as this is beneficial for overall efficiency of this technology. Herein, we have synthesized a composite of activated carbon/graphene oxide electrodes by using a simple blending process in order to improve the hydrophilic property of activated carbon. Graphene oxide (GO) of different weight ratios was blended with commercial Activated carbon (AC) and out of all the composites, AC/GO-15 (15 wt. % of GO) exhibited the best electrochemical and salt adsorption performance in all operating conditions. The as prepared AC and AC/GO-x (x = 5, 10, 15 and 20 wt. % GO) were characterized by cyclic voltammetry and their physical properties were also studied (as shown in chapter 4). The salt adsorption capacity (SAC) of AC/GO-15 at an operating window of 1.0 V is 5.70 mg g^{-1} with an average salt adsorption rate (ASAR) of 0.34 mg. g^{-1} min^{-1} at a 400 mg L^{-1} salt initial concentration and has a capacitance of 75 F g^{-1} in comparison to AC with 3.74 mg g^{-1} of SAC. This approach could pave a new way to produce a highly hydrophilic carbon based electrode material in CDI.

Keywords: electro-sorption; electrode; activated carbon and graphene oxide

5.3 Results and discussion

Electrosorption behavior of AC and modified AC is discussed. The effect of additive is further elucidated and rationalized as shown below:

5.3.1 Comparative Electrosorption capacity of pristine AC and its modified form

Introduction

As known, one of the major factors governing the performance of the CDI is the electrode materials used for the process [125, 126] therefore a great deal of effort is focused on improving this material aspect. Research in this area has focused on improvements in terms of carbon precursors through processes such as composite formation (hybridization), oxidation (for surface chemistry improvement), etc.

Hybrid composites of activated carbon offering higher performance (electrosorption) outcomes have been reported in literature [127-132] but herein, as a matter of diversification, we have successfully combined the properties of AC and graphene oxide (GO) to form hybrid composites in order to improve electrode wettability and consequently studied the electrochemical and electrosorption effects of this process. We note here that there are limited reports focusing on this area, as most wettability processes involving CDI focus on carbon oxidation [40, 41].

GO has been used for improving the hydrophilicity of many materials such as a zeolitic imidazole framework [133], membrane bioreactor [134] and cotton fabrics [135], but this application of GO in CDI can be scarcely found in the literature [136], as most research in this area is focused on GO reduction to graphene for applications in electronic improvement of AC [129-136].

Motivated by this, we have prepared a highly hydrophilic activated carbon doped graphene oxide by using a simple blending process to improve the wettability of AC. To reach the best compromise, (Here, the compromise is between reduction in specific surface area and ease of pores accessibility by solvated ions) activated carbon doped graphene oxides of different compositions were synthesized and labeled as AC/GO-x, where x represents the weight percentage of GO in the composite (x = 5, 10, 15 and 20). The electrochemical properties of the prepared electrodes (AC, AC/GO-x) were analyzed by using cyclic voltammetry as shown

in Chapter 4; afterwards, the most efficient electrode was tested in comparison with pristine AC in the home made CDI cell.

5.3.2 Simulated Feed solutions containing different concentrations

To probe the comparative ion adsorption efficiency of the pristine and modified carbon electrodes, 400 and 1200 mg L^{-1} solutions of simulated NaCl were fed to the CDI cell in a batch mode phase. Figure 5 (a) shows the concentration variation over three cycles in CDI. Close inspection of Figure 5 (a) reveals a sharp decrease at the beginning of each adsorption step, and as regeneration steps occur (desorption phase) at zero voltage, there is release of the stored ions (brine generation). Consequently, when the cell voltage is re-applied during the subsequent adsorption step, the congruent cycle is repeated.

Electrosorption test was verified by supplying NaCl solution of 400 and 1200 mg L^{-1} at a constant flow rate of 25 $mL.min^{-1}$ after applying a cell potential of 1.0 and 1.4 V for few minutes per cycle to the CDI cell as mentioned above. Three symmetrical cycles of adsorption/desorption were obtained, as shown in Figure 5 (a, b). The adsorption capacity of the composite AC/GO-15 was measured under the same conditions (400 and 1200 mg L^{-1} NaCl at the operating voltage of 1.0 and 1.4 V) with that of the pristine AC electrode. As shown in Chapter 4, AC/GO-15 possessed an outstanding electrochemical property when compared to its counterparts thus it was chosen as the electrode of interest, and its propensity for salt adsorption capacity was determined in comparison to pristine AC electrode. The introduction of GO into AC undoubtedly improved its hydrophilicity, resulting in an enhanced surface interaction of solvated ions into the pores of the composites, thus yielding a faster rate of salt adsorption (Figure 5 c) and a better charge transfer, as shown in Figure 5 (d). The salt adsorption capacity of AC/GO-15 was 5.70 mg g^{-1} while that of the AC electrode was 3.4 mg g^{-1} at 400 mg L^{-1} NaCl under an operating voltage of 1.0 V. As found in literature, Table 5 gives detailed information of the adsorption capacity of a modified hydrophilic AC electrode/doped GO electrode in CDI operation.

Other CDI operating performance matrices of these experiments under all operating conditions are presented in Table 5.1. In all cases, the AC/GO-15 showed an overall performance increase over AC.

Table 5: Electrosorption behavior of oxidized carbon based electrode in CDI as found in the literature.

Material	Adsorption capacity ($mg.g^{-1}$)	Efficiency (%)	Capacitance ($F.g^{-1}$)	Voltage (V)	References
OAC	-	15.00	73	"	40
GO/ZrO2	4.55	-	-	1.20	63
N-Doped Ti/G	9.20	98	157	"	127
OAC	-	36.10	9	2.00	140
OAC	_	55.00	_	1.00	141
OAC	5.30	-	-	"	142
GO/PVA	35.00	_-	_	"	143
AC/GO	5.70	20.10	75	1.00	This work

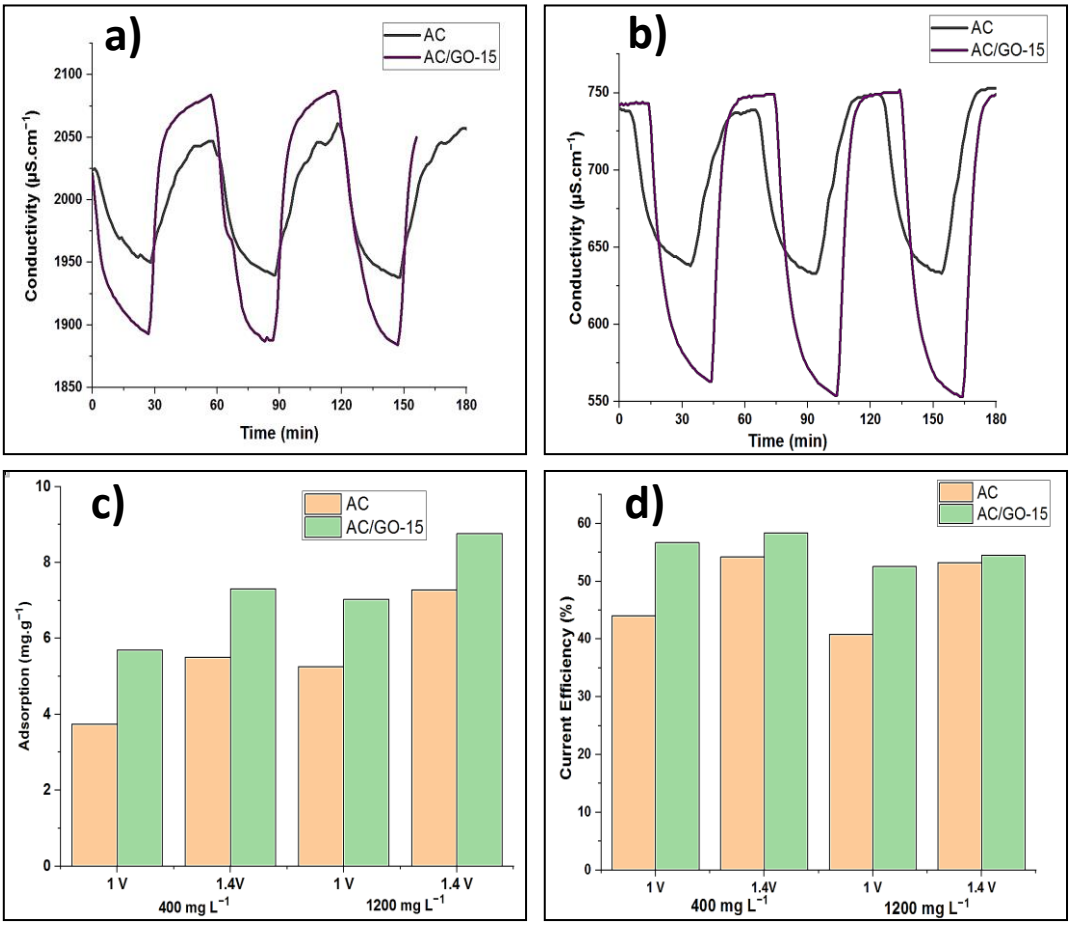

Fig 5 (a,b) Electrosorption curves of AC and AC/GO-15 electrodes at 400 and 1200 mg L^{-1} NaCl solution. (c) Salt adsorption capacity of AC and AC/GO-15 electrodes at different NaCl concentrations and operating voltage (d) Current efficiency of AC and AC/GO-15 electrodes at different NaCl concentrations and operating voltage.

Table 5.1 CDI performance matrices of AC and AC/GO-15 electrodes at all operating conditions.

Electrode	**Voltage (V)**	**Concentration (Mg L^{-1})**	**Time (min)**	**Adsorption Efficiency (%)**	**Salt Adsorption Capacity (mSAC, mg g^{-1})**	**Specific Energy Consumption (SEC) ($KWhm^{-3}$)**	**Kinetics (mg min^{-1})**	**Average Salt Adsorption Rate (ASAR mg g^{-1} min^{-1})**
AC	1.0	400	16	25.14	3.74	0.08	0.56	0.23
AC/GO-15				20.1	5.70	0.10	1.04	0.34
AC	1.4	400	16	37	5.50	0.20	1.2	0.34
AC/GO-15				25.8	7.31	0.18	1.56	0.46
AC	1.0	1200	16	11.76	5.25	0.10	0.55	0.33
AC/GO-15				8.40	7.03	0.09	0.95	0.44
AC	1.4	1200	16	16	7.28	0.26	0.96	0.46
AC/GO-15				10.3	8.77	0.20	1.34	0.55

5.3.3 Conclusion

In summary, AC and series of AC/GO-x composite electrodes (AC/GO-5, AC/GO-10, AC/GO-15 and AC/GO-20) were fabricated and characterized (as explained in chapter 4). Among the composite materials, AC/GO-15 possessed the best electrochemical properties and thereafter was utilized as an electrode of interest in comparison with a pristine AC electrode in order to elucidate this behavior on electrosorption. In all conditions, AC/GO-15 exhibited a higher electro-sorption capacity than pristine AC electrode. We believe that the incorporation of GO into AC electrode matrix increases the overall wettability (hydrophilicity) of the material and thus improves surface interaction of saline solution on the electrode; hence, the consequent effect is made manifest on the higher electro-migration and electro-sorption properties of this material. The electro-sorption capacity of AC/GO-15 was 5.70 mg g^{-1} in comparison to 3.74 mg g^{-1} for AC electrode.

5.4 Overview on desalination performance of solid electrode using pristine AC modified with reduced graphene oxide (RGO) in CDI

To understand the effect of the level of the additive (RGO) on the electrical properties of commercial pristine AC and electrosorption, we have in this section tried to understand the mechanism of ions capture in the modified electrodes by using CDI device to follow the progress of electrosorption behavior between commercial pristine AC and its modified form. By correlating electrical properties with measurements of electrodes electrosorption, we hope to understand the effect of this factor on capacitive deionization.

Some of the results provided in this section have been published in *Nanomaterials* **2021**, 13, 5185 as below:

Activated Carbon blended with Reduced Graphene Oxide Nanoflakes for Capacitive Deionization.

Gbenro Folaranmi, Mikhael Bechelany, Philippe Sistat, Marc Cretin and Francois Zaviska

Institut Européen des Membranes, IEM, UMR-5635, University of Montpellier, ENSCM, CNRS, Place Eugène Bataillon, CEDEX 5, 34095 Montpellier, France; gbenro.folaranmi@etu.umontpellier.fr (G.F.); philippe.sistat@umontpellier.fr (P.S.); marc.cretin@umontpellier.fr (M.C.)

Abstract:

Capacitive deionization is a second-generation water desalination technology in which porous electrodes (activated carbon materials) are used to temporarily store ions. In this technology, porous carbon used as electrodes have inherent limitations, such as low electrical conductivity, low capacitance, etc., and as such, improvement of electrode materials by rational design to obtain hybrid electrodes is key towards upscale in desalination performance. In this work, different compositions of mixture of reduced graphene oxide (RGO) and activated carbon have been prepared and tested as electrodes for brackish water desalination. The physico-chemical and electrochemical properties of the activated carbon (AC), reduced graphene oxide (RGO), and as-prepared electrodes (AC/RGO-x where x = 5, 10, 15 and 20 wt. % RGO) were characterized by low-temperature nitrogen adsorption measurement, scanning electron microscope (SEM), X-ray diffraction (XRD), Raman spectroscopy, X-ray photoelectron spectroscopy (XPS), Fourier transform infra-red (FT-IR), cyclic voltammetry (CV), and electrochemical impedance spectroscopy (EIS) (as shown in chapter 4). Among all the composite electrodes, AC/RGO-5 possessed the highest maximum salt adsorption capacity (mSAC) of 8.10 mg g^{-1} at an operating voltage ΔE = 1.4 V and fastest electron mobility of 55.50 cm^2/ (V.s). This shows that this simple approach could offer a potential way of fabricating electrodes of accentuated carbon network of an improved electrical conductivity that's much coveted in CDI technology.

Keywords: desalination; activated carbon electrode; reduced graphene oxide; composite electrodes

5.5 Result and discussion

Electrosorption behavior of AC and modified AC using RGO is discussed. The effect of additive is elucidated and rationalized as shown below:

5.5.1 Comparative Electrosorption Capacities of AC and hybrid AC/RGO-x

Introduction

Carbonaceous materials have always been the focus of attention as electrode materials in CDI because of their high surface area, porosity, conductivity, hydrophilicity, cheap source and biodegradability [6]. Material aspect of this technology is of utmost importance for improvement in order to achieve suitable or hybrid electrodes of high performance with

respect to the aforementioned properties; thus, there have been relentless approaches towards improving this aspect [7-10].

Activated carbon has attracted attention as electrodes in the field of CDI because of its cheap cost and the fact that it can be easily prepared from readily available biomass has made it a focal point of main electrode material in CDI. However, this cheap material is not without some challenges such as: low hydrophilicity, low electronic conductivity, reduced porosity etc., thus in order to overcome its challenges, AC surface chemistry is usually modified by various methods such as oxidation with oxidizing agents [11] or combined with additives to prepare hybrid electrode materials of high performance [5].

Reduced graphene oxide (RGO) is made of single or more layers of graphite sheets of high electrical conductivity and as found application as super-capacitor due to its high capacitance, surface area and superior electrical conductivity [144]. Since its discovery, RGO has been independently used as a promising electrode material candidate or as an additive with other carbon based materials in CDI [144]. As recently reported, advances in RGO nanoflakes has shown that methods of graphene oxide (GO) reduction to yield RGO nanoflakes could affect its textural properties. RGO synthesized by Li *et al* [145] using hydrazine reductive method on GO, yielded RGO possessing 222.01 m^2 g^{-1} specific surface area with electrosorptive performance of 1.35 mg g^{-1}. Since desalination performance of carbon based electrodes is dependent on properties such as electroactive surface area, microstructure, porosity etc., several attempts have been made to fabricate electrodes of well accentuated carbon network in order to forestall the challenges posed by RGO method of synthesis [146] However, RGO reportedly used for this purpose (as an additive) usually undergo the use of toxic chemicals for synthesis and the need of pre-treatment steps in order to improve its performance. Such pre-treatments for instance involve thermal treatment which is often time consuming. As a matter of diversity, we propose in this paper a simple and non-toxic reductive method of RGO synthesis by GO reduction using potassium hydroxide (KOH) and then subsequently used an additive to influence the electronic conductivity of commercial activated carbon (AC). The as prepared RGO was combined with commercial AC without any pre-treatment step for desalination application using CDI technique.

In the field of super-capacitors, RGO nanoflakes have found application as an additive to improve the electronic conductivity of electrochemically active double-layer materials [147-153]. Chuanyin *et al.* [152] through hydrothermal and CVD processes synthesized 3D flexible

nitrogen doped RGO (NRGO) and thereafter combined with carbon nanotubes to fabricate a flexibly hybrid super-capacitor of high specific capacitance and retention.

thus, in the same way, we propose here a series of hybrid AC/RGO-x made by combining commercial AC with RGO nanoflakes produced by KOH reduction of graphene oxide (GO). The composites were synthesized and labeled as AC/RGO-x where x represents the percentage weight composition of RGO in the composite. (x= 5, 10, 15 and 20 wt. % RGO).

5.5.2 Performance on Simulated Feed solution

It is well known that electrosorption performance does not only depend on the specific surface area of carbon electrode but on some other properties such as the electrical properties of the electrode material etc., [20]. It has been shown previously that the addition of a small amount of RGO with conventional AC improve significantly the electrochemical properties of the electrode in terms of capacitance, (74 F g^{-1}), and electron mobility (electrical properties). In order to confirm this improvement, desalination experiments were performed in a closed loop system with saline solution of 1200 mg L^{-1} NaCl at a constant flow rate of 25 mL min^{-1} and at a cell potential ΔE=1.4 V for 30 min per cycle using the different AC/RGO electrode ratio. At the end of each charging cycle (adsorption), the cell is maintained at its OCV for the same time for ions discharging (desorption). Conductivity values were recorded and plotted in form of adsorption and desorption phases (figure 5.1 a) as well as the corresponding current intensity values (figure 5.1 b). From these figures, performance indicators such as mSAC and CE (figure 5.1 c) can be extracted in order to evaluate and compare the electrosorption behavior of the pristine AC and its composite AC/RGO-x electrodes.

From figure 5.1 (a), notable sharp drops of the initial concentration of the feed solution is made evident due to creation of electric field that led to fast migration of salt ions by electrostatic attraction into their different polarized electrodes during adsorption phase. It can observed that AC/RGO-x composites showed sharper drops in comparison with pristine AC while AC/RGO-5, among all its counter-part, exhibited the sharpest drop; a behavior that is expected due to its excellent electrochemical capacitive nature (fast-track ion adsorption on the electrode surface; stable EDL formation that enables ions storage) and in all cases, it exhibited the highest maximum salt adsorption capacity and charge efficiency as shown in figure 5.1 (c) (The fast electron mobility leading to quick salt extraction in AC/RGO-5 accounts for its highest charge efficiency). The CDI performance indicators (as summarized in table 5.2) calculated from the evolution of Figure 5.1 (a) and (b) proved that our strategy

through this simple RGO synthesis and subsequent chemical agitation showed the obtained condition necessary for improvement of our electrodes for desalination. Lower desalination features of other composites AC/RGO-x (x > 5.0 wt. % RGO) at high percentage could be due to the fact that at this ratio, the dense restacking of the RGO sheets which are closely stacked (agglomerated) must have significantly affected the diffusion pathways for the electrolyte ions into the EDLC and thus, decreasing the capacitive properties of the electrodes [147-148, 154]

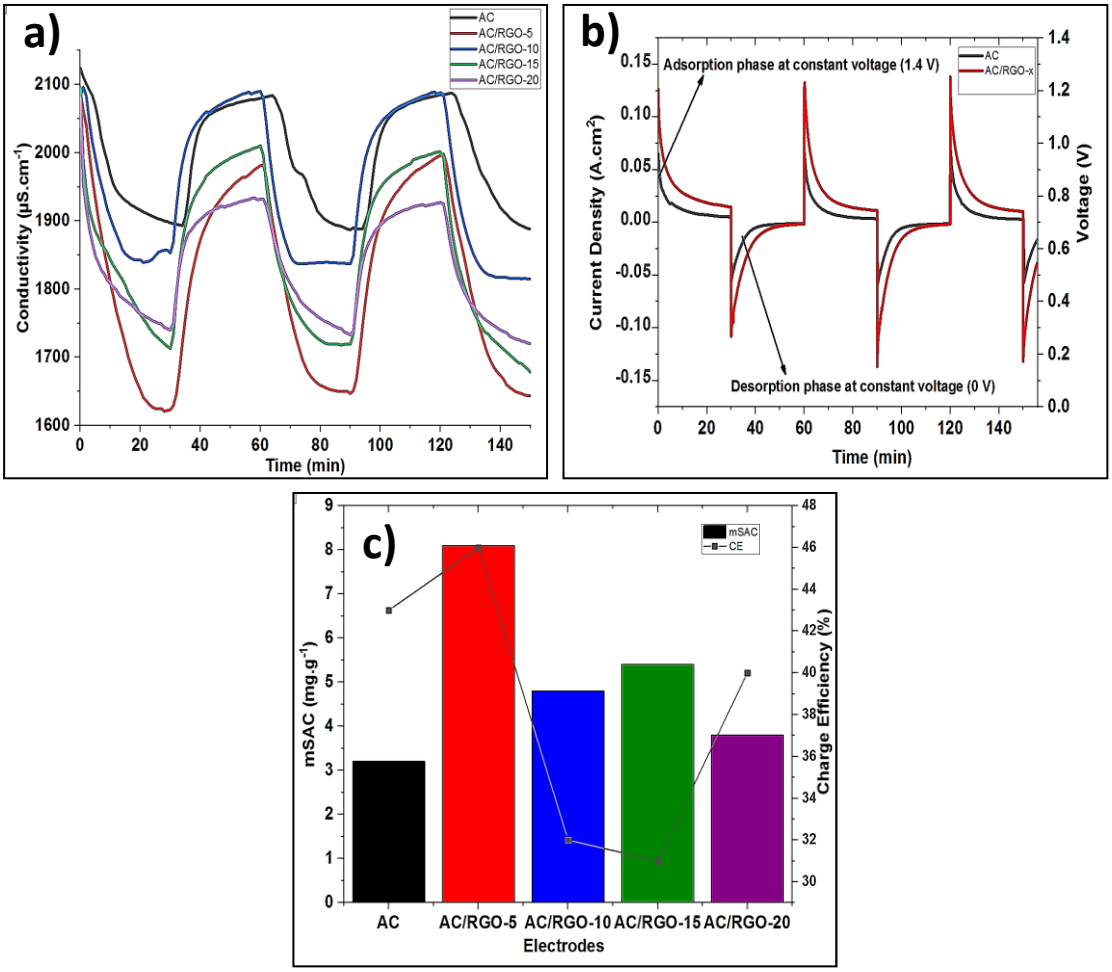

Fig 5.1 (a) Electrosorption curves of AC and AC/RGO-x at 1200 mg L^{-1} NaCl solution under applied voltage of 1.4 V (b) Current response of AC and AC/RGO-x (where x = 5 wt. % RGO) at 1.4 V (c) Maximum salt adsorption (mSAC) and Charge efficiency of AC and AC/RGO-x electrodes.

As presented in table 5.3 AC/RGO composites of high specific capacitance using different approaches of RGO synthesis as against the method adopted by our group is found in literature [155-158]. Undoubtedly, the method of synthesis and thermal pre-treatment affect

functionalities (functional groups, textural and electrochemical properties) of carbon based materials [158]. Using thermally pre-treated AC, Lanshu *et al*. [155] reported electrochemical studies of free standing AC/RGO composites with an outstanding specific capacitance of 207 F g^{-1}. Qiang *et al*. [156] synthesized a composite of ACF/RGO by electrospinning method and obtained specific capacitance of 193 F g^{-1} at the scan rate of 5 mV s^{-1}. Similar reports have been made by Haibo *et al.* [157] and Xin *et al.* [158]. Interestingly, Xin *et al.* [158] reported a low electrosorption of 2.99 mg g^{-1} which is lower than the electrosorption reported for our composites thus showing the efficacy of our method which afforded a simple, cheap and less corrosive means of obtaining RGO as a dopant for commercial AC without any pretreatment to obtain a potential EDL hybrid electrode material.

Table 5.2: CDI operating performance matrices of this experiment at all operating conditions

Electrode	**M_{SAC} (mg g^{-1})**	**SAC (mg cm^{-1})**	**ASAR (mg g^{-1} min^{-1})**
AC	3.20	0.08	0.10
AC/RGO-5	8.10	0.23	0.27
AC/RGO-10	4.80	0.14	0.16
AC/RGO-15	5.40	0.17	0.18
AC/RGO-20	6.46	0.11	0.13

Table 5.3: Advances in electrosorption of AC/RGO composite electrodes in CDI.

Electrode material	Synthesis method	Applied Voltage ΔE (V)	[NaCl]° (mg L^{-1})	**$C_{Specific}$** ($F g^{-1}$)	mSAC (mg g^{-1})	Ref
AC/RGO	Vacuum filtration process & *Th.T under N_2	-		207	-	155
CNFs/RGO	Electrospinning & *Th.T under CO_2	0.4-1.60	400	256	7.20	156
OAC/RGO	Oxidation/simple doping & *Th.T	1-2-2.0	25	181	0.81	157

	under N_2					
CNF/RGO	Electrospinning& *Th.T under N_2	2.0	400	108	2.99	158
AC/FRGO	Sono-assembly& *Th.T under N_2	1.80	117	27.9	12.58	159
NRGO-CNFs	Electrospinning & *Th.T under N_2	1.20	100	337.85	3.91	160
RGO-CNFs	Electrospinning & *Th.T under N_2	1.20	-	264.32	3.60	160
NC/RGO	Polymer templated method & *Th.T under N_2	1.2	589	137.26	17.52	161
RGO/MC	Polymer templated method & *Th.T under N_2	2.0	40	52.15	0.73	162
RGO/HCS	-	1.6	-	-	2.3	163
RGO/HPC	Dual template strategy & *Th.T under N_2	1.2	25	80.34	6.18	164
RGO/CNTs/AC	Chemical mixing method	1.2	-	93.50	2.30	165
AC/RGO-5	Simple chemical method without *Th.T	1.4	1200	74	8.10	This work

*Th.T: Thermal treatment

5.5.3 Conclusion

In summary, a series of AC/RGO-x composite electrodes were made by simple blending process without any pretreatment step and thereafter characterized (as explained n chapter 4). RGO was synthesized by GO dispersion in solution of KOH. The resulting RGO was

combined with commercial AC at different weight ratio and tested for desalination. Among all the composites, the electrode with 5 wt. % of RGO (AC/RGO-5) exhibited the highest maximum salt adsorption of 8.10 mg g^{-1} at operating potential window of ΔE = 1.4 V in 30 min in comparison with pristine AC with maximum salt adsorption of 3.20 mg g^{-1} at the same condition. Additionally, electrosorption performance and charge efficiency results of AC/RGO-5 show that the addition of RGO at this ratio is beneficial for a conducting network structure within AC, thus giving rise to electroactive species that improves the capacitive nature of the composite electrode. In conclusion, this simple approach of material improvement can pave a new way of fabricating potential electrodes of high performance in CDI technique

5.6 Introduction

As earlier explained in chapter 4, transition from solid based electrodes to flow electrodes using a flow device (FCDI) was improvised to overcome some challenges of CDI i.e., limited adsorption sites, discontinuous mode of operation etc., For this purpose, we have fabricated a flow device (see chapter 3) and dedicate this section to elaborate on the viability of a new form of activated carbon and modified activated carbon as flow electrodes in our device. We also hope to show that working at this condition provides an improved condition for electro-sorption behavior of commercially available activated carbon with that of normal activated carbon.

5.7 Overview of superfine AC as viable flow electrode in FCDI

This section documents the viability of a new form of activated carbon (superfine AC) as flow electrode in FCDI. Here, we try correlating the physico-chemical properties of the superfine AC with its electro-sorption measurements as flow electrode. By so doing, we intend elucidating how reduction in particle size of AC affects its potential as flow electrode and effectiveness for FCDI.

Some of the results provided in this section is under review and will soon be published in *chemical engineering journal* as below:

Investigation of superfine activated carbon as a viable flow electrode in capacitive deionization.

Gbenro Folaranmi, Myriam Tuak, Mikhael Bechelany, Philippe Sistat, Marc Cretin and Francois Zaviska

Institut Européen des Membranes, IEM, UMR-5635, University of Montpellier, ENSCM, CNRS, Place Eugène Bataillon, CEDEX 5, 34095 Montpellier, France ; gbenro.folaranmi@etu.umontpellier.fr (G.F.) ; philippe.sistat@umontpellier.fr (P.S.) ; marc.cretin@umontpellier.fr (M.C.)

Abstract:

Flow capacitive deionization is a variant of capacitive deionization. It offers continuous/semi-continuous desalination that is made possible via constant movement of polarized flow electrodes on conducting channels that also stand as electrode support. Performance of electrode is linked to factors such as applied voltage, feed electrode hydrophilicity, carbon loading, conductivity of the feed electrolyte, particle size, viscosity etc. In this paper, a new approach was adopted in reducing the particle size of the carbon used as flow electrode by dry milling method at different time intervals. The particle size and hydrodynamic diameter of the ground activated carbon (superfine activated carbon SFAC) was reduced after milling in comparison with pristine activated carbon (PAC) but an increase in viscosity was observed in SFAC. Increase in viscosity stems from increase in particles loosening which correlates to more stability of the slurry due to higher zeta potential with consequent less particles agglomeration effect and greater force of repulsion.

Physico-chemical analysis such as scanning electron microscopy (SEM) and particle size analyzer confirmed the reduction in size of the particles (a shown in chapter 4). On verification as flow electrode at 10 wt. % (carbon loading), superfine activated carbon exhibited a significant increase in desalination over pristine activated carbon. The improvement is linked to lower particles aggregation that enables higher ions migration and contact to the carbon pores; thus this simple method shows that superfine activated carbon at can be a viable flow electrode in FCDI.

Keywords: Flow electrode capacitive deionization, superfine AC, viscosity and desalination.

5.8 Result and discussion

Electrosorption behavior of superfine AC in comparison with normal AC is discussed. The effect in time interval during ball milling (grinding) of AC is elucidated and rationalized as shown below:

5.8.1 Investigation of superfine activated carbon as a viable flow electrode in Capacitive Deionization.

Introduction

High carbon loading in FCDI favors good connectivity network among carbon particles (favoring electron transport) but this tremendously lead to high viscosity of the slurry hence clogging is observed inside the flowing channel [166].

As found in literature, reports in FCDI using spherical or hollow carbons of regular shape and size (commercial or tailored made carbons from polymeric precursors) have shown higher desalination performance because they can afford higher carbon loading and relatively low viscosity due to the existence of corner-less and edge-less particles unlike carbons of irregular shape and size which offer corners and edges. [72, 167]. Recent approaches in improving FCDI desalination performance through different parameters such as cell potential, cell architecture to improve carbon loading and additives utilization to mitigate internal electrode resistance of carbon slurry have been reported in literature [167-169]. Aranzazu *et al.* [170], using activated carbon (average diameter of 10 µm) slurry at different weight suspensions to understand the performance of different slurries in relation to their electrochemical behavior. Using commercially made activated carbon (average diameter of 5.6 µm) of indefinite shape and size, Kuo *et al.*, [171] made carbon slurries of different mass loadings (5, 10 and 15 wt. %) and tested their mobility (static, semi flow and flow modes) in relation to desalination performance and energy consumption.

However, studies in verifying the importance of activated carbon particle size to further progress FCDI applications and its electrochemical and rheological effects should be investigated. As known, FCDI performance indices can be easily influenced by various factors such as operating condition, nature of materials etc., thus understanding the correlation of carbon based particle size to FCDI performance and working parameters under non Faradaic condition call for extensive investigation.

To reveal and understand the relationship and condition of operation between the aforementioned above and system performance, the design of activated carbon flow electrodes based on fine particles was explored for the first time in this paper. Hence, this research provides insights into the fundamental understanding of superfine activated carbon flow electrodes in comparison to normal activated carbon as flow electrodes in relation to rheology and desalination.

Superfine activated carbon (SFAC) is a new form of powdered activated carbon (PAC) that is generated by simple crushing or grinding of PAC into smaller particle size [172]. SFAC has found application in water treatment as it has been reported to provide faster adsorption rate and better adsorption capacity for naturally occurring organic matter and metals [173, 174].

5.8.2 Comparative Electrosorption Capacities of AC and superfine AC

For the desalination experiments, feed solution, saline solution of 5000 mg L^{-1} (86.5mM, 70 mL) was made to pass through the home made FCDI cell working at ΔE=1.2 V at a constant flow rate of 3 mL min^{-1} for feed solution and 40 mL min^{-1} for feed electrodes (the velocity of flow-electrode in flow channel, 0.123 ms^{-1}) as explained in Chapter 3.

The desalting behavior of SFAC ground at different time interval was verified and compared with normal AC. In all cases, SFAC flows as much as normal AC without clogging at 10 wt. % of operation. SFAC offers tremendous improvement with respect to salt adsorption on comparison with normal AC due to improved area of contact within the flow carbon network. Furthermore, SFAC ground at 90 min competes excellently well and possessed the highest desalination rate over all its counterpart and normal AC as shown in Figure 5.2 (a); this is expected due to its excellent capacitive properties.

FCDI performance indicators (chapter 3) such as DE and SRR (Figure 5.1.1 (b)), SRR calculated from Figure 5.2 (a) and CE (Figure 5.2 (c)) calculated from Figure 5.2 (a) and desalination integrated current response show that in all cases, SFAC (30, 60 and 90 min) exhibited higher performance over normal AC. More so, 90 min SFAC exhibited the highest performance among its counterpart possibly due to its improved and sufficient ions diffusion pathways (easy ion diffusion from the membrane to the pores of fine particles of flow electrode); this fact is made evident by the sharpest drop in ionic conductivity or initial concentration of 90 min SFAC in Figure 5.2 (a). Lower desalination performance of 30 and 60 min SFAC could be as a result of their high aggregation level of particles (lower force of

repulsion and higher particle size distribution) making the particle pores not easily accessible thus causing long ion diffusion pathway (between membrane and carbon slurry) to the carbon pores of the flow electrodes. This consequently leads to lower performance metrics of these flow electrodes.

Our strategy involves a very simple physical method of maximizing commercially made activated carbon particle size and through this method, a tremendous improvement in desalination was observed. With our strategy, we believe that ions in the saline solution can diffuse faster into the pores of the flow electrode due to greater area of contact created as a result of low particle size thus allowing better area of contact within the carbon network. Also, we compared our results to performance of some flow-electrode capacitive deionization (FCDI) cells recently reported in literature as presented in Table 5.4

Furthermore, the specific energy consumption (SEC) for each experiment using different flow electrodes (normal or pristine AC and superfine AC 30, 60 and 90 min) at constant voltage of operation was calculated according to Eq. (12) in chapter 3. The energy consumption for the normal or pristine AC and SFAC slurry electrodes is shown in Figure 5.3, it is obvious that the energy consumption increases with increasing grinding time and this could possibly due to the effect of viscosity.

Reports concerning energy consumption in FCDI are limited in literature. As recently reported, Seungyeon *et al.* [175] reported energy calculations using a 10, 000 mgL^{-1} NaCl showed that the energy consumption of FCDI coupled with nano-filtration unit (FCDI-NF) was 0.460 $kWhm^{-3}$ using activated carbon. Using conventional CDI, Qin *et al.* [6] calculated the energy required to treat feed salinity of 2000 mg L^{-1} NaCl to be 0.85 $KWhm^{-3}$. In comparison, using brackish water reverse osmosis (BWRO), the energy consumed for the same treatment of salinity concentration was 0.550 kWh m^{-3}. 0.35 kWh m^{-3} was reported by Qiang *et al.* [176] for a feed salinity of 9000 mg L^{-1} NaCl at 10 wt. % carbon loading and here we have reported low energy consumption (< 0.1 kWh m^{-3}) for feed salinity of 5000 mg L^{-1} NaCl using super fine AC and shows that energy consumption in desalination increases as particle size of activated carbon electrode reduces.

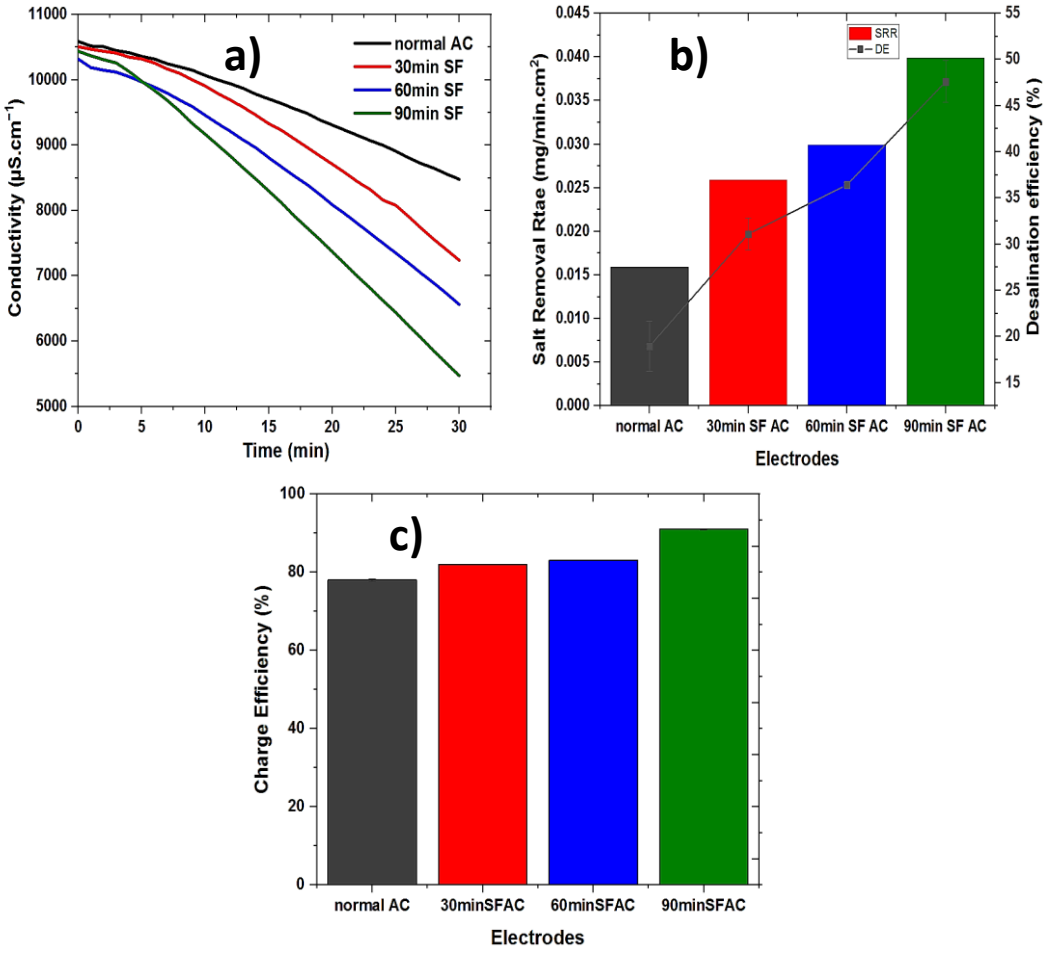

Fig 5.2 Desalination conductivity curve (a) AC and SFAC at different time (b) Salt removal rate and desalination efficiency and (c) charge efficiency of normal AC and SFAC at different time interval respectively.

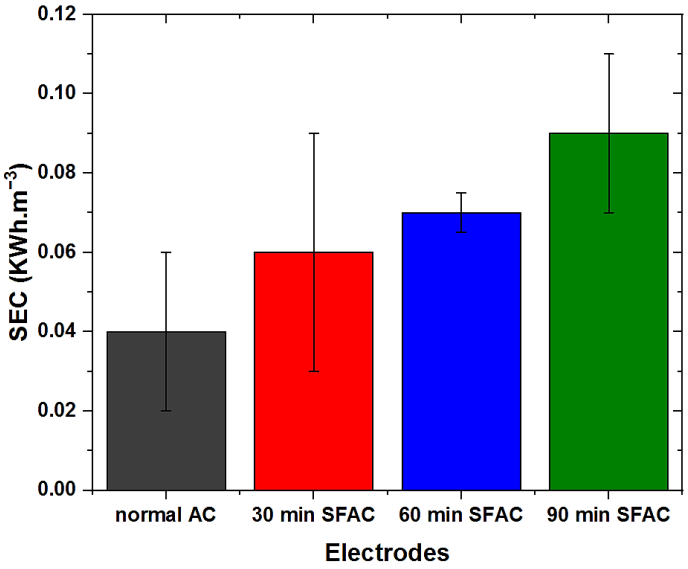

Fig 5.3 Specific energy consumption (SEC) of normal or pristine AC and superfine AC (SF AC) at 30, 60 and 90 min ball-milling time respectively

Table 5.4: Recent advances in FCDI cell performance.

Electrode material	Electrolyte	Voltage (V)	Carbon Loading (wt. %)	FS [NaCl] (g L^{-1})	SRE (%)	SRR (mg. $min^{-1}.cm^2$)	CE (%)	Ref
AC	H_2O	1.2	5	35	68	0.34	-	70
Spherical AC	NaCl+H_2O	1.2	10	35	17	-	-	72
AC+CB	Na2SO4+ H_2O	4.8	20	0.65	-	0.208	69.50	73
Spherical AC+CNT	NaCl+H_2O	1.6	7.41	11.70	-	8.32 $mg.s^{-1}$ m^{-2}	93.30	177
AC DARCO	H2Q/Q	1.2	1	2		0.42 $\mu g.min^{-1}.cm^2$	-	178
AC Norrit	H_2O	1.2	5	5.85	80	-	100	179
AC Darco +CB	H_2O	1.2	10	2	-	0.707 $\mu g.s^{-1}.cm^2$	98	180
AC MSC-30	NaCl+H_2O	1.2	5	35	62.90	-	89.70	181
AC BEADS Modified with VBTAC and S4VBS	NaCl+H_2O	1.2	35	5	27.20	5.5 $mm.s^{-1}.m^2$	85.60	182
SFAC DARCO	H_2O	1.2	10	5	47.61	0.039	90.83	TW

T W: This work

5.8.3 Conclusion

In summary, flow electrodes were made by simple grinding of powdered AC at different time interval (30, 60 and 90 min) and tested in comparison with pristine AC for desalination application by FCDI process. In all conditions, all the superfine AC (SFAC) flow just as much as pristine AC at 10 wt. % without clogging in the FCDI cell. On the basis of our findings (experimental analyses in chapter 4), particle size reduction has direct effect on viscosity but the textural, structural properties and chemical moieties of SFAC remain unchanged in comparison with pristine AC. Interestingly, the desalting performance of SFAC outperforms that of pristine AC due to improved contact area within carbon network caused as a result of reduction in particle size. As particle size reduces, the particles tend to move further apart and consequently generates stronger repulsive forces, higher viscosity and higher zeta potential. In addition, we verified that 90 min of ball milling is enough to improve the performance of AC as flow electrode at moderate weight percent of carbon loading.

5.9 Overview of Activated carbon co-mixed electrospun titanium oxide nanofibers as flow electrode in in FCDI

This section discusses the effect of physico-chemical and electrochemical properties of AC co mixed with titanium oxide nanofibers on the electro-sorption behavior of the resulting nanocomposite flow electrodes. Here, we intend understanding the effect of the additive (titanium oxide nanofibers) on the mechanism of ion transport to the pores of the flow electrodes. Correlating this factor with measurement of flow electrode electrosorption, we enable us understand the relationship between additive effect to easiness of ion transport and its direct consequence on capacitive deionization of the flow electrodes.

Some of the results provided in this section is under review and will soon be published in *materials* as below:

Activated carbon co-mixed electrospun titanium oxide nanofibers as flow electrode in capacitive deionization.

Gbenro Folaranmi, Mikhael Bechelany, Philippe Sistat, Marc Cretin and Francois Zaviska

Institut Européen des Membranes, IEM, UMR-5635, University of Montpellier, ENSCM, CNRS, Place Eugène Bataillon, CEDEX 5, 34095 Montpellier, France;

gbenro.folaranmi@etu.umontpellier.fr (G.F.); philippe.sistat@umontpellier.fr (P.S.); marc.cretin@umontpellier.fr (M.C.)

Abstract:

Flow capacitive deionization is a water desalination technique that utilizes carbon based electrodes in liquid state to obtain fresh water from brackish or seawater. This is a promising second generation water desalination technique but its performance is affected by factors such as electro-conductivity of feed electrode, concentration polarization, viscosity etc. In this study, titanium oxide nanofibers (TiO_2NFs) was synthesized via electrospinning method and subsequently mixed with commercial activated carbon (AC) to obtain a well dispersed flow electrode. Scanning electron microscope (SEM), X-ray diffraction (XRD), Raman spectroscopy, X-ray photoelectron spectroscopy (XPS) and energy dispersive x-ray (EDX) were used to characterize the morphology, crystal structure and chemical moieties of the as-synthesized composites (as shown in chapter 4). Interestingly and out of all the composites, the flow electrode containing 1 wt. % TiO_2NFs (ACTiO_2NFs-1.0) exhibited the best the highest salt removal rate of 0.033 mg/min.cm^2. Improvement in cell performance at this ratio shows that the nanofibers are well intercalated and homogeneously dispersed on the surface of the electrode thus avoiding electrode passivation and nanofibers agglomeration that could limit the flow of ions to the pores of flow electrode. This study shows that nanocomposite could be a potential flow electrode material in capacitive deionization.

Keywords: Flow electrode capacitive deionization, electrospinning, activated carbon, nanocomposite and desalination.

5.10 Result and discussion

Electrosorption behavior of titanium/AC nanocomposite flow electrode in comparison with normal AC is discussed. The effect of titanium nanofibers on the surface of AC is elucidated and rationalized as shown below:

5.10.1 Activated carbon co-mixed electrospun titanium oxide nanofibers as flow electrode in capacitive deionization.

Introduction

One of the challenges of carbon based materials used as electrodes is high resistance. concentration polarization [174]. This process leads to ions depletion at the electrode interface

due to high impedance to ion transport [183] thus finding means of reducing this phenomenon is important in achieving better stability and capacitive performance of electrical double layer capacitors (EDLCs).

Graphitic carbon materials such as activated carbon are often employed as flow electrodes because of their advantageous properties such as high surface area, porosity, adsorption capacity, availability, low cost and excellent electrochemical property [68, 184] however the polarization of AC electrodes leading to ions storage or accumulation reduction on the EDL is a growing concern hence the need for surface tailoring or modification of AC to achieve hybrid composites.

To achieve this feat, metal oxides such as zinc oxide (ZnO), tin oxide (SnO), zirconium oxide (ZrO) and titanium oxide (TiO2) have been utilized in carbon modification [63, 185, 186]. Among all these oxides, TiO_2 is an eco-friendly compound with excellent charged surface that have been exploited in reducing AC electrode interfacial resistance but its challenge of aggregation (agglomeration of TiO_2 could lead to pores blockage of AC) reduces its performance when doped with AC. To overcome this dilemma, TiO_2 nanofibers are utilized as it possesses morphology leading to reduction of intra-aggregation and inter-agglomeration in TiO_2 nanofibers; also, its large axial ratio (large surface to volume ratio) causes low charge transfer resistance (interfacial resistance) [186].

Motivated by this, we have synthesized TiO_2 nanofibers by electrospinning process and mixed it with AC to form hybrid nanocomposites. The proposed nanocomposite electrodes which consisted of different weight percentage of TiO_2NFs were labelled ACTiO_2NF-x where x represent the weight percentage of TiO_2NFs in the composite (x = 0.5, 1.0, 1.5, 2.0, 2.5 and 5.0 wt. % ACTiO_2NFs). To the best of our knowledge, it is noteworthy to state that there is little or no report in literature concerning TiO_2 nanofibers-AC as flow electrode.

5.10.2 Comparative Electrosorption Capacities of AC and AC nanocomposites

As reported in literature, the electrosorption performance of carbon based materials is linked to their electrochemical properties [96]. As explained earlier, TiO_2NFs was added at different wt. % to influence the concentration polarization of pristine AC and this factor was verified through the electrochemical characteristics of the nanocomposites. Furthermore, in order to confirm the link between electrosorption and electrochemical properties improvement, desalination experiments were carried out under a continuous system in a flow channel.

Desalination was conducted at an operational cell potential □E=1.2 V for 30 min using 5 000 mg L^{-1} NaCl as the feed solution. Difference in conductivity was monitored and recorded during the course of the experiment. Difference in conductivity was monitored and recorded during the course of the experiment. FCDI performance matrices such as salt removal efficiency (SRE, Figure 5.4 (b)), salt removal rate (SRR) and charge efficiency (CE) in Figure 5.4 (c) were used to evaluate the performance of the flow electrodes.

Obvious sharp drop of initial concentration noticed in Figure 5.4 (a) is as a result of electrostatic attraction of ions into different mobilized charged flow electrodes due to electric field creation. Notably, the nanocomposites show sharper drops than pristine AC and among all the nanocomposites, ACTiO_2NFs-1.0 exhibited the sharpest concentration drop; an expected behavior due to its excellent capacitive nature (rapid ions adsorption on the electrode surface, lower interfacial resistance, stable EDL formation that enabling better ions migration). Its highest charge efficiency (CE) implies fast ions mobility to the pores of the flow electrode thus leading to quick salt removal; a consequent effect on salt removal efficiency (SRE) and salt removal rate (SRR). Hence our strategy through this simple nanocomposites synthesis showed the obtained condition necessary for improvement of flow electrodes for desalination.

Low desalination behavior of ACTiO_2NFs-x ($x \geq 2.0$ wt. % TiO_2NFs) at high percentage could be due to the fact that at this ratio, the nanofibers tend to agglomerate among themselves (not well dispersed or less uniform) and as such, making the pores of the electrode (surface hindrance) not easily accessible for ions adsorption. Also, electrode passivation is likely to occur due to the high presence of the nanofibers [187]. This will make the electrode surface not easily permeable for ions (impermeable layer formation on electrode surface) thus significantly affecting the electrosorption performance of the electrodes as observed in our materials (whitish layers on the surface of our flow electrodes).

Due to the limited report on the electrosorption behavior of activated carbon-titanium oxide nanocomposites in flowing state, we have made a comparison report as presented in table 5.5 showing recent advances in fabrication methods of titanium nanocomposite and their electrosorption behavior in different systems.

Table 5.5: Recent advances in electrosorption behavior of activated carbon-titanium nanofiber composites

Electrode material	Synthesis method	Technique	Applied Voltage (V)	□E	[NaCl] (mg L^{-1})	SRE (%)	mSAC (mg.g^{-1})	Ref
AC/TiNF	High speed mixing	MCDI	1.2	292		89.60	17.70	125
AC/TiZrNF	Hydrothermal Tr*	CDI	1.2		100	53.08	-	187
NACTZNF	Hydrothermal Tr*	CDI	1.2		100	71.19	3.98	188
ACTiNF	Hydrothermal Tr*	CDI	1.2		500		2.70	189
ACTiNF	Simple mixing	FCDI	1.2		5000	37.30	16.72	T W

T W: This Work, Tr*: Treatment

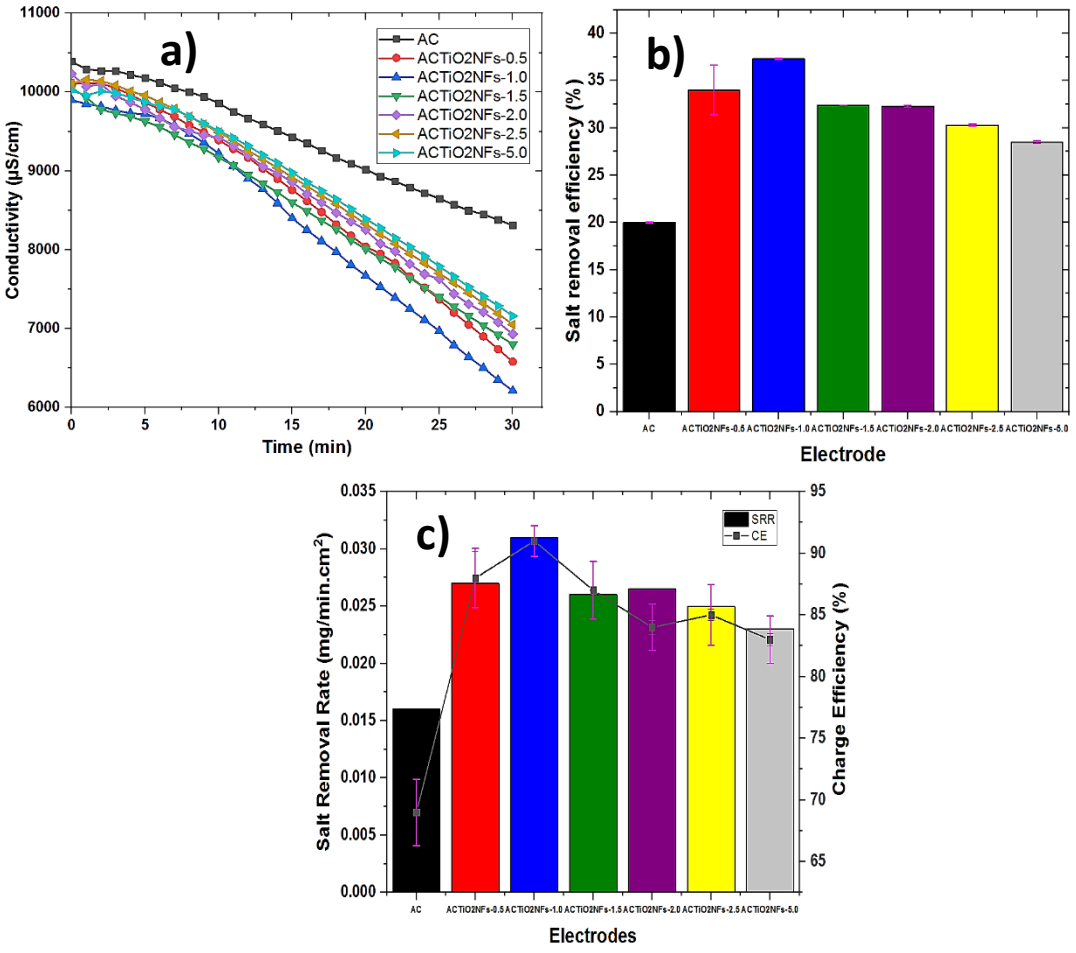

Fig 5.4: Conductivity curve (a) AC and ACTiO$_2$NFs-x (b) Salt removal efficiency and (c) salt removal rate and charge efficiency of AC and ACTiO$_2$NFs-x where (x = 0.5, 1.0, 1.5, 2.0, 2.5 and 5.0 wt. % TiO$_2$NFs) respectively.

5.10.3 Conclusion

In summary, titanium oxide nanofibers were synthesized by electrospinning process (see chapter 4). The as-spun nanofibers were rationally combined with AC through simple agitation process to form hybrid composites of ACTiO$_2$NFs-x (x = 0.5, 1.0, 1.5, 2.0, 2.5 and 5.0 wt. % ACTi0$_2$NFs) without any further post-treatment. The composites were then characterized (chapter 4) and tested as electrodes in FCDI for the first time. Interestingly, intercalation or incorporation of TiO_2 nanofibers led to an improved performance of the nanocomposite electrodes especially with ACTiO$_2$NFs-1.0 exhibiting distinguishable and outstanding desalination behavior. Nanofibrous morphology of the composites affords better anchorage within AC network thus offering better ion transport and migration to its pores. In conclusion, the demonstrated method shows a potential in achieving carbon based flow electrodes of improved morphology and desalination performance in FCDI technique

5.11 General Conclusion

In this chapter, activated carbon and its hybrid derivatives (in solid and flow state) were prepared and used as electrodes to desalinate saline solution containing NaCl (monovalent salt electrolyte) in both home-made CDI and FCDI cells.

In solid electrodes, presence of co-ion adsorption limits salt extraction and lowers charge efficiency; although improvement in properties of AC such as wettability, electrical conductivity etc., affords better performance in terms of electro-sorption.

In flow electrodes, results show that electrosorption and charge efficiency were significantly higher than in solid electrodes. These advantages could be attributed to the unlimited accessibility of ions into the pores of carbon electrodes when operated in a continuous charging phase while in liquid state. Also, FCDI affords the utilization of membranes which prevents co-ion adsorption challenge that could limit diffusion of ions. More importantly, the author believes that despite the challenges of using flow electrode (clogging, low conductivity etc.) yet, slight improvement in one of carbon properties such as particle size reduction could improve the surface area of contact among carbon-carbon network thus reducing ion diffusion

path length. This, among many factors adds to the advantage of FCDI over CDI in fresh water production.

Chapter 6 Conclusions

6.1 Thesis Summary

This dissertation is devoted to the improvement of commercial activated carbon as a cheap source of potential electrode at industrial scale for electro-sorption (brackish water desalination) application using capacitive deionization technology. Water desalination technologies such as reverse osmosis (RO), multi-stage flash distillation (MSFD) etc., makes use of membrane based processes for generating fresh water from salt solution. Basically, most of these processes operate by extracting solvent from solutes hence requiring a lot of energy input and also, cost of operation is usually high. To circumvent these challenges, electrochemical desalination techniques such as battery desalination, capacitive deionization etc., which operates in direct opposite to the aforementioned technologies by extracting solutes from solvent under electric field were improvised.

Capacitive deionization (CDI) which is the main focus of this thesis is an electrochemical technique that makes use of porous materials as electrode to temporarily separate and store salt ions under the application of potential difference. Electric field generated by the application of certain potential difference creates a situation in which the ions in solution gets separated and migrated towards oppositely charged electrodes (poles) where they are stored. Storage takes place at the electric double layer (EDL) formed inside the pores of the electrode material. EDL is an interface generated between the electrode/electrolyte solution. The spatially and temporal storage of ions depend on the formation and stability of EDL.

Materials used as electrodes in CDI usually possess some features such as high porosity, high surface area, hydrophilicity, good electrical conductivity and above all, the materials must be of low cost, readily available and of renewable source. Material such as carbon possess virtually all these characteristics and has been the choice of candidate in CDI research. Recent research projects in CDI has focused on development of advanced carbon materials to achieve high desalination capacity. However, realistic development of these fancy materials (carbons) into industrial scale is shallow as the processes involved in their synthesis or modification is either time consuming, expensive or the synthesized materials are usually of low quantity for only laboratory scale experiments.

Commercial activated carbon (AC) serves as an alternative as a good option to overcome the above aforementioned challenges of some rationally designed carbons because of its cheap

and readily available source from biomass (banana peels, coconut shell etc.) and can also be produced in huge quantity. Nonetheless, AC is not without some intrinsic challenges such as low hydrophilicity, low electrical conductivity, low porosity etc., and as such, this thesis focuses on improving its properties. To achieve this, two possible ways exist in literature which is either modification under acidic/highly oxidizing agents or forming a composite/hybrid material by combining/doping with other high performing materials. In this thesis, attention is focused on modifying activated carbon to hybrid electrode materials by simple chemistry. The generated hybrid electrodes are then evaluated and used in CDI operation. Herein, the major contributions of this thesis is summarized below:

Characterization of a novel AC/GO composite electrodes

As earlier stated, AC is of low hydrophilicity and for a good electrode material, the ease of surface interaction of the electrolyte on the solid electrode is of utmost importance in CDI. Research in this aspect focuses mainly on surface chemistry improvement of AC by using oxidizing agents such as hydrogen peroxide (H_2O_2), ($KMnO_4$), nitric acid (HNO_3) etc. As a way of diversification, we verified a new method by simple combination of AC with graphene oxide (GO). The author believes that GO, being highly rich in oxygenated functional groups (OFGs) could influence the surface chemistry of AC when combined together at a certain ratio hence the development of a novel composite electrode. Characterizations such water contact angle (WCA), shows improvement in wettability of the hybrid material and demonstration by cyclic voltammetry (CV) shows the contribution of this improvement to achieved outstanding capacitance. Result from XPS also show that incorporating GO through simple mixing with AC improved the surface properties of AC due to increase in band intensity of different OFGs of the hybrid material. This simple process resolves the fundamental hydrophilic challenge associated with AC by using a non-corrosive means as against the known methods usually reported in literature.

Resolved studies on electrical property of AC through simple experimental design

Due to low electrical property of AC, reports have shown that combining AC with additives of high electrical properties have influenced positively its desalination efficiency. Additives such as reduced graphene oxide/graphene (RGO/Gr), carbon black (CB), carbon nanotubes (CNT) etc., are usually used. However, RGO used in most of these reports are synthesized under tedious treatment steps. The synthesis approaches take time (time consuming) and the chemicals used in the reduction process are often hazardous. Thus, a novel means to resolve

this challenge was developed by simple experimental design. The experimental method requires less expensive and environmental friendly route for RGO synthesis by using KOH for GO reduction. The obtained RGO is then directly combined with activated carbon through simple chemical agitation without any further treatment. Through this approach, the obtained RGO was able to have better influence on the electrical property of activated carbon and as such yields higher desalination capacity when tested as electrode in CDI compared to other reports found in the literature

Flow capacitive deionization

The many challenges (co-ion adsorption, discontinuous mode of operation and limited surface area of adsorption) of solid based electrodes led to improvising alternative form of design in which the state of electrode is slurry (this allows unlimited active sites for adsorption) rather than solid. As a result, the aforementioned challenges were overcome. The device is designed in such a way that offers constant flow by recycling slurry electrode thus overcoming discontinuous mode of operation as electrode regeneration takes place immediately carbon slurry exits the cell compartments and get charged the moment they recycled into the cell. Flow capacitive deionization (FCDI) offers outstanding desalination capacity over conventional CDI but the challenges that comes with slurry electrode utilization is another growing concern. Challenges such as carbon clogging inside the cell, low carbon loading of the cell, low electrical conductivity, high resistance and high viscosity of carbon at higher mass have offer limitations to this variant 2nd generation technology. Here, the author focuses on improving some of the challenges of the material aspect necessary for the upscale of the technology. Key contributions emanating from this process are summarized below:

- Development of a simple form of activated carbon by simple ball milling method. The generated AC termed superfine AC (SFAC) from this method was used as flow electrodes to capture salt ions from a relatively high brackish water while operating at a semi-continuous phase. The desalination of this material was significantly effective at a shorter time when compared with pristine or normal AC. Observations from physico-chemical characterizations of this material in comparison with pristine AC offers no significant changes i.e., in defects, surface chemistry, crystallinity but significant changes were observed in their morphology and viscosity. As ball milling time progresses (grinding time), the morphology of the SFAC becomes attenuated with finer particles and the dynamic viscosity of the material also increases. Attempts

in understanding this latter behavior was rationalized by performing zeta potential of the new the materials (SFAC) and pristine AC. Observation from zeta potential shows that SFAC exhibits higher electrostatic repulsion (higher zeta potential) over pristine AC possibly due to the reason that as grinding increases, the particles become finer and more loosely bound thus moving apart from each other and consequently leads to increase in viscosity unlike particles that are tightly bound together. Also, SFAC demonstrates excellent flowing property rivalling that of pristine AC at the same level of carbon loading into FCDI cell. This feature allows SFAC to outperform pristine AC (higher desalination at a lower time) as it affords better intra-particle contact within its carbon network thus promoting faster ion transport into its pores.

- Lastly, resolution of high resistance in flow electrode was studied by using electro-spun titanium nanofibers. The development and fabrication of nanocomposite flow electrode as potential materials for improving ion transport into carbon pores was rationally designed and through experimental characterizations, reduction in charge transfer resistance (electrode/electrolyte resistance or interfacial resistance) and increase in EDL capacitance were observed. This observation shows that nanocomposite flow electrodes are well suited for electro-sorption application as their carbon structure allows efficient transport of ions due to nanofibers anchorage within their carbon stricture.

In this thesis, the author was able to show the feasibility of improving electro-sorption process for industrial application by using commercial AC. Simple methods for improving the challenges or drawbacks of AC were itemized by composite or hybrid formation and from the physico-chemical and electrochemical characterizations of these hybrid materials, improvement in electro-sorption feasibility for desalination were achieved.

Inquest into a new way to overcome the challenges of solid based electrodes and open up new way to produce fresh water from a relatively high brackish water led to innovation of FCDI. This is a promising 2nd generation technology offering high upscale in desalination. Also, it opens up understanding into new parameters such as carbon loading, viscosity and especially mechanism of ion transport in slurry electrodes.

Furthermore, the author believes that this PhD thesis will bridge a gap having proposed simple and different ways of improving AC for electro-sorption development.

6.2 Recommendations for future research

Various elaborate research projects have been performed on developing hybrid carbon materials as electrodes in CDI/FCDI process. The performance of these carbon based electrodes depend majorly on the physico-chemical properties of these materials. Attempts to make carbon electrodes of high porosity and tuned pore arrangement and investigate their electrochemical properties in relation to CDI application are still on-going [190].

Having ascertained the link between the properties of carbon electrodes and electro-sorption, the author believes that exploitation of intensive research adventures in development of microporous-mesoporous carbon material of high porosity can maximize adsorption sites as micropores offer short pathways (ions diffusion distance) for ions while mesopores provide low resistance for ions movement [191]. However, the cost of developing this such of material could be expensive and the process might be time consuming thus compromise has to been reached between advanced novel electrode development and cost. An alternative to this, is to improve and intensify research approaches in advancing the properties of cheap commercial activated carbon to function as a super hybrid electrode material (Electrode materials possessing long term stability, high electrical conductivity characteristics, and good regeneration rates). By so doing, cost reduction can be effected and this factor will be of great importance in desalting and treating water as a cheap marketable product.

Also, conducting research in the area of permeability media (IEMs) in FCDI through computational or experimental CDI (thermodynamic models) models could help predict or give more information about the diffusivity coefficients of various ions when considering multivalent ions in saline solution. Through this, sorption data and other optimized variables of these ions can be easily provided to ascertain values for a wide range of experimental conditions. [190-193]

In CDI, alternative to the usage of poly(vinyldifluoride) PVDF conductive binder during electrode preparation can be beneficial for carbon porosity and resistance reduction. Although reduced graphene oxide has been reportedly used for this purpose but its challenge of agglomeration serves a setback in reducing carbon porosity [131-132, 194].

In FCDI, an important research area should be geared towards scaling up of net production of fresh water. Although, continuous flow of operation has been introduced to tackle this challenge yet, it is still difficult to achieve mass production of fresh water because of limited

influent (feed solution) flow rate. Charge transfer in FCDI is practically low in comparison to CDI due to the water component (weak electrolyte) of the feed electrode thus impeding fast charge transfer from the current collector to the slurry. This is a major challenge; hence introduction of coupling nano-pillars such as Cu or Ni nano-pillars to graphite current collector and alternate dissolving medium instead of water could improve contact area and offer good electrical conductivity [195, 196].

Membrane incorporation in FCDI increases interfacial resistance although, as a proof of concept, Hatzell *et al.* [197] introduced FCDI without the use of membrane. Additionally, porous ceramic spacer has been recently introduced as IEMs replacement [198] although most FCDI related desalination process still use membrane. Utilization of electro-conductive membranes to improve ion permeation and reduction in resistance can also be a good innovative means of achieving high practicality in FCDI [199].

Progress in FCDI process and cell configurations have improved its performance, thus yielding better results; though still very new, this technology could pave a new dimension as an alternative future of desalination when considering vital aspects like application (for both brackish and sea water), cost, and energy recovery, thus innovation in new architectural FCDI cells and its system performance study can be a future study as the flow electrode system has inherent challenges of clogging.

Many challenges still exist (electrode selection compromise.) and the journey to CDI/FCDI aim actualization is still far-fetched albeit, predictor designs (experimental design through statistical approaches) and molecular dynamics models can be introduced i.e., for optimal material design in predicting ion transport in porous materials and parametric performance.

References

1. "Guidelines for drinking quality water. First Addendum to Third Edition," World Health Organization. **2006**. Accessed 4th Nov.2020
2. Shannon M. A., Bohn P. W., Elimelech M., Georgiadis J. G., Marinas B. J., and Mayes A.M., "Science and technology for water purification in the coming decades," *Nature*, vol. 452, pp. 301-310, 2008.
3. Zander A, Elimelech M, Furukawa D, Gleick P, Herd K, K. Jones, P. R, Sethi S, Tonner J, Vaux H, Weis J, and Wook W. "Desalination: A National Perspective," Washington 2008.
4. Elimelech M., Phillip W.A., The future of seawater desalination energy technology and the environment. *Sci*. **2011**; 333 712–717.
5. Zhao R., Porada S., Biesheuvel P.M., Van der Wal A. Energy consumption in membrane capacitive deionization for different water recoveries and flow rates, and comparison with reverse osmosis, *Desal.*, **2013;** 330., 35–41
6. Qin M, Deshmukh A., Epsztein R., Patel S., Owoseni O, Walker W., Elimelech M. Comparison of energy consumption in desalination by capacitive deionization and reverse osmosis. *Desal*. **2019**; 455, 100–114
7. Couallier E.M., Ruiz B.S., Lameloise M.L. Decloux M. Usefulness of reverse osmosis in the treatment of condensates arising from the concentration of distillery vinasses. *Desal*, **2006**; 196, 306-317.
8. Choules, P. Update on large scale ocean desalination plants. In Proceedings of the II Seminario Internacional Desalación, Antofagasta, Chile, 30 November 2010.
9. Lopez, F.; Araus, M.; Gimenez, R.; Munoz, E.; Romero, G.; Bastida, J.M. Energy consumption optimization in a large seawater desalination plant (Aguilas, 210,000 m^3/day). In International Desalination Association World Congress on Desalination and Water Reuse; International Desalination Association: Topsfield, MA, USA, Conference held in San Diego, CA, USA; **2015.** Accessed 3rd March 2020
10. Global Water Intelligence (GWI). Market Insight: GlobalWater Market in 2018; Global Water Intelligence (GWI): Oxford, UK; Available online: globalwaterintel.com (accessed on 30 June 2018).
11. Belatoui, A.; Bouabessalam, H.; Rouane Hacene, O.; De-la-Ossa-Carretero, J.A.; Martinez-Garcia, E.; Sanchez-Liza, J. Environmental effects of brine discharge from two

desalination plants in Algeria (South Western Mediterranean. *Desal. Water Treat*. **2017**, 76, 311–318.

12. Honaine Desalination Plant (Algeria). Water World Newsletter. Available online: https://www.waterworld.com/international/desalination/article/16202560/algerian-desalination-plant-reaches-production-milestone (accessed on 2nd December 2019).
13. Sajjad K.A.A.; Mohd Y.M.Y.; Abd Aziz B.M.A.; Hassimi A.H. Electrodialysis desalination for water and wastewater: A review. Che Eng. **2019**, 138, 75–82
14. Fernandez-gonzalez, C.; Ibañez, R.; Irabien, A. Sustainability assessment of electrodialysis powered by photovoltaic solar energy for freshwater production. *Renew. Sustain. Energy Rev.* **2015**, 47, 604–615.
15. Wright, N.C.; Winter A.G. Justification for community-scale photovoltaic-powered electrodialysis desalination systems for inland rural villages in India. *Desal.* **2014**, 352, 82–91.
16. Círez, F.; Uche, J.; Bayod, A.A.; Martíinez, A. Batch ED fed by a PV unit: A reliable, flexible, and sustainable integration. *Desal. Water Treat*. **2013**, 51, 673–685.
17. Hisham, M.; Mohammed, S. Activated Carbon Cloth for Desalination of BrackishWater Using Capacitive Deionization. *Desal. Water Treat.* **2018**, 45, 17–36.
18. Ryoo, M.W.; Seo, G. Improvement in capacitive deionization function of activated carbon cloth by titania modification. *Water Res.* **2003**, 37, 1527–1534.
19. Conway, B.E., Birss, V. & Wojtowicz, J. The role and utilization of pseudocapacitance for energy storage by supercapacitors. Journal of Power Sources. 1997, 66, 1–14.
20. Helmholtz. J. Theory of the double electric layer. *J. Franklin Inst.* **1883** ,110, 217-227
21. Bockris, J.O.; Reddy, A.K.N.; Gamboa-Aldeco, M. *Modern Electrochemistry*, 2nd ed.; Kluwer Academic/ Springer Publishing Company, New York, USA. **2000.**
22. Porada, S.; Borchardt, L.; Oschatz, M.; Bryjak, M.; Atchison, J.S.; Keesman, K.J.; Kaskel, S.; Biesheuvel, P.M.; Presser, V. Direct prediction of the desalination performance of porous carbon electrodes for capacitive deionization. *Energy Environ. Sci.* **2013**, *6*, 3700.
23. Yan C.; Kanaththage Y.W.; Short, R.; Gibson, C.T.; Zou, L. Graphene/Polyaniline nanocomposite as electrode material for membrane capacitive deionization. *Desal* **2014**. 344, 274-279.
24. Johnson A. M. and Newman J. "Desalting by Means of Porous Carbon Electrodes," *Journal of the Electrochemical Society*, **1971,** 118, 510-517.

25. Kotz R. and Carlen M. "Principles and applications of electrochemical capacitors. *Electrochimica Acta,* **2000**, 45, 2483-2498

26. Humplik T., Lee J., O'Hern C. S., Fellman B. A., Baig M. A., Hassan S. F., Atieh M. A., Rahman F., Laoui T., Karnik R., and Wang E. N., "Nanostructured materials for water desalination," *Nanotechnology*. **2011**, 22, 292001-292019

27. Porada S, Weinstein L., Dash R., van der Wal B., Bryjak M., Gogotsi Y., and Biesheuvel M, "Water Desalination using Capacitive Deionization with Microporous Carbon Electrodes," *ACS Applied Materials & Interfaces,* **2012**

28. Biesheuvel P. M. and Bazant M. Z. "Nonlinear dynamics of capacitive charging and desalination by porous electrodes," *Physical Review E,* 2010, 81, 03

29. Satterfield C. N., Colton C. K., and Pitcher W. H., "Restricted diffusion in liquid within fine pores," *AIChE Journal,* **1973**, 19, 628-635

30. Tsouris C., Mayes R., Kiggans J., Sharma K., Yiacoumi S., DePaoli D., and Dai S., "Mesoporous Carbon for Capacitive Deionization of Saline Water," *Environmental Science & Technology,* **2011**, 45, 10243-10249

31. Eikerling M., Kornyshev A. A., and Lust E., "Optimized Structure of Nanoporous Carbon-Based Double-Layer Capacitors," *Journal of the Electrochemical Society*, **2005,** 152, 24-33.

32. Liu, X.; Chen, T.; Qiao, W.C.; Wang, Z.; Yu, L. Fabrication of graphene/activated carbon nanofiber composites for high performance capacitive deionization. *J. Tai. Insti. Che*. Eng. **2017**, 12, 213–219.

33. Hou C.H. Development of multi-walled carbon nanotube/poly (vinyl alcohol) composite as electrode for capacitive deionization. *Sep. Purif. Technol*. **2014**, 130, 7–14.

34. Park K.K.; Lee J.B.; Park P.Y.; Yoon, S.W.; Moon, J.S.; Eum, H.M.; Lee, C.W. Development of a carbon sheet electrode for electrosorption desalination. *Desali* **2013**, 206, 86–91.

35. Sampo, T.; Marja, V.; Suvi, L.; Tiina, V.; Donald, L. Behaviour of one-step spray-coated carbon nanotube supercapacitor in ambient light harvester circuit with printed organic solar cell and electrochromic display. *Sci. Rep.* **2016**, 200, 22967.

36. Hou C.H.; Huang, J.F.; Lin, H.R.; Wang, B.Y. Preparation of activated carbon sheet electrode assisted electrosorption process. *J. Taiwan Inst. Chem. Eng*. **2012**, 43, 473–479.

37. Ajay, K.M.; Dinesh, M.N.; Murthy, K.V.; Ravikumar, C.R.; Nagaswarupa, H.P. Deposition & Electrochemical characterization of Multilayer coated electrode material for super capacitor application. *Mater. Today Proc*. **2018**, 5, 21452–21457.

38. Soffer, A.; Folman, M. The electrical double layer of high surface porous carbon electrode. *J. Electroanal. Chem. Interfacial Electrochem*. **1972**, 38, 25–43.

39. Huang, K.; Chai, S.H.; Mayes, R.T.; Tan, S.; Jones, C.W.; Dai, S. Significantly increasing porosity of mesoporous carbon by $NaNH_2$ activation for enhanced CO_2 adsorption. *Microporous Mesoporous Mater*. **2016**, 230, 100–108.

40. Teng, H.S.; Hsu, L.Y. High-porosity carbons prepared from bituminous coal with potassium hydroxide activation. *Ind. Eng. Chem. Res.* **1999**, 38, 2947–2953.

41. Huang, W.; Zhang, Y.; Bao, S.; Cruz, R.; Song, S. Desalination by capacitive deionization process using nitric acid-modified activated carbon as the electrodes. *Desali*. **2014**, 340, 67–72.

42. Mopoung, S.; Bunterm, T. KMnO4 modified carbon prepared from waste of pineapple leaf fiber production processing for removal of ferric Ion from aqueous solution. *Am. J. Appl. Sci.* **2015**, 13, 814–826.

43. Krishnamoorthy, K.; Navaneethaiyer, U.; Mohan, R.; Lee, J.; Kim, S.J. Graphene oxide nanostructures modified multifunctional cotton fabrics. Appl. *Nanosci*. **2012**, 2, 119–126.

44. Xu, X.; Liu, Y.; Lu, T.; Sun, Z. Rational design and fabrication of graphene/carbon nanotubes hybrid sponge for high-performance capacitive deionization. *J. Mater. Chem. A* **2015**, 3, 13418–13425.

45. Myint, M.T.Z.; Dutta, J. Fabrication of zinc oxide nanorods modified activated carbon cloth electrode for desalination of brackish water using capacitive deionization approach. *Desali.* **2012**, 305, 24–30.

46. Gang, W.; Qiang, D.; Zheng, L.; Chao, P.; Chang, Y.; Jieshan, Q. Hierarchical activated carbon nanofiber webs with tuned structure fabricated by electrospinning for capacitive deionization. *J. Mater. Chem.* **2012**, 22, 21819.

47. Feng, D.; Yuping, L.; Hongbin, C.; Yongbing, X.; Yi, Z. Capacitive deionization by ordered mesoporous carbon: electrosorption isotherm, kinetics and the effect of modification. *Desal. Water. Treat.* **2014**, 52, 1388–1395

48. Huanlei, W.; Qiuming, G. Synthesis, characterization and energy-related applications of carbide-derived carbons obtained by the chlorination of boron carbide. *Carbon* **2009**, 47, 820–828.

49. Jian, H.L.; Liu, B.; Lan, Y.Q.; Kuratani, K.; Akita, V.; Shioyama, H.; Zong, F.; Xu, Q. From Metal-Organic Framework to nanoporous carbon: Toward a very high surface area and hydrogen uptake. *J. Am. Chem. Soc.* **2011**, 133, 11854–11857.

50. Fan, L.Z.; Hu, Y.S.; Maier, J.; Adelhelm, P.; Smarsly, B.; Antonietti, M. High electroactivity of polyaniline in supercapacitors by using a hierarchically porous carbon monolith as a support. Adv. *Funct. Mater.* **2007**, 17, 3083–3087.

51. Tsouris, C.; Mayes, R.; Kiggans, J.; Sharma, K.; Yiacoumi, S.; DePaoli, D. Mesoporous carbon for capacitive deionization of saline water. *Environ. Sci. Technol*. **2011**, 45, 10243–10249.

52. Arulepp, M.; Leis, J.; Latt, M.; Miller, F.; Rumma, K.; Lust, E.; Burke, A.F. The advanced carbide-derived carbon based supercapacitor. *J. Power Sources* **2006**, 162, 1460–1466.

53. Shi, W.; Ye, C.; Xu, X.; Liu, X.; Ding, M.; Liu, W.; Cao, X.; Shen, J.; Yang, H.Y.; Gao, C. High-Performance Membrane Capacitive Deionization Based on Metal Organic Framework-Derived Hierarchical Carbon Structures. *ACS Omega* **2018**, 3, 8506–8513.

54. Chen, Y.Z.; Wang, C.; Wu, Z.Y.; Xiong, Y.; Xu, Q.; Yu, S.H.; Jiang, H.L. From Bimetallic Metal-Organic Framework to Porous Carbon: High Surface Area and Multicomponent Active Dopants for Excellent Electrocatalysis. *Adv. Mater*. **2015**, 27, 5010.

55. Xu, X.; Pan, L.; Liu, T.; Sun, Z. Enhanced capacitive deionization performance of graphene by nitrogen doping. *J. Colloid Interface Sci*. **2015**, 445, 143–150.

56. Jeong, H.M.; Lee, J.W.; Shin, W.H.; Choi, Y.J.; Shin, H.J.; Kang, J.K.; Choi, J.W. Nitrogen-Doped Graphene for High-Performance Ultracapacitors and the Importance of Nitrogen-Doped Sites at Basal Planes. *Nano Lett.* **2011**, 11, 2472.

57. Stoller, M.D.; Park, S.; Zhu, Y.; An, J.; Ruo, R.S. Graphene-Based Ultracapacitors. *Nano Lett*. **2008**, 8, 3498.

58. Yang, X.; Chenglin, Z.; Yong, L. Highly nitrogen doped carbon nanofibers with superior rate capability and cyclability for potassium ion batteries. *Nat. Commun.* **2018**, 9, 1720.

59. Yong, L.; Xingtao, X.; Ting, L.; Zhuo, S.; Daniel, H.C.; Likun, P. Nitrogen-doped electrospun reduced graphene oxide-carbon nanofiber composite for capacitive deionization. *RSC Adv*. **2015**, *5*, 34117–34124.

60. Jie, M.; Lei, W.; Fei, Y. Water-enhanced performance in capacitive deionization for desalination based on graphene gel as electrode material. *Electrochim. Acta* **2018**, *263*, 40–46.

61. Cao, J.; Wang, Y.; Chen, C.; Yu, F.; Ma, J. A Comparison of graphene hydrogels modified with single-walled/multiwalled carbon nanotubes as electrode materials for capacitive deionization. *J. Colloid Interface Sci.* **2018**, *518*, 69–75.

62. Ling, L.; Liuhui, L.; Qinghan, M.; Bing, C. High performance graphene composite microsphere electrodes for capacitive deionization. *Carbon* **2015**, *90*, 75–84.

63. Ahmed, E.D.; Jae, H.C.; Cheol, S.K.; Khalil, A.K.; Abdulhakim, A.; Nasser, B. TiO_2 nanorod-intercalated reduced graphene oxide as high performance electrode material for membrane capacitive deionization. *Desal* **2015**, *361*, 53–64.

64. Yasin, A.S.; Mohamed, H.O.; Mohamed, I.M.; Mousa, H.M.; Barakat, N.A. Enhanced desalination performance of capacitive deionization using zirconium oxide nanoparticles-doped graphene oxide as a novel and effective electrode. *Sep. Purif. Technol*. **2016**, *171*, 34–43.

65. Yan, C.; Zou, L.; Short, R. Polyaniline-modified activated carbon electrodes for capacitive deionization. *Desal.* **2014**, *333*, 101–106.

66. Ahmed, E.D.; Remko, B.; Hak, Y.K.; Hongwei, D.; Mary, C.P.; Jae-Hwan, C. Flexible 3D Nanoporous Graphene for Desalination and Bio-decontamination of Brackish Water via Asymmetric Capacitive Deionization. *ACS Appl. Mater. Interfaces* **2016**, *8*, 25313−25325.

67. Liu, P.; Wang, H.; Yan, T.; Zhang, J.; Shi, L.; Zhang, D. Grafting sulfonic and amine functional groups on 3D graphene for improved capacitive deionization. *J. Mater. Chem. A* **2016**, *4*, 5303.

68. Lee, B.; Park, N.; Kang, K.S.; Ryu, H.J.; Hong, S.H. Enhanced Capacitive Deionization by Dispersion of CNTs in Activated Carbon Electrode. *ACS Sustain. Chem. Eng.* **2018**, *6*, 1572−1579.

69. Porada S. Review on the science and technology of water desalination by capacitive deionization. *Prog in Mat Sci*, 2013. **58**, 1388-1442

70. Peters, P.B.; van Roij, R.; Bazant, M.Z.; Biesheuvel, P.M. Analysis of electrolyte transport through charged nanopores. *Phys. Rev. E* **2015**, 93, 053108.

71. Jeon, S.I.; Park, H.R.; Yeo, J.; Yang, S.; Cho, C.H.; Han, M.H.; Kim, D.K. Desalination via a new membrane capacitive deionization process utilizing flow-electrodes. *Energy Environ. Sci.* **2013**, 6, 1471–1475.

72. Park, H.R.; Choi, J.; Yang, S.; Kwak, S.J.; Jeon, S.I.; Han, M.H.; Kim, D.K. Surface-modified spherical activated carbon for high carbon loading and its desalting performance in flow-electrode capacitive deionization. *RSC Adv.* **2016**, *6*, 69720−69727.

73. Yang, S.; Choi, J.; Yeo, J.; Jeon, S.; Park, H.; Kim, D.K. Flow-electrode capacitive deionization using an aqueous electrolyte with a high salt concentration. *Environ. Sci. Technol.* **2016**, 50, 5892–5899104.

74. Kexin, L.; Xueliang, S.; Yanhong, B.; Helan, Z.; Xufei, Y.; Yong, J.; Panpan, L.; Xia, H. Optimized desalination performance of high voltage flow-electrode capacitive deionization by adding carbon black in flow-electrode. *Desal.* **2017**, 420, 63–69.

75. Cho, Y.; Yoo, C.Y.; Lee, S.W.; Yoon, H.; Lee, K.S.; Yang, S.; Kim, D.K. Flow-electrode capacitive deionization with highly enhanced salt removal performance utilizing high-aspect ratio functionalized carbon nanotubes. *Water Res.* **2019**, *151*, 252–259.

76. Yang, S.C.; Jeon, S.I.; Kim, H.; Choi, J.; Yeo, J.G.; Park, H.R.; Kim, D.K. Stack Design and Operation for Scaling Up the Capacity of Flow- Electrode Capacitive Deionization Technology. *Chem. Eng.* **2016**, 4, 4174−4180.

77. Gendel, Y.; Rommerskirchen, A.; David, O.; Wessling, M. Batch mode and continuous desalination of water using flowing carbon deionization (FCDI) technology. *Electrochem. Commun.* **2014**, 46, 152–156.

78. Hatzell, K.B.; Iwama, E.; Ferris, A.; Daffos, B.; Urita, K.; Tzedakis, T.; Chauvet, F.; Taberna, P.L.; Gogotsi, Y.; Simon, P. Capacitive deionization concept based on suspension electrodes without ion exchange membranes. *Electrochem. Commun.* **2014**, 43, 18–21.

79. Hatzell, K.B.; Hatzell, M.C.; Cook, K.M.; Boota, M.; Housel, G.M.; McBride, A.; Kumbur, E.C.; Gogotsi, Y. Effect of oxidation of carbon material on suspension electrodes for flow electrode capacitive deionization. *Environ. Sci. Technol.* **2015**, 49, 3040−3047

80. Długołecki, P.; Van Der Wal, A. Energy recovery in membrane capacitive deionization. *Environ. Sci. Technol.* **2013**, 47, 4904−4910.

81. Jeon, S.-I.; Yeo, J.-G.; Yang, S.; Choi, J.; Kim, D.K. Ion storage and energy recovery of a flow-electrode capacitive deionization process. *J. Mater. Chem. A* **2014**, 2, 6378.

82. Alexandra, R.; Christian, J.L.; Daniel, M.; Lisa, K.W.; Matthias, W. Energy recovery and process design in continuous flow−electrode capacitive deionization processes. *ACS Sustain. Chem. Eng.* **2018**, *6*, 13007−13015.

83. Ma, J.; Liang, P.; Sun, X.; Zhang, H.; Bian, Y.; Yang, F.; Bai, J.; Gong, Q.; Huang, X. Energy recovery from the flow-electrode capacitive deionization. *J. Power Sources* **2019**, 421, 50–55.

84. Lim, H.; Ha, Y.; Jung, H.B.; Jo, P.S.; Yoon, H.; Quyen, D.; Cho, N.; Yoo, C.Y.; Cho, Y. Energy storage and generation through desalination using flow-electrodes capacitive *deionization. J. Ind. Eng. Chem.* **2016**, 81, *317–322.*

85. Doornbusch, G.J.; Dykstra, J.E.; Biesheuvel, P.M.; Suss, M.E. Fluidized bed electrodes with high carbon loading for water desalination by capacitive deionization. *J. Mater. Chem. A* **2016**, 4, 3642.

86. El-Deen, A.G.; Barakat, N.A.M.; Kim, H.Y. Graphene wrapped MnO_2-nanostructures as effective and stable electrode materials for capacitive deionization desalination technology. *Desal*, **2014**, 344, 289–298

87. Liu, J.; Lu, M.; Yang, J.; Cheng, J.; Cai, W. Capacitive desalination of ZnO/activated carbon asymmetric capacitor and mechanism analysis. *Electrochim. Acta* **2015**, 151, 312–318

88. Li, H.B.; Pan, L.K.; Lu, T.; Zhan, Y.K.; Nie, C.Y.; Sun, Z. A comparative study on electrosorptive behavior of carbon nanotubes and graphene for capacitive deionization. *J. Electroanal. Chem*. **2011**, 653, 40–44.

89. Thommes, M.; Kaneko, K.; Neimark, A. V.; Olivier, J. P.; Rodriguez-Reinoso, F.; Rouquerol, J.; Sing, K. S. W. Physisorption of gases, with special reference to the evaluation of surface area and pore size distribution (IUPAC Technical Report). *Pure Appl. Chem.* **2015**, 87, 1051−1069.

90. Dong, Q.; Wang, G.; Qian, B.; Hu, C.; Wang, Y.; Qiu, J. Electrospun Composites Made of Reduced Graphene Oxide and Activated Carbon Nanofibers for Capacitive Deionization. *Electrochimica Acta* **2014**, 137, 388–394.

91. El-Khodary, S.A.; El-Enany, G.M.; El-Okr, M.; Ibrahim, M. Preparation and Characterization of Microwave Reduced Graphite Oxide for High-Performance Supercapacitors. *Electrochimica Acta* **2014**, 150, 269–278.

92. Konwar, L.J.; Sugano, Y.; Chutia, R.S.; Shchukarev, A.; Mäki-Arvela, P.; Kataki, R.; Mikkola, J.-P. Sustainable synthesis of N and P co-doped porous amorphous carbon using oil seed processing wastes. *Mater. Lett.* **2016**, 173, 145–148.

93. Shen, J.; Yan, B.; Shi, M.; Ma, H.; Li, N.; Ye, M. One step hydrothermal synthesis of TiO_2-reduced graphene oxide sheets. *J. Mater. Chem.* **2011**, 21, 3415–3421

94. Nishiyama, T.; Sumihara, T.; Sato, E.; Horibe, H. Effect of solvents on the crystal formation of poly (vinylidene fluoride) film prepared by a spin-coating process. *Polym. J.* **2017**, 49, 319–325

95. Wang, K.; Zhao, N.; Lei, S.; Yan, R.; Tian, X.; Wang, J.; Song, Y.; Xu, D.; Guo, Q.; Liu, L. Promising biomass-based activated carbons derived from willow catkins for high performance supercapacitors. *Electrochimica Acta.* **2015**, 166, 1-11

96. Thorogood, C.A.; Wildgoose, G.G.; Jones, J.H.; Compton, R.G. Identifying quinone-like species on the surface of graphitic carbon and multi-walled carbon nanotubes using reactions with 2,4-dinitrophenylhydrazine to provide a voltammetric fingerprint. *New J. Chem.* **2007**, 31, 958–965

97. Folaranmi G, Bechelany M, Sistat P, Cretin M, Zaviska F. Comparative Investigation of Activated Carbon Electrode and a Novel Activated Carbon/Graphene Oxide Composite Electrode for an Enhanced Capacitive Deionization. *Materials*, **2020**, 13, 5185.

98. Bryan H. R. S, Sheng C, Jingjing D, and Chuan Z. Hydrothermally driven transformation of oxygen functional groups at multiwall carbon nanotubes for improved electrocatalytic applications. *ACS Appl. Mater. Interfaces.* **2016,** 14090

99. Kim H, Miura Y, and Macosko C. W., Graphene/polyurethane nanocomposites for improved gas barrier and electrical conductivity. *ChemMats*. **2010**, 22, 3441–3450

100. Murugan A. V, Muraliganth T, and Manthiram A. Rapid, facile microwave-solvothermal synthesis of graphene nanosheets and their polyaniline nanocomposites for energy strorage. *Chem Mats*. **2009**, 21, 5004–5006

101. Chen D, Feng H, Li J. Graphene oxide: preparation, functionalization, and electrochemical applications. *Chem Rev*. **2012**; 11, 6027–53.

102. Sreekanth P, Pranitha S, Priya R and Reji P. White light Z-scan measurements of ultrafast optical nonlinearity in reduced graphene oxide nanosheets in the 400–700 nm region. *App phys Letters* 2015, **107**, 051104

103. Malas A, Das C. K., Das A. and Heinrich G. Development of expanded graphite filled natural rubber vulcanizates in presence and absence of carbon black: Mechanical, thermal and morphological Properties. *Materials and Design* **2012**, 39, 410-417.

104. Ng E. P, Mintova S. Quantitative moisture measurements in lubricating oils by FTIR spectroscopy combined with solvent extraction approach. *Micro chem. J*. **2011**. 98, 177–185.

105. Yongzhe P, Biqiong C. One pot synthesis and characterization of reduced graphene oxide –gelatin nanocomposite hydrogel. *RSC Adv.* **2016**, 6, 6171-6181

106. Beidou G, Qian L, Erdan C, Hewei Z, Liang F, Jian Ru G. Controllable N-doping of graphene. *Nano Lett.* **2010**, 12, 4975–4980

107. Wenhui M, Yunzhen C, Gaoyi H, Yaoming X, *Dongying* F and Yahui C. Capacitive Properties of the Binder-Free Electrode Prepared from Carbon Derived from Cotton and Reduced Graphene Oxide. *Chin. J. Chem.* **2017**, 35, 1844—1852

108. Ji-Hyuk C, Chongmin L, Sungwhan C, Geon D. M, Byung-su H, Hankwon C, Hee D. J. High capacitance and energy density supercapacitor based on biomass-derived activated carbons with reduced graphene oxide binder. *Carbon.* **2018**, 132, 16-24

109. Finegan I.C, Tibbetts G.G, Electrical conductivity of vapor-grown carbon fiber/thermoplastic composites. *Mater. Res. Soc.* **2001**, 16, 1668

110. Leow C, Kreider P.B, Notthoff C, Kluth P, Antonio Tricoli A & Compston P. A graphene film interlayer for enhanced electrical conductivity in a carbon-fibre/PEEK composite. *Functional Composite Materials*. **2021,** 2, 667

111. Zhi P, Lili, Ching-Yuan C, Ronggang D, Chunchui Z. High capacitance electrode materials based on layered double hydroxides prepared by non-aqueous precipitation. *Applied Clay Science.* **2013,** 74, 102-108

112. Lanshu X, Yue L, Mengying J, Qiang Z, Xiaojuan J, Chunli Y. Synthesis and characterization of free-standing activated carbon/reduced graphene oxide film electrodes for flexible supercapacitors. *RSC Adv.,* **2017**, 7, 45066

113. Qiang D, Gang W, Bingqing Q, Chao H, Yuwei W, Jieshan Q. Electrospun composites made of reduced graphene Oxide and activated carbon nanofibers for Capacitive Deionization. *Electrochimica Acta.* **2014**, 137, 388–394

114. Haibo L, Likun P, Chunyang N, Yong Liu, Zhuo Sun. Reduced graphene oxide and activated carbon composites for capacitive deionization. *J. Mater. Chem.,* **2012**, 22, 15556

115. Xin L, Ting C, Wei-chuan Q, Zhuo W, Lei Y. Fabrication of graphene/activated carbon nanofiber composites for high performance capacitive deionization *J. Taiwan Inst. Chem. Eng.* **2017**, 72, 213–219

116. Shijie Li, Kuihua H, Pengchao Si, Jinxiao Li, Chunmei Lu. High–performance Activated Carbons Prepared by KOH Activation of Gulfweed for Supercapacitors. *Int. J. Electrochem. Sci.* **2018**, 13, 1728 – 1743

117. Feng W, He P, Ding S. Oxygen-doped activated carbons derived from three kinds of biomass: preparation, characterization and performance as electrode materials for supercapacitors. *Rsc Adv.* **2016**. 6**,** 5949–5956

118. Amidon G.E., Bergren M.S., Grant D.J.W., Marshall K., Itai S., Physical test methods for powder flow characterization of pharmaceutical materials: a review of methods stimuli to the revision process, *Pharmacopeial Forum,* **1999**, 25, 8298–8308

119. Hou H., Sun C.C., Quantifying effects of particulate properties on powder flow properties using a ring shear tester, *J. Pharm.Sci*. **2008,** 97, 4030–4039.

120. Qi Z, Brian A, Ian L, Peter J. S, David A.V. M. Effect of host particle size on the modification of powder flow behavior for lactose monohydrate following dry coating. *Dairy Sci. Technol*. **2010,** 90, 237–251

121. Sven K, Antoinette Y.V, Lukas A, Thorsten T, Rainer T. Zeta potential and long-term stability correlation of carbon-based suspensions for material jetting**.** *Open Ceramics*. **2020**, 4, 100037

122. AmericanLaboratory.Zeta Potential. https://www.americanlaboratory.com/913-Technical-Articles/35729-understanding-the-Links-Between-Rheology-and-Particle-Parameters/ **2020,** accessed 02 February 2021

123. Anton Paar. Zeta potential. https://wiki.anton-paar.com/de-de/zetapotenzial/ **2020,** accessed 02 February 2021

124. Bishweshwar P, Mira P, Soo-Jin P. TiO_2 NPs Assembled into a Carbon Nanofiber Composite Electrode by a One-Step Electrospinning Process for Supercapacitor Applications. *Polymers* **2019**, 11, 899.

125. Ahmed S. Y, Ibrahim M.A. M, Chan H. P, Cheol S.K. Facile synthesis of TiO_2/ZrO_2 nanofibers/nitrogen co-doped activated carbon to enhance the desalination and bacterial inactivation *via* capacitive deionization. *Scientific report*. **2018,** 8, 541

126. Xiang, Q., Yu, J. & Jaroniec, M. Nitrogen and sulfur co-doped TiO_2 nanosheets with exposed {001} facets: synthesis, characterization and visible-light photocatalytic activity. *Physical Chemistry Chemical Physics*, **2011**, 13, 4853–4861.

127. El-Deen A.G., Choi J.-H., Khalil K.A., Almajid A.A., Barakat N A. A TiO_2 nanofiber/activated carbon composite as a novel effective electrode material for capacitive deionization of brackish water, *RSC Adv*. **2014,** 4, 64634–64642.

128. Wang, L.; Wang, M.; Huang, Z.-H.; Cui, T.; Gui, X.; Kang, F.; Wang, K.; Wu, D. Capacitive deionization of NaCl solutions using carbon nanotube sponge electrodes. *J. Mater. Chem.* **2011**, *21*, 18295–18299

129. Li, H.; Pan, L.; Lu, T.; Zhan, Y.; Nie, C.; Sun, Z. A comparative study on electrosorptive behavior of carbon nanotubes and graphene for capacitive deionization. *J. Electroanal. Chem.* **2011**, 653, 40–44,

130. Ata, S.; Banerjee, S.L.; Singha, N.K. Polymer nano-hybrid material based on graphene oxide/POSS via surface initiated atom transfer radical polymerization (SI-ATRP): Its application in specialty hydrogel system. *Polymer* **2016**, 103, 46–56.

131. Jia, B.; Zou, L. Graphene nanosheets reduced by a multi-step process as high-performance electrode material for capacitive deionisation. *Carbon* **2012**, 50, 2315–2321.

132. Kruk, M.; Jaroniec, M. Gas Adsorption Characterization of Ordered Organic−Inorganic Nanocomposite Materials. *Chem. Mater.* **2001**, 13, 3169–3183,

133. Lv, J.; Zhang, G.; Zhang, H.; Yang, F. Graphene oxide-cellulose nanocrystal (GO-CNC) composite functionalized PVDF membrane with improved antifouling performance in MBR: Behavior and mechanism. *Chem. Eng. J.* **2018**, 352, 765–773.

134. Wu, T.; Zhou, B.; Zhu, T.; Shi, J.; Xu, Z.; Hu, C.; Wang, J. Facile and low-cost approach towards a PVDF ultrafiltration membrane with enhanced hydrophilicity and antifouling performance via graphene oxide/water-bath coagulation. *RSC Adv.* **2015**, 5, 7880–7889.

135. Krishnamoorthy, K.; Navaneethaiyer, U.; Mohan, R.; Lee, J.; Kim, S.-J. Graphene oxide nanostructures modified multifunctional cotton fabrics. *Appl. Nanosci.* **2012**, 2, 119–126.

136. Khalil, K.A.; Barakat, N.A.; Motlak, M.; Al-Mubaddel, F.S. A novel graphene oxide-based ceramic composite as an efficient electrode for capacitive deionization. *Sci. Rep.* **2020**, 10, 9676.

137. Wang, Z.; Dou, B.; Zheng, L.; Zhang, G.; Liu, Z.; Hao, Z. Effective desalination by capacitive deionization with functional graphene nanocomposite as novel electrode material. *Desal.* **2012**, 299, 96–102.

138. Biswas, S.; Drzal, L.T. Multilayered Nanoarchitecture of Graphene Nanosheets and Polypyrrole Nanowires for High Performance Supercapacitor Electrodes. *Chem. Mater.* **2010**, 22, 5667–5671.

139. Alhabeb, M.; Beidaghi, M.; Van Aken, K.L.; Dyatkin, B.; Gogotsi, Y. High-density freestanding graphene/carbide-derived carbon film electrodes for electrochemical capacitors. *Carbon* **2017**, 118, 642–649,

140. Blegur, E.J.; Endarko, E. Study the effect of active carbon modified using HNO3 for carbon electrodes in capacitive deionization system. *AIP Conf. Proc.* **2016**, 1788, 030041-6

141. Villar, I.; Roldan, S.; Ruiz, V.; Granda, M.; Blanco, C.; Menéndez, R.; Santamaría, R. Capacitive Deionization of NaCl Solutions with Modified Activated Carbon Electrodes S. *Energy Fuels* **2010**, 24, 3329–3333

142. Gao, X.; Omosebi, A.; Landon, J.; Liu, K. Enhanced Salt Removal in an Inverted Capacitive Deionization Cell Using Amine Modified Microporous Carbon Cathodes. *Environ. Sci. Technol.* **2015**, 49, 10920–10926.

143. Leong, Z.Y.; Lu, G.; Yang, H.Y. Three-dimensional graphene oxide and polyvinyl alcohol composites as structured activated carbons for capacitive desalination. *Desal.* **2019**, 451, 172–181.

144. Li H, Zou L, Pan L and Sun Z. Novel Graphene-Like Electrodes for Capacitive Deionization *Environ. Sci. Technol.,* **2010,** 44, 8692–8697

145. Li H, Lu T, Pan L, Zhang Y and Sun Z. Electrosorption behavior of graphene in NaCl solutions. *J. Mater. Chem.***, 2009**,19, 6773–6779

146. Yan W. L, Yao L., Hu D. D, Liu C. D, Wang C.S.L. Progress in the preparation and application of three-dimensional graphene-based porous nanocomposites. *Nanoscale*, **2015**,7, 5563–5577

147. Böckenfeld. N, Jeong S.S, Winter M, Passerini S, Balducci A. Natural, cheap and environmentally friendly binder for supercapacitors. *J. Power Sources.* **2013**, 221, 14−20.

148. Alhabeb M, Beidaghi M. Aken K.L, Van D, B, Gogotsi Y. High-density freestanding graphene/carbide-derived carbon film electrodes for electrochemical capacitors. *Carbon.* **2017**, 118, 642−649.

149. Peiying L, Tingting Y, Liyi S, Ho Seok P, Xuecheng C, Zhigang Z and Dengsong Z. Graphene-based materials for capacitive deionization. *J. Mater. Chem. A,* **2017**, 5, 13907-13943

150. Raluca T, Otto T B, Loan P, Cosmin L, Simion A, Loan B. Reduced graphene oxide today. *J. Mater. Chem. C,* **2020**, 8, 1198-1224

151. Mohd H M Z, Jaafar A, Nor A Y, Helmi W, Yusran S, Mohd F M N, and Rahizan I. Reduced Graphene Oxide/TEMPO-Nanocellulose Nanohybrid-Based Electrochemical Biosensor for the Determination of *Mycobacterium tuberculosis*. *J. sensors,* **2020,** 2020, 1-11

152. Chuanyin X, Mengrui L, Wei Z, Chao D, Yonghao N. Flexible N-Doped reduced graphene oxide/carbon Nanotube-MnO_2 film as a Multifunctional Material for High-Performance supercapacitors, catalysts and sensors. *J. Materiomics.* **2020,** 6,523-531

153. Faten Ermala C O, Norhaniza Y, Javier G B, Xiaolei F and Ahmad Fauzi I. Electrospun Composites Made of Reduced GrapheneOxide and Polyacrylonitrile-Based Activated CarbonNanofibers (rGO/ACNF) for Enhanced CO_2 Adsorption. *Polymers*, **2020**, 12, 2117

154. Jiantong L, Mikael Ö. Prevention of Graphene Restacking for Performance Boost of Supercapacitors—A Review. *Crystals.* **2013**, 3, 163-190

155. Lanshu X, Yue L, Mengying J, Qiang Z, Xiaojuan J, Chunli Y. Synthesis and characterization of free-standing activated carbon/reduced graphene oxide film electrodes for flexible supercapacitors. *RSC Adv.,* **2017**, 7, 45066

156. Qiang D, Gang W, Bingqing Q, Chao H, Yuwei W, Jieshan Q. Electrospun composites made of reduced graphene Oxide and activated carbon nanofibers for Capacitive Deionization. *Electrochimica Acta.* 2014, **137**, 388–394

157. Haibo L, Likun P, Chunyang N, Yong Liu, Zhuo Sun. Reduced graphene oxide and activated carbon composites for capacitive deionization. *J. Mater. Chem.,* **2012**, 22, 15556

158. Xin L, Ting C, Wei-chuan Q, Zhuo W, Lei Y. Fabrication of graphene/activated carbon nanofiber composites for high performance capacitive deionization *J. Taiwan Inst. Chem. Eng.* **2017**, 72, 213–219

159. Yifan W, Shupeng Z, Wentao L, Baijun W, Changming W, Juanjuan G, Haiou S, Aimin L. Mesoporous generation-inspired ultrahigh capacitive deionization performance by sono-assembled activated carbon/inter-connected graphene network architecture. *Electrochimica Acta.* **2016**, 205, 161–169

160. Liu Y, Xu X, Lu T, Sun Z, Chua D H C and Pan L. Nitrogen-doped electrospun reduced graphene oxide–carbon nanofiber composite for capacitive deionization. *RSC Adv.,* **2015,** 5, 34117-34124

161. Wang M, Xu X, Tang J, Hou S, Shahriar M, Hossain A, Pan L and Yamauchi Y. High performance capacitive deionization electrodes based on ultrathin nitrogen-doped carbon/graphene nano-sandwiches. *Chem. Commun.*, **2017,** 53, 10784-10787

162. Zhang D, Wen X, Shi L, Yan T and Zhang J. Enhanced capacitive deionization of graphene/mesoporous carbon composites *Nanoscale,* **2012**, 4, 5440-5446

163. Wang H, Shi L, Yan T, Zhang J, Zhong Q and Zhang D. Reduced graphene oxide/highly porous carbon for capacitive deionization application. *J. Mater. Chem. A*, **2014**, 2, 4739-475

164. Wen X, Zhang D, Yan T, Zhang J and Shi L. Three-dimensional graphene-based hierarchically porous carbon composites prepared by a dual-template strategy for capacitive deionization. *J. Mater. Chem. A*, **2013,** 1, 12334-12344.

165. Zhu G, Wang W, Li X, Zhu J, Wang H and Zhang L. Design and fabrication of a graphene/carbon nanotubes/activated carbon hybrid and its application for capacitive deionization. *RSC Adv.*, **2016**, 6, 5817-5823

166. Boota, M.; Hatzell, K. B.; Beidaghi, M.; Dennison, C. R.; Kumbur, E. C.; Gogotsi, Y. Activated carbon spheres as a flowable electrode in electrochemical flow capacitors. *J. Electrochem. Soc.* **2014,** 161**,** 1078−1083

167. Xu X, Wang M, Liu Y, Lu T and Pan L. Ultrahigh Desalinization Performance of Asymmetric Flow-Electrode Capacitive Deionization Device with an Improved Operation Voltage of 1.8 V. *ACS Sustainable Chem. Eng.*, **2017, 5,** 189 —195

168. Doornbusch G. J., Dykstra J. E., Biesheuvel P. M. and Suss M. E. Fluidized bed electrodes with high carbon loading for water desalination by capacitive deionization, *J. Mater. Chem. A*, **2016, 4**, 3642 —3647

169. Ma J, He D, Tang W, Kowalski P, He C, Zhang C and Waite T. D. Development of Redox-Active Flow Electrodes for High-Performance Capacitive Deionization, *Environ. Sci. Technol.,* **2016, 50,** 13495 —13501

170. Aranzazu C.O, Robert A.W.D. Understanding the performance of flow-electrodes for capacitive deionization through hydrodynamic voltammetry. *Che Engr J.* **2021,** 406, 126826

171. Kuo F, Hui G, Wenyan H, Fei P and Kaijun W. Revealing the intrinsic differences between static and flow electrode capacitive deionization by introducing semi-flow electrodes. *Environ. Sci Water Res. Technol.,* **2020**,6, 362-372

172. Partlan, E., Davis, K., Ren, Y., Apul, O.G., Mefford, O.T., Karanfil, T., Ladner, D.A. Effect of bead milling on chemical and physical characteristics of activated carbons pulverized to superfine sizes. *Water Res.* **2016**, 89, 161–170.

173. Matsui, Y., T. Aizawa, F. Kanda, N. Nigorikawa, S. Mima, and Y. Kawase. Adsorptive removal of geosmin by ceramic membrane filtration with superpowdered activated carbon. Journal of Water Supply: Research and Technology, AQUA, **2007**. 56, 411-418.

174. Ando, N., Y. Matsui, R. Kurotobi, Y. Nakano, T. Matsushita, and K. Ohno, Comparison of natural organic matter adsorption capacities of super-powdered activated carbon and powdered activated Carbon. *Water Research*, **2010**. 44, 4127-4136

175. Seungyeon C, Barsa C, Ji Hyun K, Mamadou S.D, Jang W. Energy-efficient hybrid FCDI-NF desalination process with tunable salt rejection and high water recovery. *Journal of Membrane Science.* **2017,** 541, 580-58

176. Qiang W, Yudi H, Jian W, Qiang R, Xianhua H, Lingzhi Z, Denis.Y.W.Y , KwanSan H, Dongliang Y, Kwun N. H, Fuming C. Low energy consumption flow capacitive deionization with a combination of redox couples and carbon slurry. *Carbon,* **2020,** 170, 487-492

177. Kexin T, Sotira Y, Yuping L, and Costas T. Enhanced Water Desalination by Increasing the Electroconductivity of Carbon Powders for High-Performance Flow-Electrode Capacitive Deionization. *Sustainable Chem. Eng*. **2019**, 7, 1085−1094

178. Jinxing M, Di H, Wangwang T, Peter K, Calvin H, Changyong Z and David W. Development of redox-active flow-electrodes for high-performance capacitive deionization. *Environ. Sci. Technol*. **2016,** 50, 13495−13501

179. Daniel M and Marta C. H. Influence of Feed-Electrode Concentration Differences in Flow Electrode Systems for Capacitive Deionization. *Ind. Eng. Chem. Res*. **2018,** 57, 8802−8809

180. Calvin H, Jinxing M, Changyong Z, Jingke S and David W.T. Short-Circuited Closed-Cycle Operation of Flow-Electrode CDI for Brackish Water Softening. *Environ. Sci. Technol*. **2018,** 52, 9350−9360

181. SeungCheol Y, Sung-il J, Hanki K, Jiyeon C, Jeong-gu Y, Hong-ran P and Dong K.K. Stack Design and Operation for Scaling Up the Capacity of Flow-Electrode Capacitive Deionization Technology. *Sustainable Chem. Eng*. **2016**, 4, 4174−4180

182. Hong-ran P, Jiyeon C, Seungcheol Y, Sung J.K, Sung-il J, Moon H.H and Dong K K. Surface-modified spherical activated carbon for high carbon loading and its desalting performance in flow-electrode capacitive deionization. *RSC Adv*., **2016**, 6, 69720

183. Qu D. Studies of the activated carbons used in double-layer supercapacitors. *J. Power Sources.* **2002**, 109, 403–411.

184. Zou, L.; Li, L.; Song, H.; Morris, G. Using mesoporous carbon electrodes for brackish water desalination. *Water Res.* **2008**, 42, 2340–2348.

185. Ahmed S. Y, Ibrahim M.A. M, Chan H. P, Cheol S.K. Design of novel electrode for capacitive deionization using electrospun composite titania/zirconia nanofibers doped activated carbon. *Materials Letters.* **2018,** 213, 62–66

186. Mohamed I.M., Dao V.D., Barakat N.A., Yasin A.S., Yousef A., Choi H.-S., Efficiency enhancement of dye-sensitized solar cells by use of ZrO_2-doped TiO_2 nanofibers photo-anode, *J. Colloid Interface Sci*. **2016,** 476, 9–19.

187. Benjamin L. H, Shajahan S and Danny K.Y. W. Recent strategies to minimise fouling in electrochemical detection systems. Reviews in Analytical Chemistry. **2016**, 35, 103-111

188. Ahmed S. Y, Ibrahim M.A. M, Chan H. P, Cheol S.K. Facile synthesis of TiO_2/ZrO_2 nanofibers/nitrogen co-doped activated carbon to enhance the desalination and bacterial inactivation *via* capacitive deionization. *Scientific report*. **2018,** 8, 541

189. Yin, H. Three-dimensional graphene/metal oxide nanoparticle hybrids for high-performance capacitive deionization of saline water. *Advanced materials* **2013,** 25, 6270–6276

190. Carriazo D, Picó F, Gutiérrez M C, Rubio F, Rojo J M, del Monte F. Block-copolymer assisted synthesis of hierarchical carbon monoliths suitable as supercapacitor electrodes. *Materials Chemistry* **2010,** 4, 773-780

191. Carriazo D, Gutiérrez M C, Ferrer M L, del Monte F. Resorcinol-based deep eutectic solvents as both carbonaceous precursors and templating agents in the synthesis of hierarchical porous carbon monoliths. *Chemistry of Materials.* **2010** 22, 6146-6152

192. Fischer U, Saliger R, Bock V, Petricevic R& Fricke J. Carbon Aerogels as Electrode Material in Supercapacitors. *Journal of Porous Materials*. **1997,** 4,281–285

193. Australian National Centre of Excellence in Desalination (NCEDA). Australian ResearchersReportPortableCDITrial.Availableonline:https://www.desalination.biz/news/2/Australian-researchers-report-portable- CDI-trial/6401/ (accessed on 23 August 2018).

194. El-Khodary S.A., El-Enany G.M., El-Okr M. Ibrahim. M. Preparation and characterization of microwave reduced graphite oxide for high-performance supercapacitors, *Electrochim. Acta.* **2014,** 150, 269–278

195. Wang, S.; Tian, Y.; Wang, C.; Hang, C.; Zhang, H.; Huang, Y.; Zheng, Z. One-Step Fabrication of Copper Nanopillar Array-Filled AAO Films by Pulse Electrodeposition for Anisotropic Thermal Conductive Interconnectors. *ACS Omega*. **2019**, 4, 6092–6096.

196. Roman, A.; Ryoto, Y.; Masahiro, N. Aluminium nanopillars reduce thermal conductivity of silicon nanobeams. *Nanoscale* **2017**, 39, 15083

197. Hatzell, K.B.; Iwama, E.; Ferris, A.; Daffos, B.; Urita, K.; Tzedakis, T.; Chauvet, F.; Taberna, P.L.; Gogotsi, Y.; Simon, P. Capacitive deionization concept based on suspension electrodes without ion exchange membranes. *Electrochem. Commun.* **2014**, 43, 18–21.

198. Choo, K.Y.; Lee, K.S.; Han, M.H.; Kim, D.K. Study on the electrochemical characteristics of porous ceramic spacers in a capacitive deionization cell using slurry electrodes. *Electroanal. Chem.* **2019**, 835, 262–272

199. Patricia, F.; Elvira, P.; Giovanni, D.F.; Fiore, P.N. Electro-conductive membranes for permeation enhancement and fouling mitigation; a short review. *Membranes* **2017**, 7, 39.

Appendix A : Résumé en Francais

Cette thèse est consacrée à l'optimisation du charbon actif (CA) commercial pour la fabrication d'électrode capacitive bon marché et ce pour accroitre le développement à plus grande échelle (industrialisation) des procédés d'électro-sorption pour le dessalement de l'eau saumâtre. Les technologies de dessalement de l'eau telles que l'osmose inverse (RO), la distillation flash multi-étapes (MSFD), etc., utilisent des procédés à base de membranes pour générer de l'eau douce à partir de solutions salines. Fondamentalement, la plupart de ces procédés fonctionnent en extrayant le solvant des solutés, ce qui nécessite une grande quantité d'énergie et le coût de fonctionnement est généralement élevé. Pour contourner ces défis, les techniques de dessalement électrochimiques telles que le dessalement par batterie, l'electrodialyse, la déionisation capacitive, etc., fonctionnent à l'opposé des technologies susmentionnées en extrayant les solutés du solvant sous l'influence d'un champ électrique.Ces techniques de dessalement électrochimiques s'avère être plus énergétiquement efficace pour le dessalement d'eau saumâtre de moyenne à faible salinité (< 10 g/L de solide dissous totaux).

La déionisation capacitive (CDI), qui est l'objet principal de cette thèse, est une technique électrochimique qui utilise des matériaux poreux comme électrode pour séparer et stocker temporairement les ions sous l'application d'une différence de potentiel électrique. Le champ électrique généré par l'application d'une certaine différence de potentiel crée une situation dans laquelle les ions en solution sont séparés et migrent vers des électrodes de charge opposée (pôles) où ils sont stockés. Le stockage a lieu au niveau de la double couche électrique (EDL) formée à l'intérieur des pores du matériau de l'électrode. L'EDL est une interface générée entre l'électrode et la solution électrolytique. Le stockage spatial et temporel des ions dépend de la formation et de la stabilité de l'EDL.

Les matériaux utilisés comme électrodes pour ce procédé d'électrosorption doivent posséder certaines caractéristiques telles qu'une porosité élevée, une grande surface, une hydrophilie, une bonne conductivité électrique et, surtout, les matériaux doivent être peu coûteux, facilement disponibles et de source renouvelable. Les matériaux à base de carbone possèdent pratiquement toutes ces caractéristiques et ont été les candidats de choix pour la recherche sur les électrodes CDI. Les projets de recherche récents dans le domaine de la déionisation capacitive se sont concentrés sur le développement de matériaux de carbone avancés pour atteindre une capacité de dessalement élevée. Cependant, le développement de ces matériaux

complexes et sophistiqués à l'échelle industrielle est peu réaliste car les processus impliqués dans leur synthèse ou leur modification prennent du temps, sont coûteux ou les matériaux synthétisés sont généralement en faible quantité pour des expériences à l'échelle du laboratoire.

Le charbon actif commercial (CA) est une alternative pour surmonter les défis susmentionnés, car il est bon marché et facilement disponible à partir d'une grande diversité de biomasse (peaux de bananes, coquilles de noix de coco, etc.) et peut également être produit en grande quantité. Néanmoins, le CA n'est pas sans poser quelques problèmes intrinsèques tels qu'une faible hydrophilie, une faible conductivité électrique, une faible porosité, etc. et c'est pourquoi cette thèse se concentre sur l'optimisation de ses propriétés. Pour y parvenir, deux voies possibles existent dans la littérature, à savoir la modification sous agents acides/fortement oxydants ou la formation d'un matériau composite/hybride en combinant/dopant avec d'autres matériaux à haute performance. Dans cette thèse, l'attention est portée sur la modification du charbon actif en matériaux d'électrodes hybrides par une chimie simple. Les électrodes hybrides générées sont ensuite évaluées et utilisées dans des opérations de CDI. Les principales contributions de cette thèse sont résumées ci-dessous :

Caractérisation d'une nouvelle électrode composite AC/GO

Comme indiqué précédemment, le CA est peu hydrophile et pour un bon matériau d'électrode, la facilité d'interaction de surface de l'électrolyte sur l'électrode solide est de la plus haute importance en CDI. La recherche dans cet aspect se concentre principalement sur l'amélioration de la chimie de surface ddu CA en utilisant des agents oxydants tels que le peroxyde d'hydrogène (H_2O_2), ($KMnO_4$), l'acide nitrique (HNO_3), etc. dans le cadre de cette thèse, une nouvelle méthode a été proposée afin d'augmenter l'hydrophilicité du CA et ce par simple combinaison du CA avec de l'oxyde de graphène (GO). Le GO, étant très riche en groupes fonctionnels oxygénés (OFGs), l'hypothèse repose sur le fait que le GO pourrait influencer la chimie de surface de l'AC lorsqu'il est combiné à un certain ratio, d'où le développement d'une nouvelle électrode composite. Des caractérisations telles que des mesures d'angle de contact à l'eau (WCA), montrent une amélioration de la mouillabilité du matériau hybride et la démonstration par voltampérométrie cyclique (CV) montre la contribution de cette amélioration à l'obtention d'une capacité exceptionnelle. Les résultats de XPS montrent également que l'incorporation de GO par simple mélange avec l'AC améliore les propriétés de surface de l'AC en raison de l'augmentation de l'intensité de la bande des

différents OFG du matériau hybride. Ce procédé simple résout le problème fondamental d'hydrophilie associé à l'AC en utilisant un moyen non corrosif, contrairement aux méthodes connues habituellement rapportées dans la littérature.

Études résolues sur la propriété électrique de l'AC par le biais d'une conception expérimentale simple.

En raison de la faible conductance électrique du CA, des rapports ont montré que la combinaison de l'AC avec des additifs de propriétés électriques élevées peut influencé positivement son efficacité de dessalement. Des additifs tels que l'oxyde de graphène réduit/graphène (RGO/Gr), le noir de carbone (CB), les nanotubes de carbone (CNT), etc. sont généralement utilisés. Cependant, les RGO utilisés dans la plupart de ces rapports sont synthétisés selon des étapes de traitement fastidieuses. Les approches de synthèse prennent du temps (chronophages) et les produits chimiques utilisés dans le processus de réduction sont souvent dangereux. Ainsi, un nouveau moyen de résoudre ce défi a été développé par une conception expérimentale simple. La méthode expérimentale requiert une voie moins coûteuse et plus respectueuse de l'environnement pour la synthèse du RGO en utilisant le KOH pour la réduction du GO. Le RGO obtenu est ensuite directement combiné au charbon actif par simple agitation chimique, sans autre traitement. Grâce à cette approche, le RGO obtenu est capable d'avoir une meilleure influence sur les propriétés électriques du charbon actif et, en tant que tel, donne une plus grande capacité de dessalement lorsqu'il est testé comme électrode dans le CDI par rapport à d'autres rapports trouvés dans la littérature.

Déionisation capacitive à électrodes liquides (flow electrode capacitive deionisation FCDI)

Les nombreux défis (adsorption des co-ions, mode de fonctionnement discontinu et surface d'adsorption limitée) des électrodes à base solide ont conduit à la conception d’une nouvelle configuration de cellule d’electrosorption dans laquelle l'état de l'électrode n’est plus solide (phase continu) mais dispersée dans une solution électrolytique, appelée suspension (ce qui permet un nombre illimité de sites actifs pour l'adsorption). En conséquence, les défis susmentionnés ont été surmontés permettant un fonctionnement continu et simultanée des processus de dessalement et de régénération des électrodes (décharge). Le dispositif est conçu de manière à offrir un débit constant en recyclant la suspension d'électrode, ce qui permet de surmonter le mode de fonctionnement discontinu puisque la régénération de l'électrode a lieu dès que la boue de carbone sort des compartiments de la cellule et se charge au moment où

elle est recyclée dans la cellule. La déionisation capacitive à électrode liquide (FCDI) offre une capacité de dessalement exceptionnelle par rapport à la CDI conventionnelle, mais les défis liés à l'utilisation des électrodes en suspension sont une autre préoccupation croissante. Des problèmes tels que le colmatage du carbone à l'intérieur de la cellule, la faible charge en carbone de la cellule (concentration massique maximum limitée), la faible conductivité électrique, et la viscosité élevée du carbone à une masse plus importante ont limité cette variante de la technologie de deuxième génération. Ici, il s'agit de se concentrer sur l'optimisation de cette technologie en améliorant certains des défis liés aux électrodes liquide. Les principales contributions émanant de ce processus sont résumées ci-dessous :

- Développement d'une forme simple de charbon actif par une simple méthode de broyage à bille (broyeur planétaire). Le charbon actif généré par cette méthode, appelé charbon actif superficiel (SFAC), a été utilisé comme électrodes liquide pour capturer les ions d'une eau saumâtre relativement élevée tout en fonctionnant en phase semi-continue. Les performances de dessalement de ce matériau se sont avérées nettement supérieures par rapport au CA commercial normale. Les observations issues des caractérisations physico-chimiques de ce matériau en comparaison avec le CA vierge n'offrent aucun changement significatif au niveau des propriétés physico-chimiques (défauts, chimie de surface, cristallinité…) mais des changements significatifs ont été observés dans leur morphologie et leur viscosité. Au fur et à mesure que le temps de broyage à billes augmente (temps de broyage), la morphologie du SFAC s'atténue avec des particules plus fines aboutissant à une viscosité dynamique du matériau plus grande. Les tentatives de compréhension de ce dernier comportement ont été rationalisées en réalisant des mesures du potentiel zêta des nouveaux matériaux (SFAC) et du CA vierge. Les résultats issus des mesures du potentiel zêta montre que le SFAC présente une répulsion électrostatique plus élevée (potentiel zêta plus élevé) par rapport au CA vierge, ce qui peut s'expliquer par le fait qu'à mesure que le broyage augmente, les particules deviennent plus fines et plus lâches, s'éloignant ainsi les unes des autres, ce qui entraîne une augmentation de la viscosité, contrairement aux particules qui sont étroitement liées entre elles. Le SFAC démontre ainsi une meilleure stabilité de la suspension ainsi qu'une plus grande facilité de préparation comparé au CA commerciale et à charge équivalente en carbone dans la cellule FCDI. Le SFAC a montré des peformances de dessalement supérieure au CA vierge (dessalement plus élevé à un temps plus court) car cela permet outre l'augmentation de la surface

spécifique du matériau, un meilleur contact intra-particulaire dans son réseau de carbone, favorisant ainsi un transport plus rapide des ions dans ses pores.

- Enfin, le problème lié à la faible conductivité électrique des électrodes liquides a été étudiée en utilisant des nanofibres de titane électrofilées (electrospinning). Le développement et la fabrication d'électrodes liquide à base de matériaux nanocomposites pour améliorer le transport des ions dans les pores de carbone ont été réalisées puis caractérisées expérimentalement, montrant une réduction significative de la résistance de transfert de charge (résistance électrode/électrolyte ou résistance interfaciale) et une augmentation de la capacité de l'EDL (stockage). Cette observation montre que les électrodes à flux nanocomposites sont bien adaptées à l'application de l'électro-sorption car leur structure en carbone permet un transport efficace des ions grâce à l'ancrage des nanofibres dans leurs strates de carbone.

Dans cette thèse, l'auteur a pu montrer la faisabilité de l'optimisation du processus d'électro-sorption pour une application industrielle en utilisant des CA commerciaux. Le développement de méthodes simples basées sur la formation d'électrodes composites pour pallier les inconvénients du CA commerciale et ainsi améliorer ses propriétés ont été proposées permettant ainsi d'accroître la faisabilité de l'électro-sorption pour le dessalement.

La recherche d'une nouvelle façon de surmonter les défis des électrodes à base solide et d'ouvrir une nouvelle voie pour produire de l'eau douce à partir d'une eau saumâtre relativement élevée a conduit à l'innovation de la FCDI. Il s'agit d'une technologie de deuxième génération prometteuse, qui offre une grande capacité de dessalement. En outre, cette étude a permis de comprendre de nouveaux paramètres tels que la charge en carbone, la viscosité et surtout le mécanisme de transport des ions dans les électrodes en suspension.

En outre, l'auteur pense que cette thèse de doctorat comblera un vide en proposant des moyens simples et différents d'optimiser le CA pour le développement à plus grande échelle de l'électro-sorption.

Appendix B

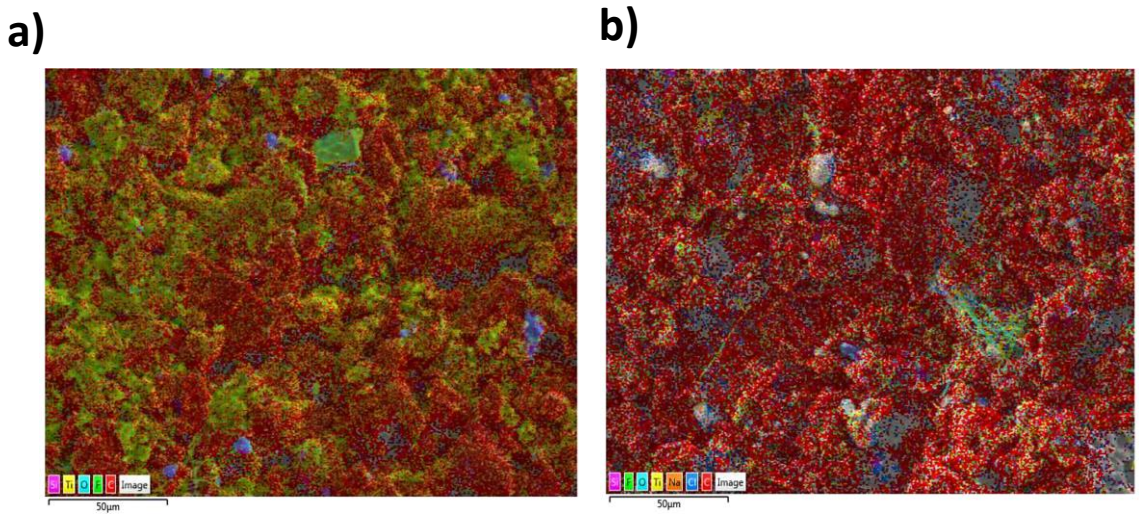

Figure B. EDX mapping of (a) ACTiO$_2$NFs-1.0 and (b) ACTiO$_2$NFs-5.0

Appendix C1

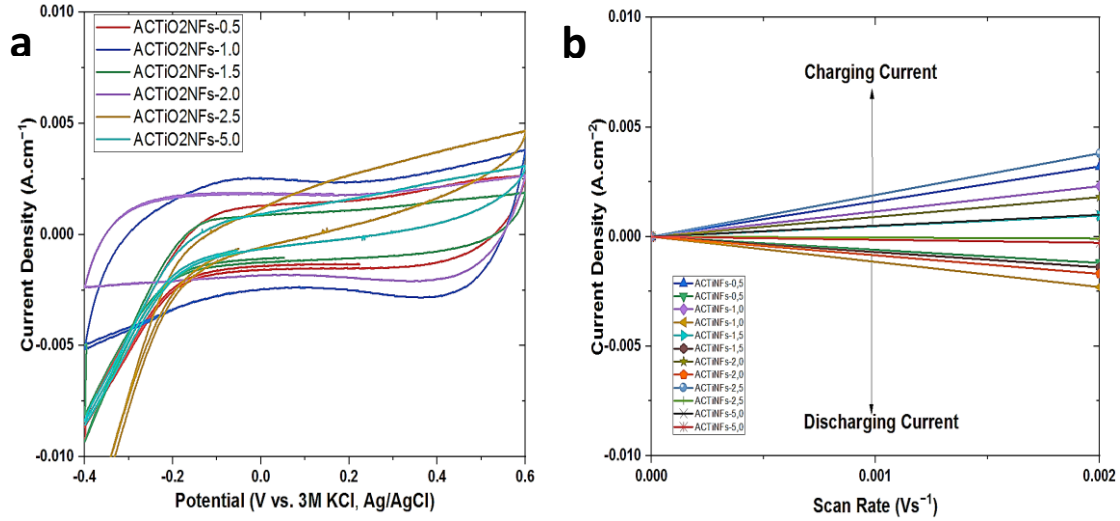

Figure C1 (a) Cyclic voltammetry curve of ACTiO$_2$NFs-x composite electrodes at the scan rates of 2 mVs^{-1} (b) Double-layer capacitance voltammetry measurements for AC and ACTiO$_2$NFs-1.0 composite electrode. Cyclic voltammetry was measured in a non-Faradaic region (0.1 V) of the voltammogram at low scan rates of 2 mVs^{-1}. The charging current (ref current density above 0 A) and discharging currents (ref current density below 0 A) plotted as a function of scan rate (Vs^{-1}). The determined double-layer capacitance of the system was taken as the average of the absolute value of the slope of the linear fits to the data

Appendix C2

Table B2: Electrical double layer capacitance (C_{DL}) of $ACTiO_2NFs$-x electrodes.

Electrode material	C_{DL} ($F.cm^{-2}$)
$ACTiO_2NFs$-0.5	0.60
$ACTiO_2NFs$-1.5	0.80
$ACTiO_2NFs$-2.0	0.70
$ACTiO_2NFs$-2.5	0.60
$ACTiO_2NFs$-5.0	0.30

Appendix D1

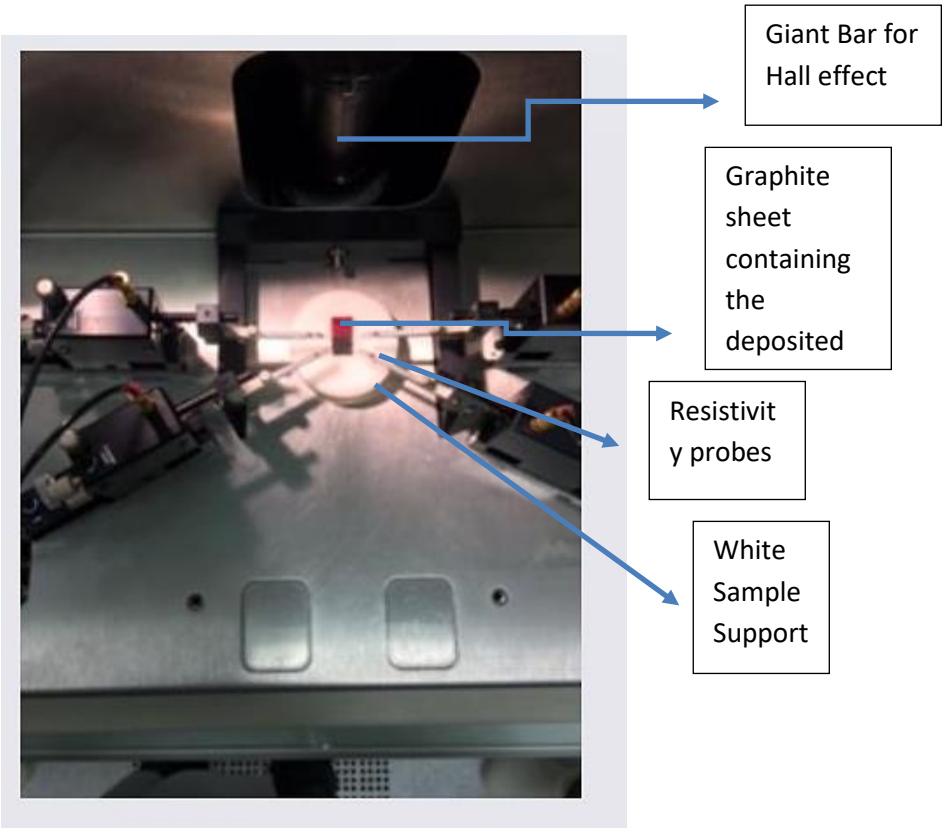

Figure D1. Laboratory set-up of a four probe resistivity and electron mobility experiment

Table D2: Table showing the resistivity and conductivity of the prepared electrodes

Materials	Sample thickness (µm)	Resistivity ($ohms.cm^2$)	Conductivity (1/Resitivity)
AC	488	0.033	30.33

AC/RGO-5	200	0.030	33.33
AC/RGO-10	420	0.048	20.83
AC/RGO-15	435	0.039	25.64
AC/RGO-20	280	0.038	26.31

Appendix E

Table E1: Solid electrode composition (AC/G0-x)

Electrode material	AC (g)	PVDF (g)	CB (g)	RGO (g)	NMP (mL)
AC	3.20	0.4	0.4	0.00	25
AC/GO-5	2.64	0.4	0.4	0.16	25
AC/GO-10	2.48	0.4	0.4	0.32	25
AC/GO-15	2.32	0.4	0.4	0.48	25
AC/GO-20	2.16	0.4	0.4	0.64	25

Table E2: Solid electrode composition (AC/RG0-x)

Electrode material	AC (g)	PVDF (g)	CB (g)	RGO (g)	NMP (mL)
AC	3.20	0.4	0.4	0.00	25
AC/RGO-5	2.64	0.4	0.4	0.16	25
AC/RGO-10	2.48	0.4	0.4	0.32	25
AC/RGO-15	2.32	0.4	0.4	0.48	25
AC/RGO-20	2.16	0.4	0.4	0.64	25

Table E3: Flow Electrode composition of superfine AC.

Electrode material	FE (10 wt. %) (g)	DH_2O (70 mL)	FS (g/L) [NaCl]
AC	7.80		5.0
Superfine AC	7.80		

FE: Feed electrode, FS: Feed solution, DH_2O: Distilled water.

Table E4: Flow Electrode composition of AC co-mixed electrospun titanium nanofibers

Electrode material	FE (10 wt. %) (g)	DH_2O (70 mL)	TiO2NFs (g)	FS (70 mL)	FS (g/L) [NaCl]
AC	7.80				5.0
ACTiO2NFs-0.5	7.76		0.039		5.0
ACTiO2NFs-1.0	7.72		0.078		5.0
ACTiO2NFs-1.5	7.68		0.12		5.0
ACTiO2NFs-2.0	7.64		0.16		5.0
ACTiO2NFs-2.5	7.60		0.20		5.0
ACTiO2NFs-5.0	7.40		0.40		5.0